Abstract

Ferguson, Stephen Scott. The expression, purification, and characterization of metallo-adducts of the histidine-containing phosphocarrier protein (HPr) from *Bacillus Subtilis* and two of its engineered mutants. (Under the direction of Charles R. Cornman)

Expression of recombinant HPr and its mutants HPrγ (S12Y, R17H, E84Y) and HPrβ (S12Y, R17H) was performed in the *Escherichia coli* organism. The proteins were purified via calmodulin affinity resin to yields of ~40 mg/L of culture. The native HPr protein was shown to be active by mutant complementation assays, while the engineered mutants HPrγ, and HPrβ were inactive to phosphotransfer reactivity. Mass spectroscopy analyses verified the masses of the proteins relative to that predicted from the constructed DNA sequences.

Iron-binding studies with HPrγ were designed to coordinate iron (III) ions in a manner analogous to the metalloenzyme protocatechuate 3,4 dioxygenase. This mode of coordination, however, was not observed with iron in our examination of HPRγ. Alternate metal-binding studies with copper and manganese revealed that HPrγ, at physiological pH values, does not form stable complexes with several transition metal ions. The HPrβ mutant protein and, to a degree, native HPr , however, do show transition metal-binding properties through UV-Vis and EPR spectroscopies.

A plausible cause for our inability to form an HPrγ-iron complex is the formation of a hydrophobic pocket at pH = 8.0, between the engineered pairs of proximal histidine and tyrosine residues of HPrγ. CD denaturation studies to examine this possibility revealed that HPrγ has an increased stability to thermal denaturation from 60 ^{o}C for HPr and HPrβ, to 65 ^{o}C for HPrγ.

Design, Preparation, and Characterization of Metallo-adducts of the Histidine-Containing Phosphocarrier Protein from *Bacillus subtilis*

by

Stephen Scott Ferguson

A dissertation submitted to the Graduate Faculty of
North Carolina State University
in partial fulfillment of the
requirements for the Degree of
Doctor of Philosophy

Chemistry

Raleigh

2000

APPROVED BY:

Charles R. Cornman_____ Edmond F. Bowden_____

Hosni M. Hassan_____ Russell J. Linderman____

Biography

Stephen Scott Ferguson was born on August 27, 1970 in Chapel Hill, North Carolina to Herbert and Lillie Ferguson. He was raised near Pittsboro, North Carolina. In 1989, he graduated from Northwood High School in Chatham County, and that fall enrolled at North Carolina State University. After struggling with tuition and classwork for his first two years, he entered the Cooperative Education Program by taking a job at the Chemical Testing Unit of the NC Department of Transportation. Through alternating semesters of work and classwork, he excelled with a lightened workload (work no longer necessary during academic semesters) and a fresh, practical outlook on chemistry. By his senior year Stephen was showing an increasing desire to study the biological aspects of chemistry, and in the Fall of 1994 began his graduate education at NCSU under professor Charles R. Cornman. During his first two years, Stephen took coursework in biotechnology, and excelled at teaching undergraduates as evidenced by winning three teaching awards. Additionally, he was initiated into the Phi Lambda Upsilon Chemistry Honor Society for outstanding academic performance. Upon successful completion of his dissertation defense, Stephen will begin a postdoctoral position at the National Institute of Environmental Sciences under Dr. Joyce Goldstein, where he will further his knowledge and experience in both chemical and biological sciences.

Acknowledgments

Several people have been instrumental in the completion of this thesis-work. First of all, I want to acknowledge my advisor, Dr. Charles R. Cornman. His passion for the biological aspects of chemistry fueled my ambitions to learn and grow as a scientist. This research project was his baby, and he gave me the tools and insight to carry it out. He has been patient beyond reason, enthusiastic, and above all else a role model for me to better myself as a scientist and a person.

I would like to acknowledge Dr. Hosni Hassan. I first met him in a bioinorganic chemistry class, and the literature discussions we had opened my eyes to the fascinating world of oxygen, and left a lasting impression on me. The next fall, I came to him to ask for the temporary use of some laboratory space and equipment to conduct our biological experiments. Neither of us had any idea it would turn into a four-year stay. Dr. Hassan has always made time to answer my numerous questions and share his ideas. He has been a steadying in force in a sometimes-rocky world, and I truly thank him for his generosity.

I also want to thank several members of my research group and Dr. Hassan's group. Yvette Boyajian introduced me to Dr. Cornman, and has been an excellent example of how a graduate student should function. Her guidance both in classwork and research was more helpful than she will ever know. Thad Stauffer has been a good friend who always found time to listen and to offer advice in the numerous obstacles in this research project. Jason Andrus has been a great friend who has helped me expand my knowledge and technical abilities in biological research, and has a contagious enthusiasm for science and philosophy. Donna Joyce-Gray has been a great friend who has always found time to listen to my research quandaries, and offer her opinions and ideas. Dr. Steven Bowen was very helpful by introducing me to the subcloning procedure that helped solve our biggest experimental obstacle. Yvette, Thad, Jason, Donna, and Steven have all been great coworkers and I thank all of them for their help with this research.

I definitely want to thank my parents Herbert and Lillie Ferguson, and my parents-in-law Richard and Lee Bradley. All four have been there for me through the good and bad times, and I love them dearly.

Finally, I would like to thank my beautiful wife Dr. Rebecca Ferguson, DVM. Her strength and love for the last 10 years have kept me going when it seemed like I would never succeed.

Table of Contents

List of Tables

List of Figures

Table of Abbreviations

Chemical Abbreviations

Arg	Arginine
Asp	Asparagine
CABB	Calcium binding buffer
CBP	Calmodulin Binding Peptide
Cys	Cysteine
Cu	Copper
DIG	Digoxigenin
DMG	Dimethylglutaric acid
DNA	Deoxyribonucleic acid
DTT	Dithiothreitol
EB	Elution buffer
E	Escherichia
EDTA	Ethylenediaminetetraacetic acid
EGTA	Ethyleneglutaminetetracetic acid
Fe	Iron
Glu	Glutamate
His	Histidine
HPr	Histidine containing phosphocarrier protein
HPrβ	Mutant HPr S12Y, R17H
HPrγ	Mutant HPr S12Y, R17H, E84Y
IPTG	Isopropyl-1-thio-b-D-galactopyranoside
Mn	Manganese
ONPG	o-nitrophenyl-β-D-galactoside
PEP	phosphoenolpyruvate
Ser	Serine
SDS	Sodium dodecyl sulfate
SDS-PAGE	Sodium dodecyl sulfate poly acrylamide Gel electrophoresis
Taq	Thermus Aquaticus
Tyr	Tyrosine
V	Vanadium

Units Abbreviations

Å	Angstroms
C	Celsius
cm	Centimeter

g	Gram
G	Gauss
GHz	Gigahertz
K	Kelvin
M	Molar
Mg	Milligram
µg	Microgram
min	Minute
mL	Milliliter
µL	Microliter
mM	Millimolar
µM	Micromolar
mmol	Millimoles
N	Normal
nm	nanometers
V	Volts
W/w	Weight by weight
V/v	Volume by volume

Other Abbreviations

A	Absorbance
CD	Circular Dichroism
EPR	Electron Paramagnetic Resonance
NMR	Nuclear Magnetic Resonance
T	Temperature
ε	Extinction coefficient
λ	Wavelength

Chapter 1

INTRODUCTION

1.1 Metalloenzymes in biology

From physical chemistry to microbiology, the study of proteins and their role in life has been fundamental in discovering how nature has evolved its intricate systems of checks and balances. Specialized proteins, enzymes are capable of catalytically converting specific substrates to biologically useful products.

Metalloenzymes in particular carry out some of the most rapid and unique transformations in biology. They differ from other enzymes in that covalently-bound metal ions, or an incorporated metal-containing cofactor, play a key role in their structure and reactivity. Table 1 shows a list of some naturally occurring metalloenzymes, the identity of the covalently bound metal ion(s), and their function. This abbreviated list of

Metalloprotein	**Metal**	**Reactivity**
Catalase	Fe-heme	$H_2O_2 \rightarrow 2H_2O + O_2$
Cytochrome c	Fe-heme	e^- transfer, cyt. C → cyt. C oxidase
Cytochrome c oxidase	Fe-heme, Cu	$2H^+ + ½O_2 + 2e^- \rightarrow H_2O$
Cu-Zn superoxide dismutase	Cu, Zn	$2O^{2-} + 2H^+ \rightarrow O_2 + H_2O_2$
Ferrodoxin	Fe-S clusters	Electron transfer reactions
Nitrogenase	Fe-Mo, Fe-S clusters	½N2 + $^3/_2$H2 → NH3
Oxygen evolving complex	Mn cluster	$2H_2O \rightarrow 4H^+ + O_2 + 4e^-$
Protocatechuate 3,4 dioxygenase	Fe	Protocatechuate ring cleavage
Ribonucleotide reductase	Binuclear Fe center	Ribonucletide→Deoxyribonucleotid
Tyrosinase	Binuclear Cu	Phenolic substrates → Catecholates
Xanthine oxidase	Fe-S, Mo-pterin	Xanthine → Uric Acid

Table 1.1: Naturally occurring metalloenzymes

some of the more widely studied metalloenzymes shows the structural and functional diversity found in these catalysts. Nitrogenase, for example, fixes nitrogen from atmospheric N_2 at ambient temperature and pressure, while industrially this reaction requires high temperature (300-500 ^{o}C) and pressure (> 300 atm) to overcome the sizeable activation energy. Nitrogenase utilizes both iron and molybdenum containing metal clusters as incorporated cofactors to afford the enzyme its remarkable redox properties, and catalytic ability.

Copper-Zinc Superoxide Dismutase is another example of the unique redox properties that can be found in metalloenzymes. This enzyme is crucial to aerobic organisms because it rapidly converts the highly reactive superoxide ion to hydrogen peroxide and water, and in concert with catalase, protects life from the consequences of living in an O_2 atmosphere. Unlike Nitrogenase, Cu-Zn SOD binds two transition metal ions directly to the protein amino acids, and not in a cofactor cluster. Both enzymes, however, can rapidly and specifically carry out the chemistry they have evolved to catalyze. The diversity observed in metalloenzymes is spectacular, and exploring their structure and function will allow us to harness their potential.

An attractive idea that has great technological potential is the preparation of "designer enzymes" capable of performing specific transformations. To this end, researchers have studied the reactivity and physical properties of enzymes to elucidate how they perform such highly specific and rapid transformations. Towards the ultimate goal of preparing "designer metalloenzymes," research efforts have successfully utilized the unique properties of antibodies, through their mode of production within living

organisms, to generate catalytic antibodies that facilitate specific transformations.[1] In general, however, it is difficult to design proteins. At present we are not capable of predicting protein structure based solely on sequence information.[2] Furthermore, our ability to strategically incorporate metal ions within the protein scaffold is in its infancy,[3] thus hindering our ability to create "designer metalloenzymes." In the following sections, I will describe examples of metalloproteins that have been produced and how our research will further expand this field.

1.2 METALLOPROTEIN DESIGN AND SYNTHESIS

Research on metalloprotein design and synthesis is an emerging field of protein chemistry. A simple "his tag" is now a standard method of protein purification in which a poly-histidine peptide is incorporated adjacent to a protein terminus. Subsequently passage over a Ni^{2+} affinity column is used to purify the target protein.[4]

Peptide synthesis has been utilized to create specific protein sequences and study the incorporation of metal ions into these small protein molecules.[5] Zinc finger-type peptides have been frequently reported due to their small size and predictable secondary structure.[6] These zinc finger domains, are naturally occurring proteins, with conserved amino acids that have been shown to specifically bind and modulate nucleic acid structures in the presence of zinc ions. Synthetic peptides, derived from this sequence, have also been made by incorporating non-natural metal binding ligands and studying protein-metal interactions on a small peptide model of known structure.[7]

Larger peptides based on *de novo* design have also been synthesized in which metal ions are bound by natural and/or modified amino acid residues within α-helix bundles.[8] As with the zinc finger sequence, conserved residues are found in peptide helical structures, and re-design of these sequences in locations that are not essential to the helical structure allows substitution with non-natural amino acid derivatives. Protein engineering, based on these protein structures, has lead to the self-assembly of these protein helices into bundles, formed by strategic incorporation of hydrophilic residues and hydrophobic residues on directed faces of the helical structure. Thus, strategic incorporation of metal-binding derivatives on these known bundle structures can provide a probe of the protein structure, and the potential to study metal-protein, and metal-metal interactions on the structure of a designer protein.

Sollazzo and coworkers have created a zinc binding site within a "minibody" structure analogous to a portion of an antibody V_H domain.[9] This type of engineering is similar to the peptide synthesis approaches in that a conserved segment of antibody structure is re-designed. However, the sequence modifications in this study are made *in vivo* via gene transcription/translation of an antibody fragment, engineered to bind zinc via a short peptide loop in two proximal domains of the minibody structure.

Metalloprotein design has often utilized pre-existing clefts within a protein of known structure. Studies by Lu and coworkers have produced both Cu and Mn containing metalloproteins, which display similar physical properties to naturally occurring metalloenzymes.[10] This represents the next step in metalloprotein synthesis by constructing metal sites with the ability to perform directed functions. These constructs

by Lu and coworkers produced metal-binding proteins that have physical characteristics analogous to metalloenzymes, however their function was not defined.

Hellinga and coworkers have developed the molecular modeling program "Dezymer" that searches three-dimensional protein structures for geometric clefts suitable for metal incorporation.[11] This approach represents a more general approach to metal incorporation by searching an entire protein structure for suitable clefts for metal coordination. Utilizing this program, Caradonna and coworkers have prepared a cuboidal Fe_4-S_4 site, and a Fe-histidine site within thioredoxin mutants.[12] In addition, Hellinga and coworkers subsequently prepared a tetrahedral blue copper site and a tetrahedral Fe-S_4 site within thioredoxin mutants.[13] However, this approach of searching for the best three-dimensional space for metal-binding is limited, at the very least, by the number of proteins that have been structurally characterized.

Our research efforts attempt to contribute to in this emerging field through the development of a novel approach to metalloprotein design.

1.3 HYPOTHESIS

We hypothesize that phosphate-binding sites represent a structural motif that can be readily converted to form a metal-binding site. If successful, this will provide a more general method for incorporating metals into proteins due to the ubiquity of phosphate-binding sites in nature. It also focuses design efforts on a more specific set of templates, phosphate-binding sites, thereby greatly reducing the number of variables.

1.4 SCOPE OF THIS RESEARCH

We will test the "phosphate-to-metal binding site" hypothesis by attempting to prepare a known metal binding site (the target) using a phosphate-binding site as the scaffold. The experimental details of this work are presented in Chapter 2. Chapter 3 details the criteria we have used for choosing a target metalloenzyme site and the phosphate-binding protein to be converted into the target. The genetic manipulations used to convert the scaffold into the target are discussed in Chapter 4. We will discuss the steps taken to create the constructs of both native and mutant proteins, and provide results showing the success of these methods. The expression of these genetic constructs to provide the proteins is presented in Chapter 5. Chapter 6 focuses on the inorganic aspects of these research efforts. Here we will explore the ability of our mutant proteins to coordinate metal ions in a manner analogous to the target metalloprotein. Chapter 7 summarizes the results and draws conclusions regarding the correctness of our hypothesis and the potential for this approach in the preparation of designer metalloenzymes.

1.5 References

[1] Schultz, P. G.; Lerner, R. A. *Acc. Chem. Res*, **1993**, *26*, 391-395.
[2] Smith, C.K.; Regan, L. *Acc. Chem. Res.* **1997**, *30*, 153-161.
[3] Regan, L. *Trends Biochem. Sci.* **1995**, *20*, 280-284.
[4] Hengen, P. N. *Trends Biochem. Sci.* **1995**, *20*, 285-286.
[5] Cheng, R. P.; Fisher, S. L.,; Imperiali, B. *J. Am. Chem. Soc.* **1996**, *118*, 11349-11356.
[6] Struthers, M. D.; Cheng, R. P.; Imperiali, B. *J. Am. Chem. Soc.* **1996**, *118*, 3073-3081.
[7] Cheng, R. P.; Fisher, S. L.; Imperiali, B. *J. Am. Chem. Soc.* **1996**, *118*, 11349-11356.
[8] Mutz, M. W.; Case, M. A.; Wishart, J. F.; Ghadiri, M. R.; McLendon, G. L. *J. Am. Chem. Soc.* **1999**, *121*, 858-859.
[9] Pessi, A.; Bianchi, E.; Crameri, A.; Venturini, S.; Tramontano, A.; Sollazzo, M. *Nature* **1993**, *362*, 367-369.

[10] Hay, M.; Richards, J. H.; Lu, Y. *Proc. Natl. Acad. Sci.* **1996**, *93*, 461-464. Yeung, B. K.; Wang, X.; Sigman, J. A.; Petillo, P. A.; Lu, Y. *Chem. & Bio.* **1997**, *4*, 215-221.

[11] Hellinga, H. W.; and Richards, F. M. *J. Mol. Biol.* **1991**, *222*, 763-785.

[12] Pinto, A. L.; Hellinga, H. W., and Caradonna, J. P. *Proc Natl. Acad. Sci.* **1997**, *94*, 5562-5567. Coldren, C. D., Hellinga, H. W., and Caradonna, J. P. Proc Natl. Acad. Sci. 1997, 94, 6635-6640.

[13] Hellinga, H. W. *J. Am. Chem. Soc.* **1998**, *120*, 10055-10066. Benson, D. E.; Wisz, M. S.; Liu, W.; Hellinga, H. W. *Biochemistry* **1998**, *37*, 7070-7076.

Chapter 2

EXPERIMENTAL PROCUDURES

2.1 SUPPLIES AND MATERIALS

The reagents and materials are listed in Table 2-1

Table 2-1: Reagents, materials, and suppliers

Name	Suppliers
Acetone	Fisher
Acetonitrile (HPLC Grade)	Fisher
Acrylamide	Fisher
Agar, McConkey	Difco
Agarose	Fisher
Ammonium Acetate	Fisher
Ammonium Chloride	Fisher
Ammonium Persulfate	Fisher
ampicillin	Fisher
Ascorbic Acid	Sigma
BamHI	Boehringer Mannheim
Bis-Acrylamide	Fisher
Brilliant Blue Coomasie G-250	Fisher
Bromophenol Blue	Fisher
Calcium Chloride	Sigma
Catechol	Sigma
Centriprep-10	Amicon
Centricon-10	Amicon
Chloramphenicol	Sigma
Chloroform	Fisher
CM Sephadex C-25	Sigma
Copper Sulfate	Fisher
D_2O	Cambridge Laboratories
Dialysis Tubing (Snakeskin) 10,000 MWCO	Acros
Dialysis Tubing (Cellulose) 10,000 MWCO	Fisher
2,2-Dimethyl Glutaric Acid	Acros
DIG® Starter Kit	Boehringer Mannheim
DNA Ligase	Boehringer Mannheim
DNA Molecular Weight Markers	Promega
dNTP's	Promega
Dithiothreitol	Sigma
Ethidium Bromide	Fisher
E. coli (BL21-(DE3))	Novagen
E. coli (BL21-(DE3)-pLysS)	Novagen

Table 2-1 cont…

E. coli (XL1-Blue-tet^R)	Hassan Lab
EcoRI	Boehringer Mannheim
Ethylene diamine tetraacetic acid	Sigma
Ethylene glutamine tetraacetic acid	Sigma
Ethyl Alcohol	Fisher
Ferric Chloride	Fisher
Ferrous Sulfate	Fisher
Filters (sterilization)	Millipore
Filters (Qualitative #3)	Fisher
Glacial Acetic Acid	Fisher
Glucose	Fisher
Glycerol	Sigma
HEPES Buffer	Sigma
HindIII	Boehringer Mannheim
Hydrochloric Acid	Fisher
IPTG	Fisher
Kanamycin Sulfate	Sigma
Magnesium Acetate	Sigma
Maleic Acid	Sigma
Magnesium Chloride	Promega
Manganese (II) Chloride	Fisher
2-Mercaptoethanol	Sigma
Methanol	Sigma
Mineral Oil	Sigma
Nde I	Boehringer Mannheim
Oligonucleotides	Genosys
o-nitrophenyl-β-D-galactopyranoside	Sigma
Ovine serum albumin	Sigma
pCal-n expression system	Stratagene
pET-9a	Novagen
pGem-3Z	Promega
pGem-T	Promega
p-nitrophenyl phosphate	Eastman Kodak
pNotA/T7 PCR Cloning System	5-prime 3-prime
Phenol (biological grade)	Fisher
phenylmethylsulfonylfluoride	Sigma
Phosphoenolpyruvate	Sigma
Polyethylene Glycol	Sigma
Potassium Ferricyanide	Fisher

Table 2-1 cont…

Potassium Permanganate	Sigma
2-Proponal	Fisher
Protein Molecular Weight markers	Promega, BIO-RAD
Proteinase K	Sigma
Protocatechuate	Sigma
Qiaex II gel purification system	Qiagen
Qiaprep plasmid purification system	Qiagen
Qiaquick purification system	Qiagen
RNAse One	Promega
Sac I	Boehringer Mannheim
Sca I	Promega
Sma I	Stratagene
SSP I	Stratagene
Sephadex G-50, G-100	Sigma
Shrimp Alkaline Phosphatase	Boehringer Mannheim
Sodium Acetate	Fisher
Sodium azide	Sigma
Sodium Carbonate	Fisher
Sodium Chloride	Fisher
Sodium Cyanide	Fisher
Sodium Dithiothionite	Matheson
Sodium dodecylsulfate	Fisher
Sodium Ethylene Diamine Tetraacetic Acid	Fisher
Sodium Hydroxide	Fisher
Sulfuric Acid	Fisher
Taq DNA polymerase	Boehringer Mannheim
TEMED	Fisher
Tetracycline (HCl)	Fisher
Thiamine (HCl)	Sigma
Tris Base	Fisher
Tris (HCl)	Fisher
Trypsin	Sigma
Tryptone	Fisher
Tween-20	Sigma
Urea	Fisher
X-gal	Fisher
Yeast Extract	Fisher

2.2 Equipment

Molecular Modeling procedures were performed on a Silicon Graphics Workstation in the Biochemistry Department at NCSU in the laboratory of Dr. Paul Agris. Visualization and modeling procedures were carried out with Molecular Simulations InsightII modeling software package utilizing its builder, biopolymer, discover and discover3 modules.

Agarose gel electrophoresis analysis of DNA fragments was performed on a Fisher Biotech FB-SB-710 mini-horizontal unit purchased from Fisher Scientific. The power supply was an E-C 105 model purchased from E-C Apparatus Corporation.

Sodium Dodecyl-Sulfate Polyacrylamide Gel Electrophoresis (SDS-PAGE) was performed on an E-C 120 mini-vertical gel box purchased from Fisher Scientific. All gels were run under denaturing conditions (in SDS). The E-C 105 power supply provided the voltage potential, and was typically maintained at a constant current of 30 mA for 45-90 minutes.

Gel documentation was performed with a camera and computer interface purchased from UVP. The software for capturing and saving the gel images was the Laboratory Imaging and Analysis System from UVP. This software also assisted in the quantitation of image intensities for concentration comparisons and counted bacterial colonies on solid media placed in petri-dishes.

Polymerase Chain Reactions (PCRs) and other reactions requiring temperature profiles were performed on a Perkin-Elmer Gene Amp 2400 thermocycler with a 0.5 mL

tube sample holding block and a heated lid. For PCR reactions, no oil was applied, and samples retained > 97% of their volume throughout a 30 cycle reaction.

Centrifugations were performed with an Eppendorf 5417R, 5417C, or 5415C unit for samples of 2.0 mL or less. For larger samples, a Sorvall RC-5B centrifuge with the SS-34, GSA, or GS3 rotors was utilized, typically run between 4 ^{o}C and 15^{o}C.

Incubators utilized to grow bacterial cultures include: New Brunswick Scientific Co. Byrotory Water Bath Shaker, Queue Radial Shaker model 4730, Thelco 5DG Scientific Incubator. Typical shaking and growth experiments were performed at 125 rpm and 37 ^{o}C.

Shakers utilized for a variety of experiments included: Red Rotor PR70 shaker from Hoeffer Scientific Instruments, and Lab-Line Orbit 3527 shaker. Rocking procedures were performed on a Red Rocker PR50 rocker from Hoeffer Scientific Instruments.

The optical density of cultures was measured at 600 nm using a Novaspec model 4049 spectrophotometer in 0.8 mL cuvettes.

DNA quantitation using absorbance measurements at 260nm of (50 µl samples) was performed on a Cary spectrometer equipped with a micro cuvette holder**.** Estimates were made by either comparison with known concentration standards, or via estimation with the value of (50 ng DNA/(mL)). Both methods gave concentration values within 40 % of each other in most cases, which was sufficient for the methods utilized herein.

Protein chromatography was performed using a Bio-RAD Fraction Collector 4500D utilizing its drop counting mode of sample collection. Two different collection racks (5 cm and 10 cm) were used depending on the desired fraction size.

Ultraviolet-visible spectroscopy was performed on a Hewlett-Packard 8452A Diode Array spectrophotometer in a UV transparent 1.0 mL cuvette with pathlength of 10 mm. Spectra were taken in the general scanning mode, utilizing water or buffer as blank samples, and the region between 800 nm and 820 nm was set at the reference absorbance of 0.0 for all metal addition experiments.

Electron spin resonance (ESR) spectroscopy was performed using an IBM ER200D instrument operating at X-band ($\nu \sim 9.45$ GHz). Microwave frequency was measure with a Hewlett Packard 5350B frequency counter and the field at $g = 2.0037$ was calibrated with DPPH. Spectra at 77K were acquired using a quartz finger Dewar and cylindrical quartz sample tubes. Typical spectra were the average of five scans taken at rate of 100 seconds per scan.

Circular Dichroism measurements were made on a JASCO J600 spectrophotometer with a 10 mm cuvette. The temperature profiles were generated with an Isotemp temperature controller. Data were collected between 250 nm and 200 nm for each temperature.

Vanadium NMR was performed on a General Electric Omega 300 NMR instrument equipped with a 10 mm broad band probe and sample tube. Typical scans were recorded in water with a sweep width of 90,000 Hz, at a frequency of 79.0 MHz,

gain between 1000 and 3000, and obtaining ~10,000 scans per spectrum. Spectra were referenced to external VOCl3 and the baseline was corrected by subtraction of a blank.

2.3 Polymerase chain reaction protocols are as follows:

A. To a 0.5 mL thin-walled microcentrifuge tube were added, 1 ng of template DNA, 10 μl of 10 mM primers (upstream and downstream), 10 μl of 10X Taq buffer, 2 μl of 5 μM dNTPs, and deionized water to a make a final reaction volume of 99 μl.

B. The reaction was placed in the thermocycler and the "hot start" cycle was initiated as follows: template and primer denaturation at 99^{o}C for 10 minutes, annealing of primers to template at T_m (typically 55^{o}C) for 1 minute, then movement to the optimal temperature for Taq DNA polymerase activity at 72^{o}C for 1 minute.

C. At the initiation of the 72^{o}C step, the program is held until all samples have been treated with 1 μl of Taq DNA polymerase. This minimizes the polymerase degradation during the initial 10 minute denaturation step. This completes the "hot start" cycle.

D. Twenty-five to thirty cycles are performed with 1 minute denaturations at 93 ^{o}C (the lower denaturation temperature minimizes the activity loss of the Taq enzyme), followed by equilibration at T_m for 1minute, and finally extension at 72 ^{o}C for 1 minute.

E. After completion of the last cycle, the reaction was cooled to 4 ^{o}C for storage and subsequent analysis.

2.4 Enzymatic Modification of DNA Protocols

A. Restriction endonuclease digestion were typically performed by combination of 1-5 μg of DNA to be cleaved, 2 μL of 10X digest buffer, deionized water to a final reaction volume of 18 or 19 mL (depending on single or double digest), and finally 1 μL of restriction endonuclease (1μL of each if a double digest). The reaction was placed in a 37^{o}C water bath for 2 –16 hours, depending on the star activity (non-specific cleavage activity) of the enzyme. Reactions are then cooled to 4^{o}C for storage and subsequent characterization.

B. Vector DNA dephosphorylation was accomplished as follows: 1-5 μg of digested, purified vector DNA (see below), 1 μL of 10X dephosphorylation buffer, and water to a final volume of 9 μL were combined, and treated with 1 μL of shrimp alkaline phosphatase. The reaction is run for 30 minutes at room temperature, and cooled to 4^{o}C for storage and subsequent analysis. Prior to dephosphorylation, cleaved vector was prepared by purification with the Qiaquick system or the QiaexII system (described in section 2.7 C and D).

C. Ligations of vector and insert DNAs were performed using a variety of methods. The following description illustrates a typical set of reactions. Vector-to-insert molar ratios of 1:1, 1:3, and 1:5 were utilized to optimize our conditions for ligation. A typical 1:1 reaction was performed by the combination of 100 ng of

cut, dephosphorylated vector, 1 equivalent of insert DNA (for a 300 bp insert, we would apply 5.3 ng), 1 μL of 10X ligation buffer, water to a final volume of 9 μl, and followed by addition after the 1st annealing step of 1 μL of T4 DNA ligase. After incubation at 17 ^{o}C for ~16 hours, the sample was cooled to 4^{o}C for storage and subsequent analysis and/or transformation.

2.5 Agarose Gel Electrophoresis

Agarose gel electrophoresis was performed on all of the above DNA manipulations. Typical experiments employed a constant voltage of approximately 75 V, with typical currents produced near 30 mA, for 30-45 minutes. Both Tris-Borate-EDTA and Tris-Acetate-EDTA buffers were utilized as conductive electrolytes at pH = 7.0 (typical) under standard concentrations. Agarose gels were stained with ethidium bromide and the intercalated fluorophore was exposed to UV light from a UVP (Ultra-Violet Products®) transilluminator. Typical gel setup and analysis was performed as follows. First, a 1% solution of agarose in gel buffer (TAE) is made to a final volume of 50 mL. This solution was placed in a microwave oven for 3 minutes to heat the water and melt the agarose. This solution was cooled to approximately 40 ^{o}C, and 2 mL of 0.1 % ethidium bromide was added, mixed thoroughly, then placed in the gel box along with a 10 well comb, and allowed to solidify and cool to room temperature. Once solid, the gel was submerged in approximately 200 mL of TAE buffer, and the samples were loaded into the wells and a voltage of 75 V is

then placed on the gel box. The DNA begins to migrate toward the anode through the gel matrix, which differentiates the DNA fragments by size. Comparison with a molecular weight marker was used to estimate fragment sizes.

2.6 DNA Transformation Protocols

A. Preparation of competent E. coli cells using $CaCl_2$ was achieved in a manner analogous to the method described in Current Protocols in Molecular Biology.[1] Typical preparations were performed as follows. First, bacterial cultures of the desired strain were grown overnight, then subcultured into 100 mL of fresh media. This culture was shaken and incubated at 37^{o}C for 3-4 hours until the cultures optical density at 600 nm is between 0.3 and 0.5 absorbance units. The culture was then immediately chilled on ice for 30 minutes. After centrifugation at 5,000xG for 10 minutes, the supernatant was removed and discarded, and the wet paste was resuspended in 10 mL of sterile 0.1 M $CaCl_2$ and equilibrated for 30 minutes. This process was repeated once more, and the final pellet was resuspended in 1.0 mL of a solution of 0.1 M $CaCl_2$ and 40 % glycerol. Aliquots were placed in sterile 1.5 mL microcentrifuge tubes for transformation.

The transformation protocol is as follows: target DNA (100 ng) was added to the prepared cells and chilled for 30 minutes on ice. The mixture was heat shocked for 90 seconds at 42 ^{o}C, followed by rapid addition of 1.0 mL of

fresh media, cooling on ice, and recovery at 37 ^{o}C for 45 minutes. The cells were then ready to be plated out on selective media.

B. Preparation of competent E. coli cells by electroporation followed the procedure in Current Protocols in Molecular Biology with minor changes.[2] A culture of the desired stain was grown overnight, and subcultured into 1 L of fresh media. At a culture density of OD600 from 0.3-0.6, the bacteria were placed on ice and cooled for 30 minutes. The cells were centrifuged at 3000xG for 10 minutes and resuspended in 500 mL of fresh, sterile water. This process was repeated twice to lower the ionic strength of the bacterial solution, and the final pellet was resuspended in 10 mL of water. These cells were aliquoted into 1.5 mL tubes, for electroporation or were frozen for future usage.

DNA was added to the prepared cell aliquots, and gently mixed. The solution was placed in an electroporation cuvette, and a voltage of 2.5 V was applied to open small pores in the bacterial cell walls, thereby allowing the target DNA to migrate into the cells. One mL of sterile media was immediately added to the cells, and they are allowed to recover at 37^{o}C for 30 minutes before plating out on selective media.

2.7 Plasmid Purification Protocols

A. Qiagen mini-prep kits were used to isolate plasmid DNA from cultures derived from a single colony forming unit. Minor modifications to the protocol provided

with the kit included, culture sizes, centrifugation times and speeds, and elution conditions.[3]

B. Qiagen midi-prep kits were utilized to prepare large quantities of DNA using the recommended protocol provided.[4]

C. Qiagen PCR-prep kits were utilized to purify PCR product DNA from the other reaction components with modified elution conditions.[5]

D. QiaexII gel purification kits were used to purify DNA from agarose gel slices with some modification to the drying and elution steps.[6]

2.8 PCR products were subcloned into pNoTA/T7 using the supplier's instructions without modification.[7]

2.9 DIG colony hybridization screening of putative clones used the following procedure.[8]

A. The first step in the DIG technique is the generation of the DNA probe by denaturing the template DNA and then adding 4 μL of the DIG High Prime reagent and incubating the reaction at 37 ^{o}C overnight. This usually resulted in > 1 μg of probe DNA.

B. Nylon membranes were placed on the test and control plates for 1-2 minutes, and marked for orientation and plate identification. The membranes were treated for 10-15 minutes each in glass dishes containing wetted 3M Whatman paper soaked in denaturant, neutralization solution, and SSC buffer.

C. DNA control spots were placed on the membranes, and the membrane was crosslinked with UV light for 2 minutes. Proteinase K was added to the membranes and incubated for 1 hour at 37^{o}C. Then the cellular debris was removed from the membranes with wet Whatman paper by pressing down and rolling a reagent bottle over a stack comprising of aluminum foil, Whatman paper, membrane, Whatman paper, and aluminum foil (from bottom to top).

D. The clean membranes were sealed in a bag with 10 mL of hybridization solution containing denatured probe DNA and shaken at 65^{o}C overnight.

E. Detection of the DNA-bound using the supplier's instructions with one modification. The DIG substrate was added to the membranes, sealed in a water tight bag, and then incubated at 37 ^{o}C for 1 hour. Subsequently, the chemiluminescent film was placed above the bag, and exposed overnight.

2.10 DNA sequencing was performed at either the North Carolina State University DNA Sequencing Facility, or at the Iowa State University DNA Sequencing Facility, "In house" primers appropriate for the vector DNA sequence from each facility were used unless otherwise indicated.

2.11 Reagent solutions

A. Media

All media utilized in these studies were Lauria-Broth (LB) solutions containing 10 mg of tryptone, 5 mg of yeast extract, and 10 mg of NaCl per liter of solution.

These solutions were autoclaved for 30 minutes to 1 hour and cooled to 37 ^{o}C prior to addition of antibiotics.

B. Buffers

Several buffer solutions were utilized during these experiments.

CABB400: 2 mM $CaCl_2$, 50 mM Tris-HCl, 400 mM NaCl brought to a pH = 8.0

EB400: 2 mM EGTA, 50 mM Tris-HCl, 400 mM NaCl brought to a pH = 8.0

Tris Dialysis Buffer: 20 mM Tris-HCl, 20 mM NaCl brought to a pH = 8.0

HEPES Dialysis Buffer: 20 mM HEPES, 20 mM NaCl brought to a pH = 8.0

DMG Dialysis Buffer: 20 mM DMG 20 mM NaCl brought to a pH = 8.0

Acetate Dialysis Buffer: 20 mM $NaC_2H_3O_2$, 20 mM NaCl brought to pH = 4.8

Thrombin Digest Buffer: 2.5 mM $CaCl_2$, 20 mM Tris-HCl, 50 mM NaCl brought to a pH = 8.0

Phosphate Buffer: 20 mM Na_2PO_4, 20 mM NaCl brought to pH = 8.0

C. Metal solutions

Iron (III): 10 mM iron (III) chloride dissolved in 0.1 M HCl

Iron (II): 10 mM iron (II) sulfate in deionized water

Copper (II): 10 mM copper (II) sulfate in water

Manganese (II): 10 mM manganese (II) nitrate in water

Vanadium (IV): 10 mM vanadyl sulfate in water

Vanadium (V): 10 mM sodium orthovanadate in water for 1 week

D. Other reagents

PCA: 5 mM 3,4 dihidroxybenzoic acid in appropriate buffer

$K_3Fe(CN)_6$: 10 mM $K_3Fe(CN)_6$ in water

H_2O_2: 10 mM hydrogen peroxide in water

BME: β-mercaptoethanol added directly into from pure stock as needed

DTT: sodium dithiothreitol stock at 100 mM in water

2.12 Protein concentration determination

A. Biuret assays were performed as described in Protein Methods without further modification.[9]

B. Hartree-Lowry assays were performed as described in Current Protocols in Protein Science.[10]

C. A_{280} measurements were performed on an HP 8542 diode array spectrometer, and were used to determine protein concentrations of pure protein samples for which the E280 was known or determined. For HPr ε = 0.71 (mg/mL), HPrγ ε = 0.81 (mg/mL), and for HPrβ ε = 0.77 (mg/mL).

2.13 SDS-PAGE analyses were accomplished using a three gel method designed for examining small proteins and performed as follows:

1. Solutions of acrylamide stock (48% acrylamide/1.5% bisacrylamide), gel buffer (3 M Tris, 0.3% SDS pH=8.45), 80% glycerol, 10% APS and TEMED were acquired or prepared.

2. The resolving gel and spacing gels were simultaneously prepared as follows: The resolving gel was prepared with 5.0 m/mL of acrylamide stock, 5.0 mL of gel buffer, 2.5 mL of deionized water, 2.5 mL of glycerol solution, 75 μL of APS, and 7.5 μL of TEMED. The spacing gel contains 1.25 mL of acrylamide stock, 2.0 mL of gel buffer, 2.75 mL of deionized water, 0 mL of glycerol solution, 30 μL of APS, and 3.0 μL of TEMED.
3. Approximately 4 mL of resolving gel is poured between clean, dry glass plates, followed by about 0.75 mL of spacing gel prepared solution. A thin (50 μL) layer was applied to the top of the spacing gel to create a smooth interface, and the gels are allowed to polymerize.
4. The stacking gel is then prepared with 1.0 mL of acrylamide stock, 3.1 mL of gel buffer, 8.4 mL of deionized water, 0 mL of glycerol solution, 100 μL of APS, and 10 μL of TEMED. This solution is poured onto the solidified spacing gel, and a 10 well comb (typical) is inserted.

Once solidified, the gel was placed into the EC 120 apparatus and a voltage is applied to deliver a constant current of approximately 30 mA. Upon completion of the electrophoresis run, the gels were removed and stained with R-250 Coomassie Blue Staining solution (50% MeOH, 10% $HC_2H_3O_2$, and 0.25% R-250) for 1 hour. Destaining in 10% MeOH and 5% $HC_2H_3O_2$ was performed overnight to remove unbound Coomasie stain, and the gel was photographed under a white light source with the UVP equipment.

2.14 Protein expression of native and mutant proteins was typically initiated by inoculation of 10 ml of LB/Amp (50 μg/ml) media with 10 μl of bacterial frozen stock and growth overnight at 37^{o}C. From this culture, a 50 μl aliquot was removed, and added to 100 ml of fresh LB. At a growth level with an optical density at 600 nm of 0.6, the culture was treated with IPTG to a final concentration of 1.0 mM. This growth level typically took 3.5 - 4.0 hours to attain. The culture was allowed to grow under inducing conditions for an additional 4 hours then chilled to 4^{o}C. The chilled bacterial cells were centrifuged at 10,000 g for 10 minutes, and the wet paste was resuspended in 2.5 ml (1/25 volume of the culture) calcium binding buffer containing 50 mM NaCl (CABB-50). This expression was scaled up by factors of 10 and 20 depending on the preparation.

2.15 Four methods Bacterial cell lysis were utilized including Lamelli solution lysis, French Pressure lysis, Sonication lysis, and Bead Beating lysis.

A. Lamelli lysis was performed by addition of 3X Lamelli solution to resuspended bacterial cells to a final concentration of 1X. Then the mixture was placed in boiling water for 10 minutes, and the cellular debris was spun down at 10,000xG for 10 minutes.

B. French Pressure lysis was performed in a 40 mL Aminco French Pressure Cell. Concentrated cell resuspensions were loaded into the piston chamber, and the cell was subjected to 5 minutes of constant internal pressure of 10,000 PSI. Then, maintaining a constant pressure, the pressure valve was slowly opened, and the

bacterial solution was aspirated out of the cell to rupture the bacterial walls. This process was repeated 3 times for each 40 ml of concentrated, resuspended bacteria.

C. Sonication procedures were modeled after the protocols outlined in Maniatis.[11] In our lyses, we utilized a probe-type sonicator with the following protocol. First, we froze the concentrated, resuspended bacteria at –80 ^{o}C for 1 hour. Upon thawing, we placed the cells in a 15 mL Falcon tube, and started the sonicator at a setting of 300 mA for 1 minute, then chilled the tube on ice for 2 minutes. This process was repeated 4-6 times to achieve complete lysis.

D. Bead beating lysis was applied to the *S. aureas* strain donated by Dr. Wolfgang Hengstenberg for the complementation assays. This is the most efficient method, in our hands, for the lysis of this S797A strain. The method involves addition of approximately 100 µl of glass beads to a microcentrifuge tube along with 1 mL of concentrated, resuspended bacterial cells. The tube(s) are then vortexed briefly, and placed in a sample holder positioned at the top of a mechanical piston. Once secured, the sample is rapidly shaken by the action of the oscillating piston. After 2 minutes of beating, the samples are placed on ice for 2 minutes, then reinserted in the sample holder for another 2-3 passages. Once complete, the cell free extract was centrifuged away from the glass beads and cellular debris at 14,000 rpm for 10 minutes.

2.16 Protein purifications were accomplished on small and large scales with several protocols. Chapter 5 contains a general analysis of these procedures that can be summarized with the following general method.

A. Small Scale Purifications

Bacterial wet pastes were resuspended in CABB-50, then lysed with sonication, followed by centrifugation at 10,000*g for 20 minutes. These cell free extracts were then transferred to a microcentrifuge tube containing 50 μL of calmodulin affinity resin (CAR). The slurry was allowed to rock for one hour at 60 rocks per minute at 4 ^{o}C. The resin was spun down at 3000xG for 1 minute, then washed with 5 100 μL washings with CABB-50. Finally the resin was treated with 100 μL of elution buffer containing 50 mM NaCl (EB-50), spun down and the supernatant was removed for SDS-PAGE analysis.

B. Large-Scale purifications

1. Cell free extracts are clarified by centrifugation a 15,000xG for 20 minutes, and then shaken on ice with calmodulin affinity resin (amounts varied depending on scale and method employed) at 50 revolutions per minute for approximately 1 hour.
2. Slurries were separated by centrifugation (small scale) or column frits (large scale) to allow the unbound column “flow through” to be removed. Then the resin was washed with 10-20 column volumes of calcium binding buffer (CABB, variable components) to remove all unbound extract components.

3. The resin was eluted with 5-10 column volumes with elution buffer (EB, variable components), and the protein containing fractions were grouped and dialyzed for further analysis.

2.17 Metal binding studies were performed by careful additions of 10 mM metal solutions into 0.8 mL solutions of proteins from 70 μM to 200 μM. Additions were performed in a sequential manner with small changes in total solution volume from 0.5 to 5.0 metal equivalents corrected during analysis. After each metal addition, each sample was mixed thoroughly and allowed to equilibrate for 1 minute prior to recording the UV-Vis spectra.

2.18 EPR samples were taken directly from the UV-Vis titration samples with 5.0 equivalents of metal ion, and were recorded by averaging 5 scans over the window of interest at a scan time of 100 s.

2.19 HPr mutant complementation assays were performed utilizing the procedure developed by Dr. Wolfgang Hengstenberg and coworkers.[12] The *Staphyloccus aureus* strain (S797A) deficient in a functional ptsH gene (HPr's gene) was graciously donated by Dr. Hengstenberg. Cell free extracts of the S797A strain were generated by the bead beating lysis method as described in section 2.13. Aliquots of HPr were added to the cell free extract in the presence of 2.0 mmoles of phosphoenolpyruvate and 2.0 mmoles of o-nitrophenyl-β-D-galactoside.

Absorbance at 410 nm (ε = 6,000 $M^{-1}cm^{-1}$) was used to detect the formation of o-nitrophenol, indicating HPr phosphotransfer activity.

2.20 MALDI-TOF mass spectrometric analysis of protein samples was performed on a Bruker instrument (Proflex III) using stainless steel targets. The samples were prepared by addition of addition of 2 μl of protein (0.25-0.75 mg/mL) to 3 μL of solvent (2:1 H_2O:CH_3CN). This solution was then added to 5 μL of sinnapinic acid matrix, and 1 μL of this resultant mixture was spotted on the target and allowed to dry at room temperature.

2.21 CD data were obtained on native HPr, HPrγ, and HPrβ proteins dialyzed in 20 mM phosphate buffer at pH = 8.0 to provide the cleanest CD window. For A222 measurements, the proteins were diluted 1/15 (~ 3 μM) to allow adequate measurements down to 200 nm in a 10 mm cuvette. A280 measurements were recorded on 700 μM protein solutions due to the much weaker CD signal at 280 nm (tyrosine absorbance).

2.22 REFERENCES

[1] Ausubel, F.M. et al., eds 1991 Current Protocols in Molecular Biology method, Wiley Interscience, New York ppXX-XX.
[2] Ausubel, F.M. et al., eds 1991 Current Protocols in Molecular Biology method, Wiley Interscience, New York pp XX-XX.
[3] QIAprep purification system manual, 1997, Qiagen Ltd.

[4] Qiagen midi-prep purification system manual, 1994, Qiagen Ltd.
[5] QIAquick purification system manual, 1997, Qiagen Ltd.
[6] QiaexII gel extraction purification system manual, 1996, Qiagen Ltd.
[7] PCR Cloner system manual, 1997, 5-prime 3-prime Inc.
[8] Miltenburg R. v. et al. eds. 1995 *The DIG System User's Guide for Filter Hybridization*, Boehringer Mannheim GmbH, Biochemica, Germany
[9] Bollag, D. M.; Rozycki, M. D.; Edelstein, S. J. *Protein Methods*, 2nd ed, 1996, Wiley-Liss, Inc. New York.pp 76-79.
[10] Pain, R. Current protocols in Protein Science, 1996, Wiley & Sons, Inc. pp. 7.61-7.6.23
[11]Sambrook, J. et. al. eds (1989) *Molecular cloning: a laboratory manual*, 2nd ed., Cold Spring Harbor Laboratory Press, Cold Spring Harbor.
[12] Hengstenberg, W.; Penberthy, W. K.; Hill, K. L.; Morse, M. L. *J. Bacteriol*. **1969**, *99*, 383-388

Chapter 3

TARGET DEVELOPMENT & PROTEIN RE-DESIGN

3.1 INTRODUCTION

To test our hypothesis that pre-existing phosphate-binding sites can serve as generalized scaffolds for the construction of metal-binding sites, we needed to attempt the conversion, and characterize its success. Phosphate sites in biology typically bind one to three phosphates within their structures through hydrogen bonding interactions, or covalent attachment to specific amino acid side chains.[1] This variety affords us the opportunity to create mononuclear or polynuclear metal sites analogous to the parent scaffold. For our initial studies we have focused on the creation of a mononuclear site. This approach represents the simplest system we can generate. Experimental results from this system can subsequently provide a foundation to expand to more complex design strategies. Thus our first step in testing our hypothesis is to choose a mononuclear phosphate-binding protein, and attempt to strategically convert its active site to a metal-binding site.

3.2 PHOSPHATE-BINDING TEMPLATE

Our initial design strategy entailed defining a set of criteria for the scaffold protein we believe are essential to effectively evaluate our hypothesis. Through these criteria, we chose the Histidine-containing phosphocarrier protein (HPr) from the *Bacillus subtilis* organism as our template protein. This section will delineate these criteria, and demonstrate the rationale behind our choice of HPr from *Bacillus Subtilis* to test our hypothesis.

First criterion -- the template protein should contain an active site, that binds mononuclear phosphate ions instead of polynuclear phosphate ions. This will minimize the potential number of variables (numbers of ligands, metals, potential coordination geometries etc…) in the design strategy, and allow a more direct correlation between the physical characteristics observed and the structural properties of the active site. Our choice of HPr fits this criterion because its natural mode of action is to transfer

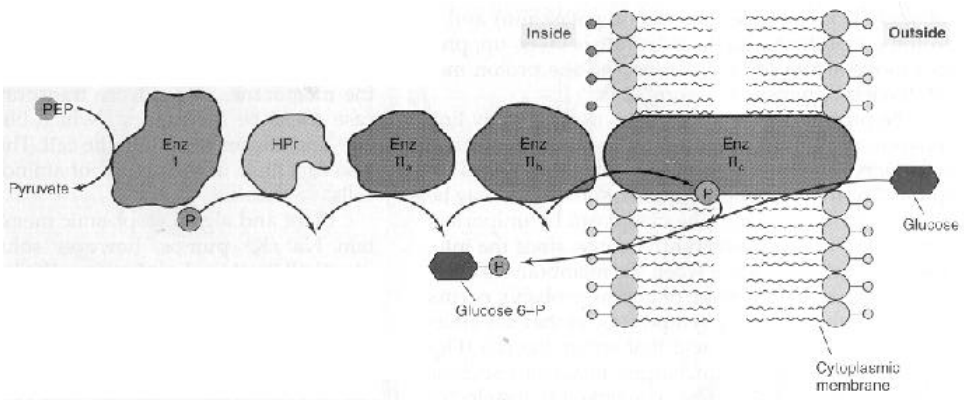

Figure 3-1: Generalized mechanism of the phosphoenolpyruvate phosphotransferase system depicting the role of HPr in the transport of specific sugars across cellular membranes in *E. coli*..

a single phosphate ion from Enzyme I to Enzyme II (Enzyme III in *B. subtilis*) in the phosphoenolpyruvate phosphotransferase system (PEP-PTS).[2] Figure 3-1 illustrates the role of HPr in sugar translocation within the PEP-PTS.[3] HPr itself is not an enzyme, but a cytoplasmic protein that can be phosphorylated by Enzyme I, and dephosphorylated by Enzyme II. Both Enzyme I and HPr are non-specific components in that they participate in all phosphotransferase reactions regardless of specific sugar involved. HPr's interaction with phosphate has been demonstrated to be a covalent attachment of a single phosphate ion to the N-1 nitrogen of a histidine residue within the phosphate-binding

site.[4] This histidine residue is universally conserved within all organisms utilizing the PEP-PTS, thus demonstrating its critical role in HPr function.[5] In summary, HPr contains a mononuclear phosphate-binding site, which makes it a suitable choice of template to test our hypothesis. Although polynuclear phosphate-binding proteins such as those in the Ras family of NTP hydrolysis enzymes could provide useful scaffolds for *polymetallic* proteins, we have chosen to test our hypothesis with the simplest case, and HPr meets this requirement.

Second criterion -- the phosphate-binding protein should be structurally characterized. This is critical to allow us to design our experiments. By visualizing the three-dimensional structure of the template protein, we can evaluate the possibilities of protein mutation and the potential metal coordination afforded within those mutants. Structural knowledge is also important to evaluate the experimental results. Knowledge of the local and global environment around the potential metal-binding sites can often provide an explanation of experimental results. In addition, utilizing the structural information of the template protein, one can often anticipate potential problems associated with neighboring protein residues (metal coordinating side chains or hydrogen bonding interactions) or more global hindrances such as disulfide bonds, hydrophobic interactions, or ion channels. Clearly a structurally defined template is critical in testing our hypothesis and our choice of HPr from *B. Subtilis* fulfills this requirement. Both a three-dimensional X-ray crystal structure and a solution structure solved by two-dimensional NMR have been reported.[6,7]

The structures obtained from both the NMR and X-ray crystallographic studies are very similar, and informative. HPr is a monomeric protein of approximately 9,000 Daltons which is devoid of cysteine residues or disulfide bonds. Both of these characteristics are favorable for our experiments. The small size of HPr is extremely helpful because characterizations of the protein structure and spectroscopic analyses of its metal-binding properties are more readily evaluated with a smaller set of potential ligands. The strong solubility of HPr in conjunction with its small size enables the facile generation of high concentration HPr solutions and use fewer milligrams of protein to achieve them (high number of moles of HPr, relative to other, much larger proteins using fewer g/mL). In addition, the accuracy of mass determinations with mass spectrometry (MS) is enhanced since errors of 0.1% - 0.01% are typical for common MS techniques. This results in a typical error of 1 to 10 Da for a protein the size of HPr, which is accurate enough to identify the both mutation and metallation effects. The lack of disulfide bonds and cysteines is also extremely helpful because it negates the necessity of utilizing reducing agents such as β-mercaptoethanol or dithiothreitol in protein buffer solutions (which can often form metal complexes, and complicate the spectroscopic characterization of metal-binding). In addition, potential metal-cysteine interactions, which are common in naturally occurring proteins, are avoided by the fortuitous absence of cysteine residues in HPr. These structural observations taken together suggest that HPr has the potential to be an ideal template protein to evaluate our hypothesis.

Details of the HPr structure give a clear picture of the phosphate binding site, and the global geometry, which affords the protein scaffold the ability to carry out its

function. Figure 3-2 contains a ribbon diagram of HPr depicting the folding of the secondary and tertiary structure. The overall folding topology is an open-face β-sandwich with four antiparallel β-strands packed against three α-helices. The phosphate-binding site is located at the N-terminus of the first α-helix, and contains the universally conserved Histidine 15 residue. This imidazole side chain is located on the protein

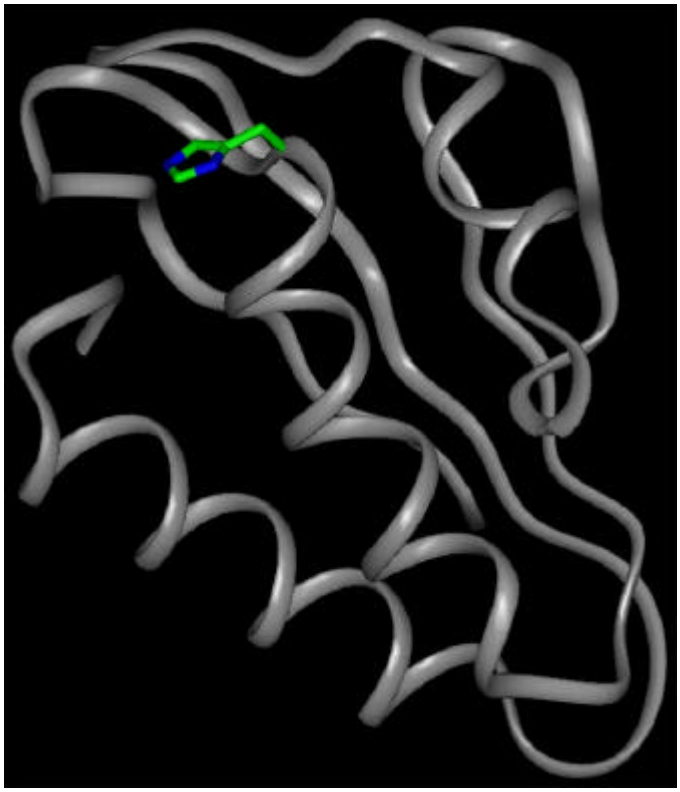

Figure 3-2: Ribbon diagram of the HPr structure from *B. subtilis*. Histidine 15 has been three dimensionally rendered, and is the universally conserved site of phosphorylation

surface, thus the phosphate-binding site is solvent accessible. A second residue, arginine 17, which is also highly conserved, has been demonstrated to be essential for phosphotransfer activity.[8] It is located adjacent to His-15, and in the crystal structure by Herzberg and coworkers, forms a salt bridge via a sulfate ion with His-15. They suggest

that the sulfate ion's association with these functionally essential residues implies that the crystal structure resemble the phosphorylated state of HPr.[6] Another key structural observation is the location of HPr's C-terminus. As with all known HPr proteins, the glutamate at residue 84 (*B. subtilis*) or 85 (*E. coli*) is spatially close to the histidine-

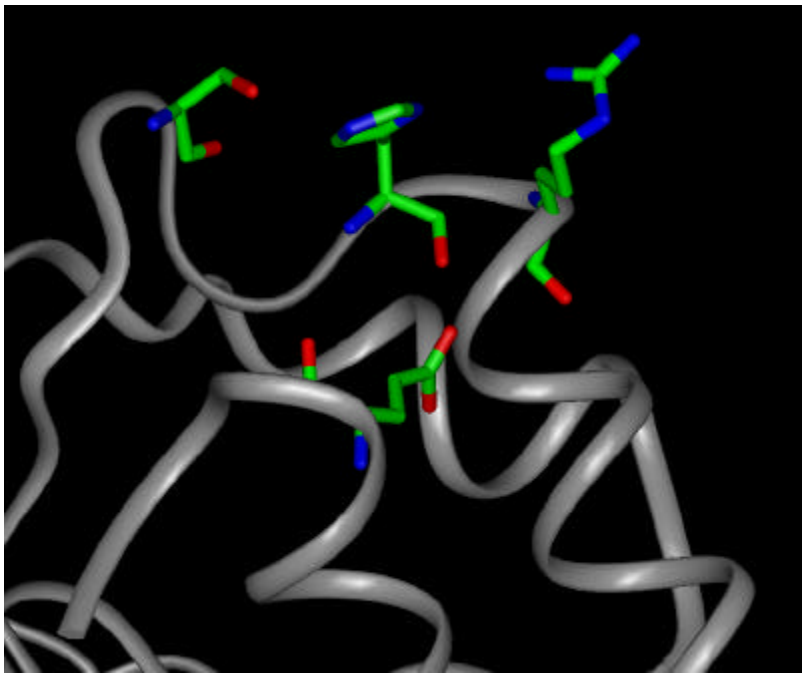

Figure 3-3: Native HPr structure depicting the phosphate binding pocket with rendered residues His-15, Arg-17, Ser-12, and Glu-84.

containing active site.[9] Curiously, deletions or mutations of this residue do not result in greatly diminished activity, thus it is suggested that perhaps its role is to stabilize the protein structure against denaturation.[9] Figure 3-3 illustrates a close-up view of the HPr active site, with functionally important residues rendered. Proline 18 is another residue which has been found to be a conserved of HPr proteins, and is critical to HPr function. Substitution of Pro-18 with alanine greatly diminishes HPr's activity. It is thought that the proline helps stabilize the phosphate-binding region at the helix terminus, and

facilitates structural integrity of the active site.[9] These and other structural observations give us a detailed insight into HPr's structural properties afford it the ability to transfer a single phosphate ion between two different enzymes. This information is essential for us to strategically modify the phosphate-binding site of HPr into a metal-binding site, and makes it an ideal candidate to test our hypothesis.

Third criterion – Our phosphate-binding template should have a quantifiable reactivity. This property is critical to determine the reactivity of our native protein, its mutants, and its metallo-adducts. First, by producing a native protein which is active, we demonstrate that our preparation of HPr was successful, and that it is folded in the proper form to allow natural reactivity with Enzyme I. In addition, by comparison of the native reactivity with that of the generated mutants and their metal-adducts, we can show the effects of our mutations and metallation on the native function. In our studies we plan to utilize the mutant complementation assay developed by Dr. Wolfgang Hengstenberg and coworkers. This assay produces colorimetric data to rapidly evaluate the functional integrity of the tested protein. Thus the activity of HPr can be monitored, which meets our third criterion for our scaffold phosphate-binding protein.

Fourth criterion -- The gene sequence for the phosphate-binding protein has been isolated and available. One of the most difficult steps in the genetic manipulation of a target gene is isolation of the native gene sequence from the target organism. This can often take years to accomplish, thus we wanted to choose a phosphate-binding protein in which the gene has been previously isolated. HPr has been extensively examined, and several genes from both gram-positive and gram-negative organisms have

been isolated, sequenced, and cloned. We contacted Dr. Jonathon Reizer at the University of San Diego in La Jolla California, and he graciously agreed to donate the isolated gene from the *B. subtilis* organism. This meets our fourth and final requirement of genetic availability, and greatly reduces the difficulty of generating the recombinant phosphate-binding protein and its mutants

From the above, it is clear that HPr satisfies the desired criteria for our scaffold phosphate-binding protein, and thus appears ideal as a template to test our hypothesis.

3.3 SELECTION OF A TARGET SITE

Another step in the design process is to select a target metalloprotein site as an idealized goal for the transformation of our phosphate-binding protein. Successful conversion of a phosphate site into this target metal site would both establish the validity of our hypothesis and serve as a building block for future research. We defined a set of criteria for this target metal site we felt were important, and would give us the best opportunity to synthesize and characterize the desired complex. In this section, we will outline these criteria, and for each, demonstrate why we chose the iron complex found in the active site of protocatechuate 3,4 dioxygenase (PCD) to test our hypothesis.

First criterion -- The target metal site contains a single metal that is covalently coordinated directly to the protein residues. This is the simplest case imaginable of direct metal coordination to the protein, thus it minimizes the potential number of structural variables for both the design and synthesis processes. PCD satisfies this criterion because it contains a mononuclear iron (III) ion within its active site, which

is directly coordinated to the amino acid residues of the enzyme. Figure 3-4 illustrates a structural model of the PCD metalloenzyme solved by X-ray crystallography.[10]

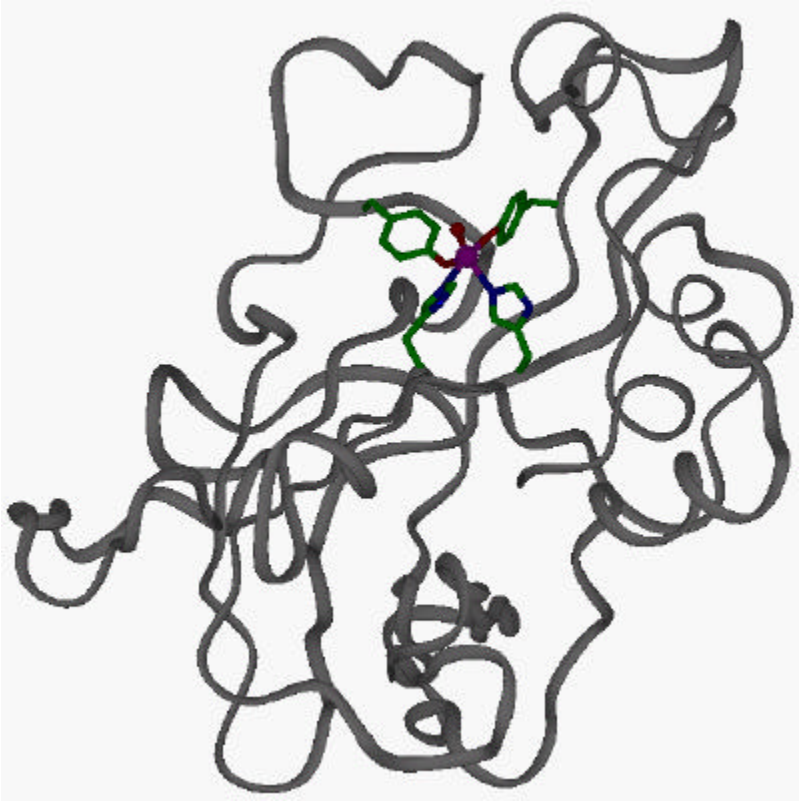

Figure 3-4: Structural model of a PCD β-subunit containing an highlighted Fe^{3+} active site. Notice the coordinating ligands (2-Tyr, 2-His) and a solvent exchangeable H_2O. Arg 457 (not shown) is poised above the tyrosine residues and has been also been implicated in the reaction mechanism

Second criterion – The target should originate from a naturally occurring metalloenzyme that has functional importance. With our ultimate goal of developing a systematic strategy for the preparation of *designer metalloenzymes*, it is important that we choose a target metal site derived from a metalloenzyme. This will afford us the opportunity to prepare a functional metal binding site within our formerly

non-reactive phosphate binding protein. If we can successfully prepare this metal site, we can accomplish several goals.

- We validate our hypothesis.
- We evaluate the minimum requirements for reactivity and substrate specificity of our target. It is important to test the critical factors involved in substrate specificity so that we may engineer this ability within our designer metalloenzymes. Our successful preparation of an active metalloenzyme could be accompanied with a lack of substrate specificity, which, although a negative result, could provide valuable insight into the fundamental factors for its incorporation. Our choice of PCD certainly fits this criterion because it is an active metalloenzyme that has been demonstrated to be substrate specific for the protocatechuate molecule.
- We will have generated a synthetic metalloenzyme that has functional/industrial applications. PCD is naturally occurring metalloenzyme that catalyzes the specific breakdown of the aromatic molecule protocatechuate (Figure 3-5). This reaction is one of the evolved pathways for the breakdown of aromatic hydrocarbons.

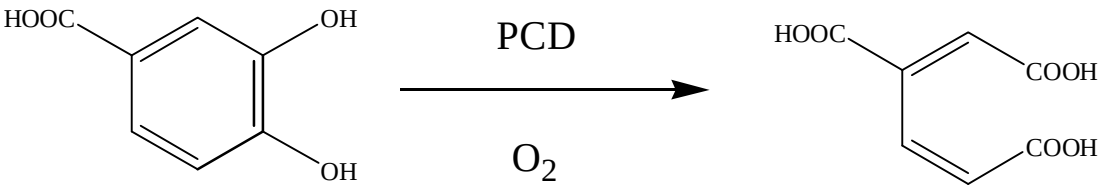

Figure 3-5: Chemical transformation catalyzed by protocatechuate 3,4 dioxygenase in atmospheric concentrations of oxygen.

Third criterion -- Our target metalloenzyme should be structurally characterized. The target metalloenzyme should have a structure that has been solved by physical methods to provide a physical (or virtual) model of the target site. Inspection and comparison of this target site, with the three-dimensional environment of our phosphate-binding protein cleft, allows for strategic re-design of the template into a target-type protein/ligand environment. PCD has been structurally solved by X-ray crystallography from the *Pseudomonas aeruginosa* organism.[11] This protein contains four structurally similar subunits; two α-type and two β-type. The β subunits contain catalytic iron centers as depicted in Figure 3-5. Figure 3-6 illustrates a view of the iron

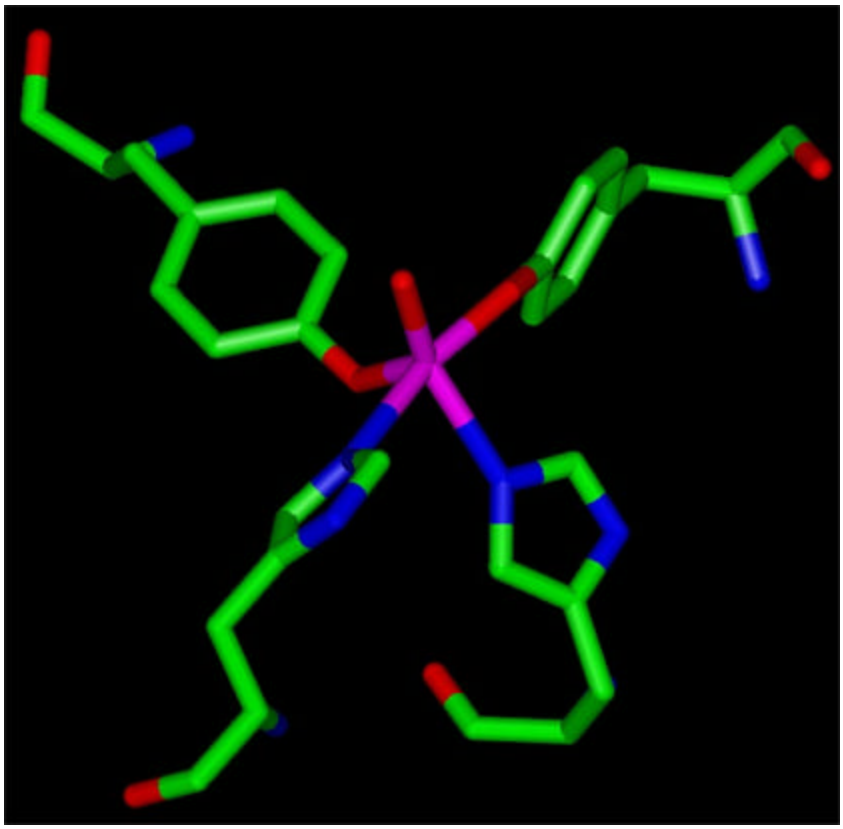

Figure 3-6: The active site of protocatechuate 3,4-dioxygenase from Pseudomonas aeruginosa. The iron center is coordinated directly to the protein via covalent bonds with two tyrosine and two histidine residues.

center. The iron ion is coordinated in a distorted trigonal bipyramidal geometry with four side-chains covalently coordinated to the iron center. In both the axial and equatorial positions, a phenolate (tyrosine) and imidazole (histidine) group are covalently coordinated to the iron, with the third equatorial position occupied by a solvent exchangeable water/hydroxide ion. Knowledge of these and other structural details of PCD satisfies our third criterion, and provides essential information to convert our phosphate-binding site into an iron site analogous to PCD.

Fourth criterion -- The target site should possess spectroscopic characteristics that can be monitored and correlated with the structural properties of the active-site geometry. This is an important feature because spectroscopic methods often allow non-destructive characterization of the physical properties. This allows for incremental perturbation of sample conditions and analysis at each step. PCD is a distinctive metalloenzyme in that it possesses several spectroscopic properties that can be readily monitored.

- It contains Fe (III)-phenolate coordination. This can be identified by an intense absorbance at 460 nm giving PCD its distinctive red-burgundy color. Thus successful synthesis of Fe (III)-tyrosine coordination should be readily observable. In addition, resonance Raman (RR) spectroscopy has been widely used to probe the vibrational profile of this coordination and confirm tyrosine coordination.

- PCD contains a paramagnetic iron nuclease in its active site that has been extensively examined by electron paramagnetic resonance spectroscopy to probe the environment of valence electrons of the iron center.

These and other physical probes such as Mossbauer spectroscopy, Resonance Raman spectroscopy, NMR of paramagnetically shifted protons, magnetic susceptibility, and stopped flow studies of reaction intermediates of PCD have been applied to PCD, and its distinctive characteristics should allow us to evaluate our effectiveness at creating an analogous site in our former phosphate site.

Fifth criterion -- The target metalloenzymes reactivity should be monitorable and mechanistically characterized. Upon successful generation of the target site within the former phosphate site, we would like to evaluate the catalytic reactivity of our designer metalloenzyme with respect to the target metalloenzyme performance. If full reactivity is observed, this is a significant accomplishment. However, if the reactivity of the target metalloenzyme is not achieved, it is important to understand why we missed the target. This knowledge could guide us to modify our approach to achieve our goal. PCD, due to its spectroscopically friendly iron center, has been extensively examined to determine the mechanism of action. Numerous substrate and inhibitor studies have been performed to demonstrate how PCD interacts with substrate, how it achieves its specificity, and how the dicarboxylic acid product is evolved.[12,13] This knowledge will be extremely helpful in evaluating the success of our attempts to create a designer metalloenzyme from a former phosphate-binding site. Clearly PCD meets this fifth criterion.

In summary, PCD is an extensively studied enzyme that has a mononuclear iron center, which is spectroscopically friendly. It is an important enzyme in nature, and has been mechanistically characterized. The combination of all these properties makes PCD an ideal choice for our target metalloenzyme. Thus, the metal-site structure of PCD will serve as an ultimate goal, a guide, and a measuring stick to test our hypothesis that phosphate-binding sites can be modified to serve as metal-binding sites.

3.4 RE-DESIGN OF HPr

With both a template protein and a target metalloenzyme chosen, we set out to redesign HPr. In redesigning a protein it is important to avoid modifications that could drastically change the protein secondary and tertiary structure. These types of modifications nullify the advantage of choosing a structurally defined template, and can complicate subsequent studies. Thus, we chose to use protein molecular modeling to design and evaluate our native and modified proteins. This approach gives us a strategic advantage to generate and test multiple mutation sets of the template protein, and evaluate how the modifications we create could affect the local and global folding of the phosphate-binding site. Molecular modeling of proteins and nucleic acids has become a common technique in designing complex experiments, visualizing the potential interactions, and evaluating resulting data.[14] Thus, we set out to model HPr, and redesign its phosphate-binding site to adopt a structure capable of supporting the coordination requirements of an iron ion analogous to that found in PCD.

We obtained the protein structural coordinates from the Brookhaven National Laboratory Protein Data Bank.[15] As mentioned above, we chose HPr from the *B. subtilis* organism because it meets our outlined criteria. However, our initial examinations revealed that HPr from *E. Coli* also satisfies many of these criteria. Therefore, we began to closely examine the structure of the PCD active site and how it compared with the phosphate-binding pocket from *B. Subtilis* and *E. coli*. Figure 3-7 shows a comparison of the two structures, which show a striking resemblance. Both contain the β-sandwich

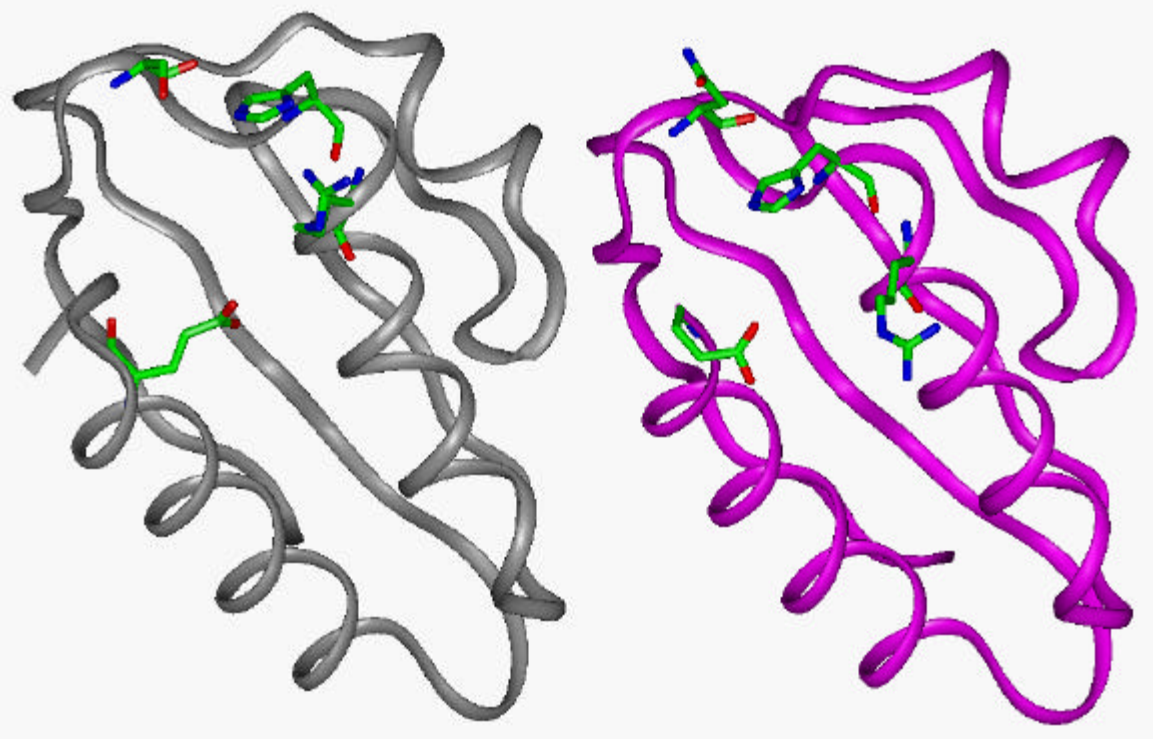

Figure 3-7: Comparative view of HPr structure from *B. subtilis* (left) and *E. coli* (right). Both structures models of X-ray diffraction structures obtained from the Broohaven National Laboratory Protein Data Bank.

tertiary structure, and structural alignment of their backbone models demonstrates their structural homology on both secondary and tertiary levels. From this comparison, notice

that in the *B. subtilis* structure (left) that residue 12 is serine (hydroxyl side chain), while *E. coli* contains asparagine (amide side chain). The serine hydroxyl points directly into the phosphate binding site, while the amide group of the *E. coli* protein is directed outward toward the solvent. Residues 15 and 17 are conserved amino acids between the two proteins, but arginine 17 is positioned slightly farther from His-15 in the *E. coli* structure, and has alternate backbone dihedral angles directing it away from the His-15 side chain. Also, glutamate 84 in the *B. subtilis* structure differs in positioning from the matching glutamate 85 residue from *E. coli*. Glutamate 85 is the terminal residue in the *E. coli* structure, while four additional residues follow glutamate 84 in the *B. subtilis* protein. Most importantly, the distance from the closest Glu-85 oxygen to His 15 is greater than 10 Angstroms in the *E. coli* structure, while Glu-84 from *B. subtilis* is only 6 angstroms away. Collectively, the *E. coli* active site side chains are directed more away from the center of the phosphate-binding pocket, while the *B. subtilis* active center is more compact, and its residues are directed into the phosphate-binding cavity. From these and other structural observations (with ML_5 complexes, discussed below), the phosphate site from *B. subtilis* would require much less perturbation (relative to the defined protein structures) to bind an iron ion in the center of the phosphate binding pocket in a geometry analogous to PCD than HPr from *E. coli*. This is an important feature. Increasing the perturbations required for metal coordination from the native protein structure will increase the likelihood of destabilization of the protein scaffold, and limit our ability both to support metal coordination and compare the native and mutant metallated structures. From this comparison, and the existence of extensive literature on

each protein's structure and phosphotransfer ability, we concluded that the redesigning of HPr from *B. subtilis* would give us the best chance for successful coordination of iron in the former phosphate-binding site.

With a definitive scaffold protein chosen as our template phosphate-binding protein, we set out to perform molecular modeling calculations on the native protein to test how the protein structure responds to potential amino acid changes. For all our molecular modeling studies, we utilized the InsightII suite of molecular modeling modules from Molecular Simulations as described in the experimental section. Our first step in the structural minimization of HPr was to assign a set of potentials for the protein that assigns charges to the various residues. We chose to perform all our calculations at a

Residue	Charge
Lysine 4	+1
Lysine 7	+1
Aspartate 11	-1
Histidine 15	0
Arginine 17	+1
Lysine 28	+1
Aspartate 30	-1
Aspartate 32	-1
Glutamate 36	-1
Lysine 40	+1
Lysine 45	+1
Lysine 57	+1
Glutamate 60	-1
Aspartate 69	-1
Glutamate 70	-1
Aspartate 72	-1
Glutamate 78	-1
Glutamate 79	-1
Lysine 82	+1
Glutamate 84	-1
Glutamate 88	-1

Table 3-1: Charge Assignments for HPr at pH = 7.2.

pH = 8.0. This is the predominant pH utilized in the HPr activity studies, and is close to the widely accepted physiological pH of 7.2. Table 3-1 contains a list of charged residues. With potentials assigned, the next step was to choose a mathematical forcefield to approximate the vibrational and intermolecular interactions of the protein. We chose the standard ESFF forcefield developed by Molecular Simulations. This forcefield is described in Figure 3-8.

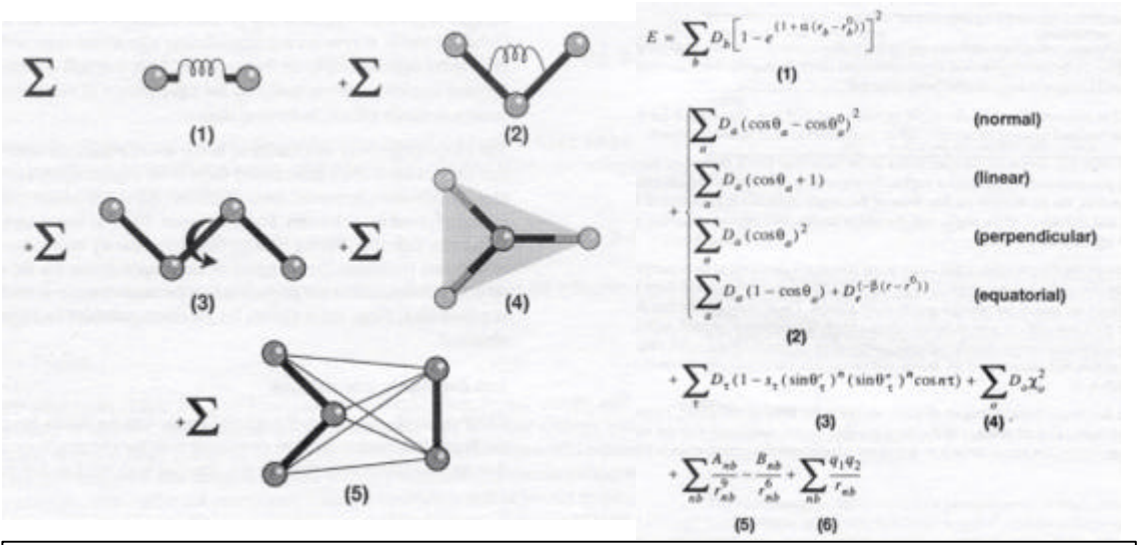

Figure 3-8: Graphical and mathematical description of the ESFF forcefield utilized in the Discover® module of the InsightII molecular modeling program. Terms including bond stretching (1), bending (2), torsional motions, out-of-plane bending, term (5) is for Van der Walls interactions, and term (6) accounts for the Coulombic interactions.

Now the protein structure is ready for the minimization process. All the calculations presented here were performed *in vacuo*. Water box calculations were also attempted, but the calculations were time-consuming and did not cause discernable structure changes over 2-3 day minimizations. Therefore, we chose to perform our minimizations *in vacuo* because of their speed and heightened response to calculations variables. For our initial minimizations, we chose 300 iterations of steepest descents

minimization to a RMS derivative of 1.0 followed by the conjugates method from 1.0 down to a value of 0.01 for the RMS derivative. Figure 3-9 contains a comparative look at the pre and post minimization native HPr structures. Notice there is little structural alteration in the secondary and tertiary structure. This is not unexpected since the process of crystallization produces a stable protein conformation that is likely to be the lowest energy structure achievable. We tested the limits of this minimization, and found that by greatly exaggerating the Van der Waals and/or electrostatic forces, or by allowing large structural movements in a single iteration, we could cause drastic changes in the protein structure. After performing numerous minimizations and testing different variables, we observed the simulation results, and established a set of parameters that gave reproducible, chemically meaningful results of its potential energy through the ESFF forcefield. With this background, we can now comparatively test the performance of our mutant HPr proteins under similar conditions to probe their structural stability upon mutation.

To generate the mutations in HPr's phosphate-binding site, the only predetermined restriction made was that the native histidine-15 residue (which is universally conserved in all HPrs) would not be modified. There are two rationale for imposing this limitation. First, HPr mutants containing alternative amino acids for His-15 show no phosphotransfer reactivity.[16] This is attributable to the direct coordination of the phosphate ion to the imidazole ring. Furthermore, mutation of this residue could also cause perturbations in the HPr secondary structure, and altering the integrity of the phosphate-binding pocket. A second reason to leave His-15 unchanged is that conversion

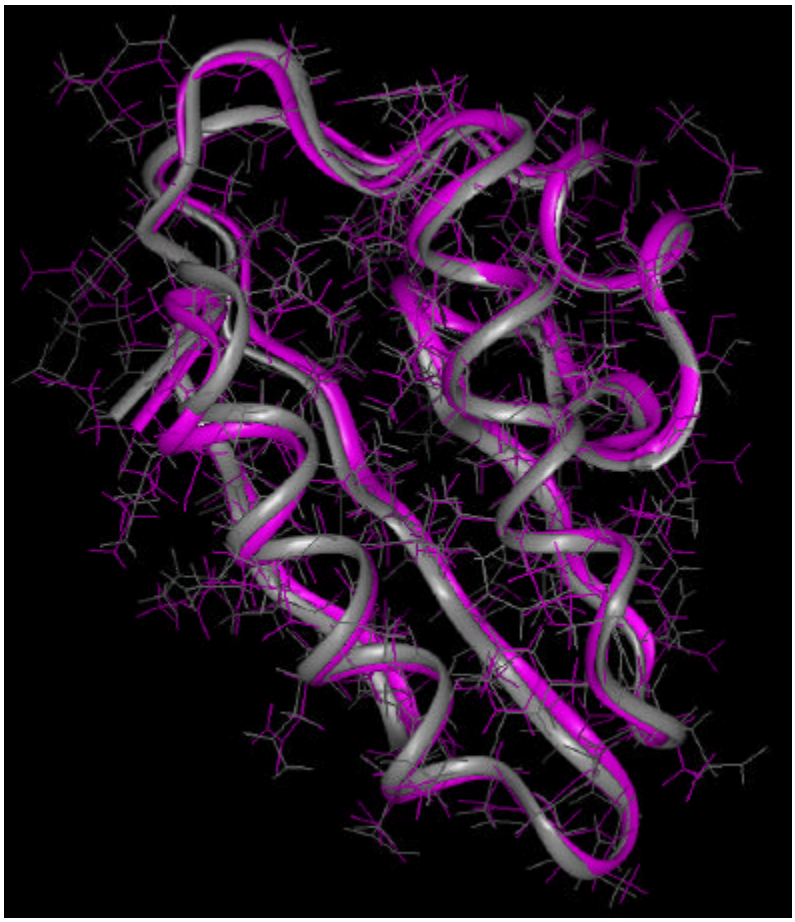

Figure 3-9: Comparison of HPr upon minimization. In gray is the native HPr crystal structure, while the purple structure is a minimized protein structure achieved with the conjugates method of *in vacuo*.

of HPr to a PCD-like metalloprotein requires two histidine and two tyrosine residues. By avoiding mutation of His-15 to tyrosine, we reduce the number of required modifications to HPr and the number of potential mutant sets to examine. We believe this limitation gives us the best chance to successfully create a PCD-like site within HPr and comparatively evaluate the resulting metal-adducts with native HPr.

To generate structural models of potential HPr mutants containing two tyrosine and two histidine residues, we utilized the Biopolymer module in the InsightII suite of

modeling programs. Careful examination of the phosphate-binding site in HPr showed that four of the amino acid side-chains were directed into the phosphate-binding pocket. These residues are illustrated in Figure 3-3 and include Serine-12, Histidine-15, Arginine-17 and Glutamate-84. All four are important factors in phosphotransfer reactivity.[17] Their orientation to the site of phosphorylation suggests that they are associated with phosphate binding and likely remain directed toward the active site during this activity. As a result of this observation, we limited the number of possible mutation sets to these four residues. Keeping His-15 unchanged, our limitations resulted in three potential combinations of two tyrosine and two histidine residues: H12, H15, Y17, Y84; Y12, H15, H17, Y84; and Y12, H15, Y17, H84. Maintaining the backbone dihedral angles of native HPr, we created each of these HPr mutants. We then measured the intramolecular distances between the potential metal ligand atoms (phenolate oxygen and imidazole N(δ)). All of the mutant sets were reasonably proximate (4-10 Angstroms) to provide a proximal ligand set for a metal ion. Thus, we performed minimization experiments analogous to the native protein for each of the mutant proteins. The results of these calculations were consistent with those of the native protein, with no significant deviation in the secondary or tertiary structure observed. This results suggests that the phosphate-binding pocket of HPr could be stable to mutation under the conditions of our analysis, and demonstrates the potential of HPr's phosphate-binding pocket to serve as a scaffold for the construction of a metal-binding site.

With three feasible mutant HPr structures to choose from, we generated a generic ML_5 complex, that contains the exact bond distances and angles as those of the iron site

in PCD. We placed this complex within the three mutant HPr binding pockets, and reoriented it to achieve the best match (tyrosine and histidine pair both axial and equatorial) to the geometry of the HPr pockets. By monitoring the bond distances, we positioned the complex to minimize the sum of the distances to the four potential ligand atoms. Through this process, the Y12, H15, H17, Y84 mutant was chosen as the best

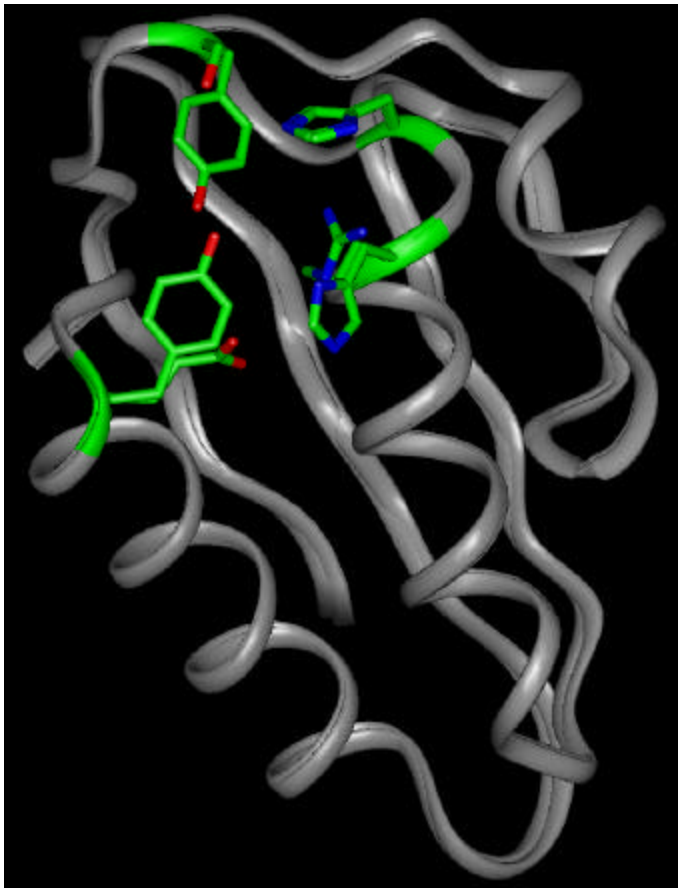

Figure 3-10: Comparison of the native HPr and mutant structures

candidate (Figure 3-10). This mutant HPr, named HPrγ is shown in comparison with native HPr without modification of the amino acid backbone dihedral angles. HPrγ mutant HPr had the lowest mean bond distance (4.91 Angstroms), and more importantly,

its amino acid orientations were a near perfect match to the requirements of the PCD-like ML_5 complex. In summary, this design process differentiated the feasibility of the three potential mutant sets, and led us to a candidate HPr mutant that reasonably approximates the iron ligand set found in PCD.

Construction of a structural model of the mutant HPr-metal complex was performed to test its structural ability to support the rigid constraints of iron coordination analogous to PCD. Our first goal was to place an iron atom in the HPrγ pocket, and run molecular minimizations analogous to those performed for the apoproteins. However, this proved difficult because the ESFF forcefield does not have parameters for iron, and development of such reliable parameters is not a trivial process.[18] The AMBER forcefield has been developed to handle iron atoms, but only for small molecules.[19] Thus the combination of the size of HPr and the unique properties of iron made this goal unachievable at the time of this development process. Consequently, we took a different approach.

The fundamental issue we wanted to address with these calculations was how does the HPrγ secondary and tertiary structure respond to the stress of iron complexation. Will the coordination constraints of the iron atom to these four residues cause HPrγ to collapse, denature, or retain some or all of its structural integrity? To answer this question, we utilized the Discover3 module of the InsightII molecular modeling software, which allows for the constraint of certain bond distances, bond angles, and dihedral angles. We placed a pseudoatom (a dummy atom) within the active site, and created bonds to the oxygen and nitrogen atoms of the HPr ligands. Then we imposed a

constraint set on the local environment of the pseudoatom shown in Table 3-2. The structure was then minimized. This was repeated under various conditions (Van der

Parameter	Value
Metal-O bond lengths	1.8 Å
Metal-N bond lengths	2.2 Å
Tyrosine α-C to backbone C	1.0 Å
Histidine α-C to backbone C	1.0 Å
Metal-O-C eq. bond angle	150^o
Metal-O-C axial bond angle	170^o
Metal-N-C bond angles	120^o
Metal-O-C-C dihedrals	varied to match PCD
Metal-N-C-N dihedrals	0 or 180^o
Metal-N-C-C dihedrals	0 or 180^o
O-Metal-N axial bond angle	173^o
O-Metal-N equatorial bond angle	120^o

Table 3-2: Important parameters utilized to restrain the active site of HPrγ to generate the HPr-metal minimized complex. Other parameters were also required to maintain the exact planarity of the aromatic rings of histidine and tyrosine, however, only α-carbon bond length restrictions were placed on the peptide backbone to allow simulation of the restraint effects on the secondary structure.

Waals forces, electrostatic forces, etc…). The structure produced from these simulations is shown in Figure 3-11 along with the native HPr structure for comparison. The structural comparison shows that there are some small perturbations near the phosphate-binding pocket. This is result is not unexpected result since the structure must collapse to a certain extent to satisfy the coordination requirements of the iron atom. What is evident is that restraint to the iron was accomplished without grossly altering the HPr secondary or tertiary structure. This suggests that the HPr scaffold can support the constraints of iron coordination analogous to PCD. Figure 3-12 shows a closer view of the resulting metal site, with a comparative

Figure 3-11: Shown here is HPrγ with metal that has been constrained to a pseudoatom with the geometric properties of the metal site found in PCD. This structure (gray with metal center rendered) represents the average minimized structure, and can be compared to the ribbon diagram of native HPr (purple)

view of the PCD active site. This view shows the striking similarity generated by this constrained minimization, and in conjunction with the lack of global movement required to achieve this similarity to the PCD site, supports our contention that this HPr mutant set is plausible.. There are subtle differences in the ligand orientations, but the overall comparison of the two suggests that this is a feasible mutant to support the coordination requirements of iron analogous to PCD. From these calculations, we feel HPrγ is a good mutant choice for the generation of a PCD-like iron complex with HPr.

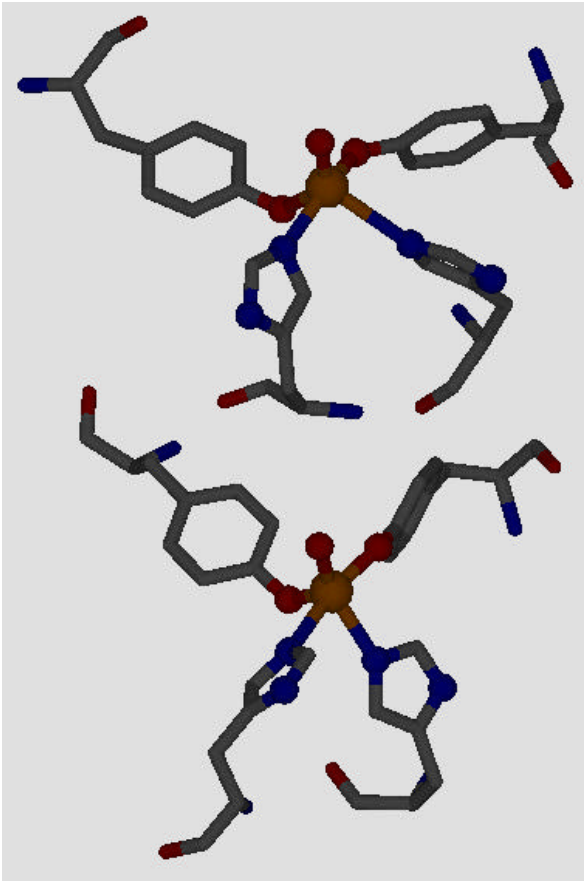

Figure 3-12: Shown here is a close-up view of restrained HPrγ (top). On the bottom, the PCD active site is shown for comparison. Notice the different orientation of the histidine residues, yet overall their structures compare favorably with each other

In summary, the structural knowledge of our template and target protein structures has afforded us the opportunity to strategically re-design HPr, and mutate its sequence. Our design strategy has resulted in a definitive choice of mutant HPr that possesses the potential to coordinate iron in an analogous manner to that found in PCD without significantly disturbing the protein secondary or tertiary structure..

3.5 SUMMARY

We have outlined the desired criteria for our template phosphate-binding protein and target metalloprotein. We have shown how HPr and PCD satisfy these criteria. We have discussed our molecular modeling of HPr, and how we applied this tool to evaluate

our native and candidate mutant structures. We described our method of rational re-design of HPr and reported the resulting choice of mutant proteins to test our hypothesis. This mutant HPr has the potential to bind iron in a manner structurally analogous to our target site from PCD. This concludes our design strategy from which we can proceed to the laboratory, and test the validity of our design strategy and hypothesis.

3.6 REFERENCES

[1] Guan, K.; Dixon, J. E. *J. Biol. Chem.* **1991**, *266*, 17026-17030.
[2] Wiegal, N.; Waygood, B. E.; Kukuruzinska, M. A.; Nakazawa, A.; Roseman, S. *J. Biol. Chem.* **1982**, *257*, 14461-14469.
[3] Figure taken directly from: Brock, T. D.; Madigan M. T.; Martinko, J. M.; Parker, J., **1984**, Biology of Microorganisms, 7th ed., Prentice-Hall, Inc. Englewood Cliffs, New Jersey.
[4] Kalbitzer, H. R.; Hengstenberg, W.; Rosch, P.; Muss, P.; Bernsmann, P. *Biochemistry* **1982**, 21, 2879-2885.
[5] Meadow, N. D.; Fox, D. K.; Roseman, S., *Annu. Rev. Biochem*. **1990**, *59*, 497-542.
[6] Herzberg, O.; Reddy, P.; Sutrina, S.; Saier, M. H., Jr.; Reizer, J.; Kapadia, G. *Proc. Natl. Acad. Sci*. **1992**, *89*, 2499-2503.
[7] Wittedind, M.; Reizer, J.; Klevit, R. E. *Biochemistry* **1990**, *29*, 7191-7200.
[8] Kluse, R.; Hengstenberg, W.; Beneicke, W.; Kalbitzer, H. R. *Protein Engineering*, **1993**, *6*, 417-423.
[9] Kluse, R.; Hengstenberg, W.; Beneicke, W.; Kalbitzer, H. R. *Protein Engineering*, **1993**, *6*, 417-423.
[10] Whittaker, J. W.; Lipscomb, J. D.; Kent, T. A.; Munck, E. *J. Biol. Chem*., **1984**, *259*, 4466-4475.
[11] Ohlendorf, D. H., Lipscomb, J. D.; Weber, P. C. *Nature*, **1988**, *336*, 403-405.
[12] Lauffer, R. B.; Que, L., Jr. *J. Am. Chem. Soc*. **1982**, *104*, 7324-7325.
[13] Orville, A. M.; Lipscomb, J. D. *J. Biol. Chem*. **1989**, *264*, 8791-8801.
[14] Levitt, *M. J. Mol. Biol.* **1992**, *226*, 507-534.
[15] Reizer, J.; Sutrina, S. L.; Wu, L. F.; Deutscher, J.; Reddy, P.; Saier, M. H.; *J. Biol. Chem.* **1992,** *267*, 9158-9169.
[16] Poolman, B.; Modderman, R.; Reizer, J. J. Biol. Chem. 1992, 267, 9150-9157.
[17] Seok, Y. J.; Lee, B. R.; Zhu, P. P.; Peterkofsky, A. *Proc. Natl. Acad. Sci.* **1996**, *93*, 347-351.

[18] Weisemann, F. *Inorganic Chemistry* **1994**, *33*, 1891-1899
[19] Jimenez, B. J.; Asenio, J. L. *Biopolymers* **1995**, *35*, 55-74.

Chapter 4

GENE CONSTRUCTION & CLONING

4.1 INTRODUCTION

To conduct our metal-binding experiments on HPr and its mutants, we chose a strategy to generate pure native and mutant proteins in high concentrations. To accomplish this, we needed to harness the genetic information within the target gene sequence, and equip it with the machinery to produce large quantities of the desired protein. In this chapter I will delineate the steps taken to genetically manipulate the native and mutant HPr genes to achieve these goals.

4.2 NATIVE HPr GENE PREPARATION AND CLONING

Generation of HPr and its mutant proteins requires several steps. The first step is to obtain the gene sequence from the organism of choice. We Chose the HPr gene from *Bacillus subtilis* for these studies. Thus, the ptsH gene, which encodes for the native HPr protein must be isolated from the genomic DNA of *B. Subtilis* and incorporated in a recombinant manner within a vector DNA construct. This process allows one to manipulate the gene by providing a method of replication, and affords antibiotic resistance to selectively choose organisms that contain the desired DNA. Fortunately, this task was completed by Dr. Jonathon Reizer and coworkers of the University of San Diego, who graciously donated the *B. subtilis* gene to us. As offered, the gene was in the pCPP shuttle vector.[1,2]

The pCPP shuttle vector affords replication and low level function in both E. coli and B. subtilis. However, to produce high levels of protein (overexpression), this ptsH gene must be removed from the pCPP shuttle vector and placed in an expression vector

that has the ability to overexpress foreign proteins. We chose to utilize the commercially available pCal-n system from Stratagene®.[3] Briefly, the pCal-n vector is a modified pET11-a vector utilizing a T7 RNA polymerase under the control of the lacUV5 promoter (Figure 4-1). Preceding the target gene sequence, the vector DNA contains a sequence that codes for a calmodulin-binding peptide purification tag. Thus, induction of protein expression with the lactose analog IPTG (isopropyl-1-thio-β-D-galactopyranoside) will initiate RNA transcription of the calmodulin binding peptide immediately followed by your target sequence. This "purification tagging" affords a method for rapid purification of protein, and has the advantage of a thrombin protease cleavage site between the tag and target sequences. Modification of ptsH is required to insure that incorporation into pCal-n gives a construct with correct position, orientation, and reading frame. The pCal-n vector requires that a 5' BamHI restriction endonuclease recognition site immediately precede the target gene sequence for proper function. The 3' recognition site can vary among any of the polylinker sites shown in Figure 4-1 including BamHI. We chose BamHI and HindIII sites for our initial experiments due to the strong buffer compatibility of these restriction endonucleases. This type of "forced cloning" strategy demands that the insert DNA bind to the vector in the correct orientation, and precludes "backwards" ligation in the vector reading frame.

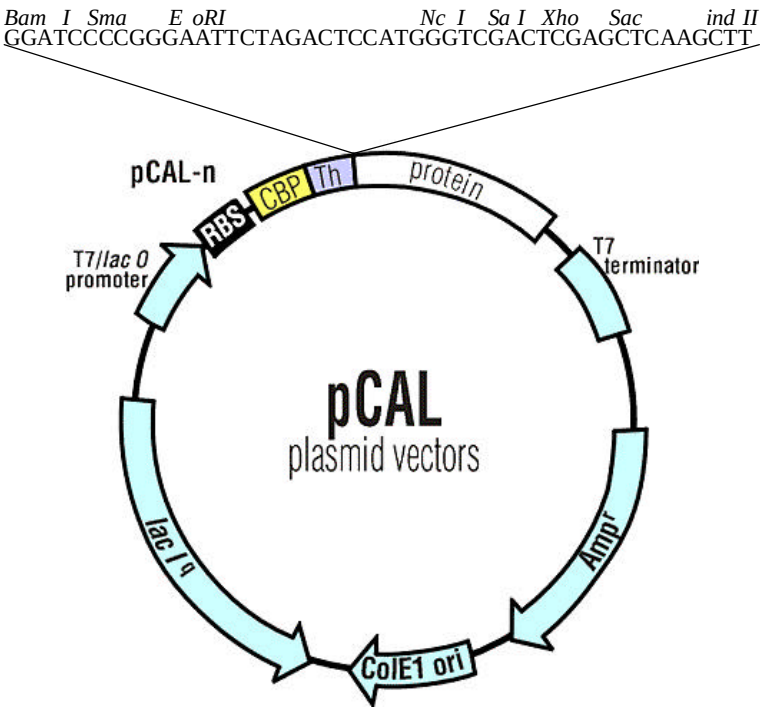

Figure 4-1: A pCal-n expression vector map depicting the key functional segments. From an expansion of the polylinker region it is shown that in-frame ligation to the BamHI site followed immediately by the target sequence and a second cut site will produce a construct capable of producing the tagged target protein.

In order to generate these new termini, we chose to copy the gene out of the pCPP vector using the Polymerase Chain Reaction (PCR). This approach does not require prior knowledge of the flanking regions of the target gene sequence, and provides the capability, through the oligonucleotide primer design, to add variable termini. Figure 4-2 depicts our initial strategy. In this reaction, the upstream and downstream primers bind to the denatured template strands as shown, and provide 3'-hydroxyl ends, from which DNA polymerase enzymes can extend the strand in the presence of deoxynucleotides. This process creates a new strand containing the primer sequence, which can now serve as a template for subsequent cycles. The additional sequence flanking the cleavage sites in the primers (Figure 4-2) was included to increase the efficiency, near the product termini, of endonuclease cleavage.

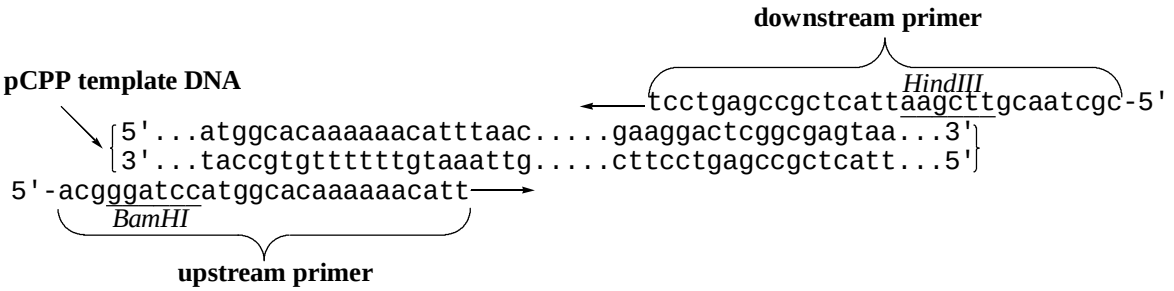

Figure 4-2: PCR setup showing the designed primers and their binding orientation to the native pCPP template DNA. Incorporated restriction endonuclease sites are underlined.

in subsequent manipulations.

We obtained the illustrated primers, and ran the PCR reaction (as described in section 2.3). The resulting product was analyzed on a 1.2 % agarose gel along with double digested (BamHI/HindIII) pCal-n vector, as is shown in Figure 4-3.

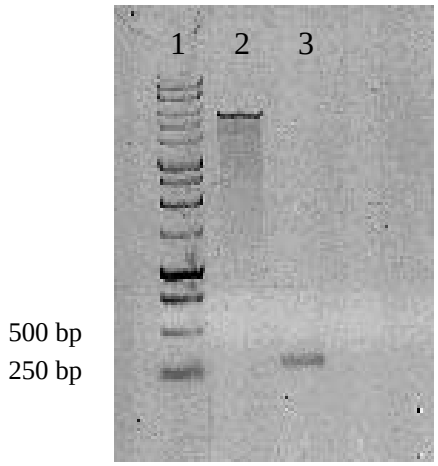

Figure 4-3: 1.2 % agarose gel electrophoresis of 1 kb molecular weight marker (1), double digested (BamHI/SacI) pCal-n vector (2), and purified PCR product.

A single PCR product was produced, and is in the correct mass range to conclude that we are most likely amplifying the correct segment of the pCPP template DNA.

Following the PCR amplification reaction, the product was purified to remove the residual oligonucleotides, primers, and other reaction components that could inhibit

subsequent digestion and ligation reactions. Using a Qiagen PCR Prep column (see section 2.7-A). The resulting purified product was then double-digested with BamHI/HindIII, and subsequent passage through a second PCR Prep column completes its preparation for ligation to the pCal-n vector. For optimal ligation, the pCal-n polylinker segment was removed from the digested vector along with the excess reaction components. Initial attempts used agarose gel purification (see section 2.7-D) to remove these unwanted digest components. However, later we found that the Qiaquick DNA purification method could produce much higher yields of pure, double digested vector, and additionally could successfully remove the <50 bp polylinker DNA fragment.

Direct incorporation of the initial PCR product into the pCal-n expression vector was attempted (with exhaustive repeats with variable conditions). Unfortunately, the lack of a facile colony screening method for pCal-n, low plasmid copy number, and an apparent poor ability to cleave near the ends of a PCR product and re-ligate into the pCal-n vector necessitated an interim step to solve this difficult problem. The pNoTA/T7[4] vector, which is specifically designed to incorporate PCR product DNA in a blunt-end manner (see section 2.8) was chosen for this step. This vector affords blue/white color screening of putative clones,[5] multiple cleavage sites, and high copy-number plasmid production. Thus, subcloning into the pNoTA/T7 vector allowed us to more rapidly evaluate the integrity of our PCR products, by selecting a construct that contains the desired sequence before proceeding further.

Our first pNoTA/T7 cloning and transformation experiment was performed with I:V molar ratios of 2:1 and 4:1. The resulting growth on LB/Amp plates produced

approximately 50% blue, and 50% white colonies on each insert-containing transformation. White colonies indicate disruption of the pNoTA/T7 vector sequence potentially by the presence of incorporated insert. Plasmid were isolated and purified from four white colonies and agarose gel electrophoresis was used to analyze the BamHI/HindIII digests as shown in Figure 4-4. From this image, an ~270 bp band is present in lanes 3, 4, and 5, which is consistent with the anticipated fragment size and demonstrates our first successful PCR product incorporation.

Figure 4-4: First agarose gel showing insert incorporation. Intense marker band at 500 bp. Lanes 2-5 contain digests of purified plasmid from white colonies.

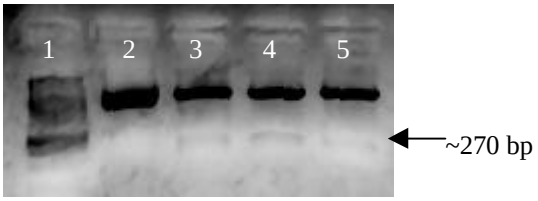

The plasmid from lane 4 along with its precursor PCR product to the NCSU DNA sequencing facility, and the resulting sequencing data confirmed that we indeed had incorporated the targeted PCR product containing a copy of the ptsH gene into the pNoTA/T7 vector. Additionally, this sequence solved the enigma of our earlier cloning difficulties. As seen in Figure 4-5, desired guanine nucleotide has been replaced with cytosine nucleotide in the primer-binding region. This most likely resulted from incorrect primer synthesis, and subsequent incorrect PCR amplification, thereby yielding CCATCC rather than a BamHI site (GGATCC).

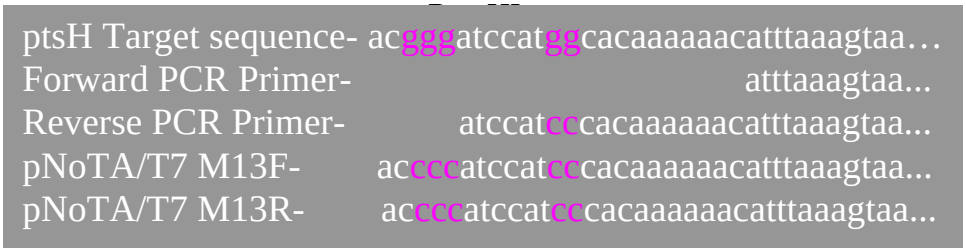

Figure 4-5: Sequence analysis from the BamHI/HindIII PCR product experiments

With these eye-opening results, we immediately designed a new PCR experiment, to take advantage of the pNoTA/T7 subcloning strategy. Although use of this subcloning step appears to be a longer route, it allows us to rapidly and efficiently screen sequence incorporation using with the advantages of blue/white selection and higher plasmid copy numbers relative to pCal-n experiments. This new experiment utilized an upstream primer identical to the earlier design except the 5' terminal acg was not added. This sequence is not necessary with the utilization of the blunt-end ligating pNoTA/T7 subcloning strategy. The downstream primer in this new experiment, however, is very different from our earlier efforts. During our troubleshooting experiments, we sequenced the pCPP vector's ptsH gene and flanking regions to both confirm we do have an intact ptsH gene from *B. subtilis*, and to gain sequence information on the flanking regions of the gene. We found that at ~80 bp downstream of the ptsH gene, a pre-existing SacI site was present. SacI has adequate buffer compatibility with BamHI, and is present in the pCal-n polylinker. So we designed our new downstream primer to bind downstream of this SacI site. This strategy is summarized in Figure 4-6, and affords both a larger insert fragment of ~350 bp (easier to visualize than the smaller 270 bp fragment) and precludes

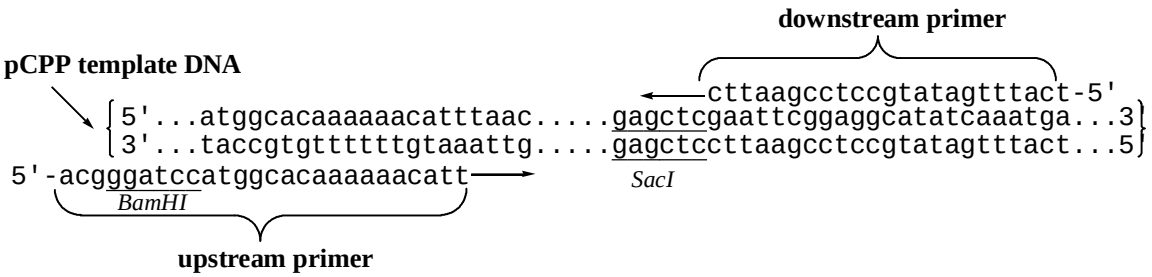

Figure 4-6: PCR setup showing the designed primers and their binding orientation to the native pCPP template DNA. Incorporated restriction endonuclease sites are underlined.

the need to mutate the downstream segment of the gene to effectively clone it into pCal-n.

With our new strategy outlined, we ordered new primers and performed the PCR reaction with an analogous setup to our earlier reactions. The primary difference for this reaction was that the temperature profile was modified with a new Tm of 60 ^{o}C. Figure 4-7 shows a 1.2% agarose gel analysis of these reactions (with varying conditions) revealing production of high concentrations of ~350 bp DNA fragments (as expected) in lanes 1, 2, 3, and 5.

Figure 4-7: PCR reactions with the new primers purchased from Genosys, Inc. run on a 1.2 % agarose gel. Lane 1, standard 100 bp ladder; Lane 2, standard conditions (1 mM Mg^{2+}); Lane 3, 1.5 mM Mg^{2+}; Lane 4, 2.0 mM Mg^{2+}; Lane 5, no template control; Lane 6, Stragene® Taq DNA polymerase in place of Boehringer Mannheim.

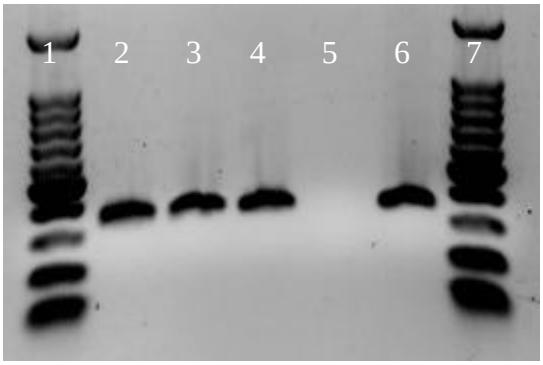

The PCR product from lane 2 was purified via the Qiagen PCR prep method, and subcloned into the pNoTA/T7 vector as previously described. Following, transformation

of the ligation reaction (3:1 insert:vector), three single white colonies were cultured and plasmid DNA was isolated. Double-digestions of the plasmids with BamHI/SacI were analyzed on a 1.0 % agarose gel electrophoresis and is shown in Figure 4-8.

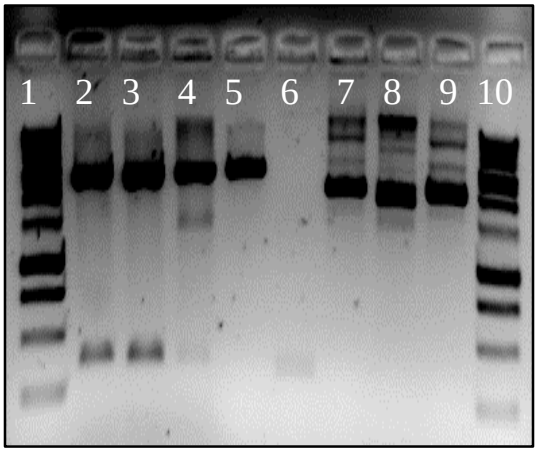

Figure 4-8: 1.0 % agarose gel of isolated plasmids and digests from three cultured white colonies from the pNoTA/T7 system.

Lane	Contents
1	1 kb ladder
2	Cut plasmid 1
3	Cut plasmid 2
4	Cut plasmid 3
5	Cut pNoTA/T7
6	Pure PCR product
7	Uncut plasmid 1
8	Uncut plasmid 2
9	Uncut plasmid 3
10	1 kb ladder

The sequences from the plasmid in lane 2 shown in Figure 4-9 confirms that we have successfully copied the ptsH gene from the pCPP vector, and added a BamHI restriction endonuclease site to its 5' terminus. In addition the targeted SacI site, downstream of the gene sequence is present and intact. Some anomalies in the sequence are present; however, the complementary sequence from the opposite direction in both cases is consistent with the correct sequence, and significant radioactive intensity for the correct nucleotide was observed on the sequence spectrum for both anomalies.

With the correct gene fragment subcloned into the pNoTA/T7 vector, our final genetic manipulation was to cleave it out, and ligate it within the pCal-n expression vector. We began the cloning process by double-digesting the pCal-n vector and the pNoTA/T7 plasmid containing our gene with BamHI and SacI (see section 2.4(A)). The pCal-n vector and the pNoTA/T7 plasmid containing the target ptsH gene were gel

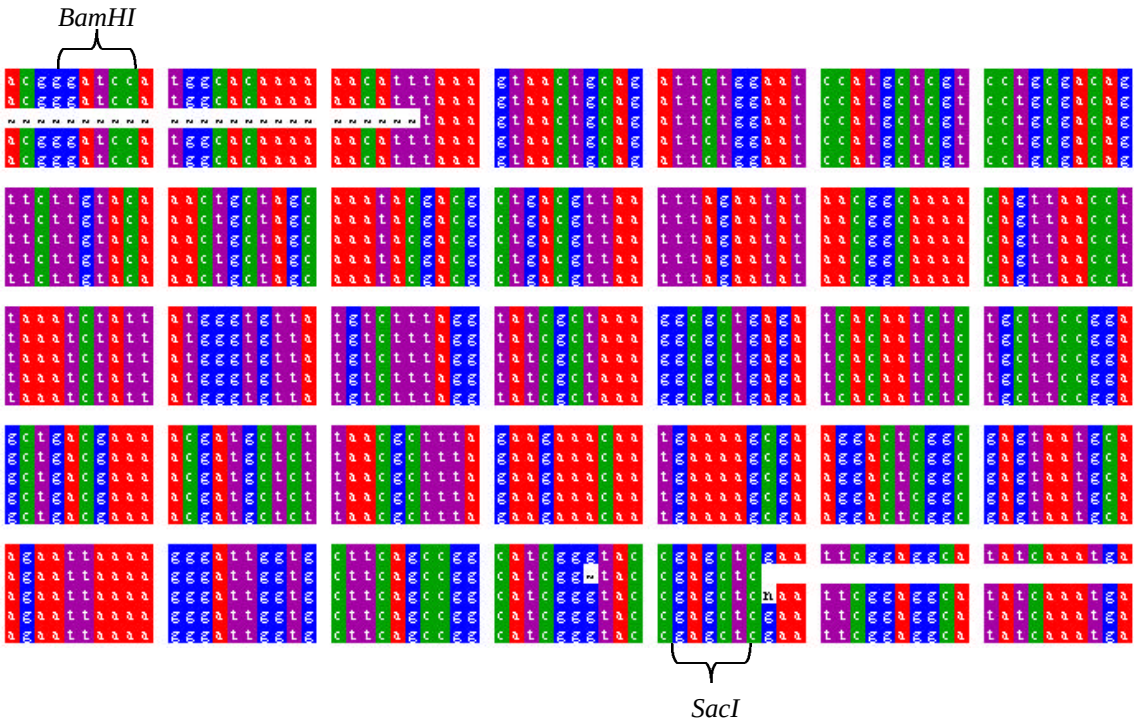

Figure 4-9: pNoTA/T7 + ptsH gene sequence with BamHI and SacI sites. Sequence generated with the designed PCR primers described above. The top strand is the target ptsH sequence, the second is the downstream PCR sequence, the third is the upstream PCR product sequence, the fourth is the pNoTA/T7 subclone sequence in the forward direction, and the bottom is the reverse subclone sequence.

purified on a 2 % agarose gel (see experimental 2.4(D)). Figure 4-10 shows the separation prior to excising the target bands. The observed smearing is the result of

Figure 4-10: Left lane contains double digested pCal-n, while the right lane contains the insert digest which is clearly distinguishable from its parent vector sequence.

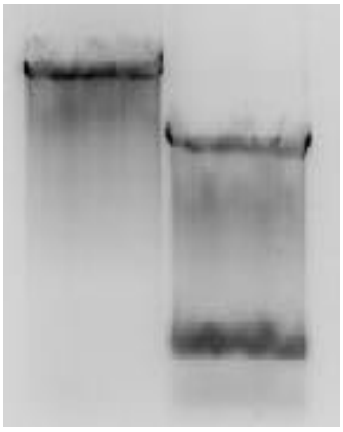

overloading the lanes and some nuclease activity that was alleviated by use of nuclease-free deionized water.

Purified digests were run on a 1.1 % agarose gel along with controls and (shown in Figure 4-11) to evaluate our effectiveness in removing the pNoTA/T7 vector DNA, and cleaning up the pCal-n samples. Figure 4-11 confirms that we were able to successfully cleave the insert and control pET-9a vectors, and effectively gel purify the vector and insert DNAs.

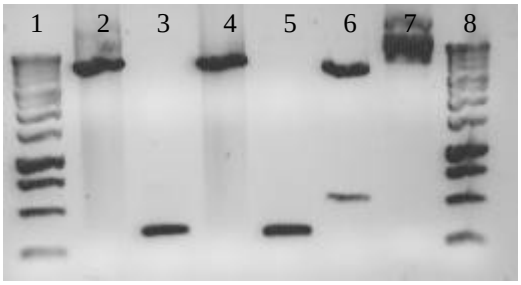

Figure 4-11: 1.1% agarose gel electrophoresis of the preparation of the pCal-n vector and ptsH gene insert for ligation. Lanes 1 and 8, 1 kb ladder; Lane 2, unpurified pCal-n digest; Lane 3 gel purified insert DNA; Lane 4, Qiaquick purified pCal-n digest; Lane 5, reference insert. Lane 6, digest control of pET-9a; Lane 7, uncut pCal-n vector.

Ligations of the pCal-n vector with the ptsH gene fragment were performed (see section 2.4 (C)) with insert to vector ratios of 1:1, 3:1, and 5:1. The subsequent transformations were plated on LB/Amp media and grown overnight. The colony counts produced in this experiment were encouraging. The controls worked as anticipated, and the ligation containing plates had 200-500 colonies each. With these large numbers of colonies, and the lack of a blue/white selection method for pCal-n, it would be difficult to culture, isolate plasmids, digest, and run gel electrophoresis on three plates of >200 colonies each.

Colony hybridization was used to screen an entire set of transformation plates in one experiment. We used the DIG® colony hybridization method from Boehringer Mannheim (described in section 2.9). Briefly, the gene of interest is labeled with a modified nucleotide at every thymine position in an extension reaction similar to PCR. These probe DNA strands now have both high affinity for their complementary strands from the target gene and a specialized antibody conjugate designed to bind to the modified thymine nucleotides. The antibody contains an alkaline phosphatase conjugate that in the presence of a specialized phosphatase substrate, emit light. Treatment of a nylon membrane, crosslinked to the cellular DNA, with probe, antibody, and substrate produces a chemiluminescent film that highlights the position of specific probe binding and thus, the desired plasmid construct. With this capability, we proceeded to screen the transformations of the insert plus pCal-n ligations and control reactions. The results of utilizing this procedure on our 1:1, 3:1, 5:1, (+), and (-) controls are shown in Figure 4-12. Here the negative control is essentially devoid of intense signal in the large, linear streak of bacterial cells. The positive control clearly displays a large (+) symbol, and the three insert containing spot tests can be seen while the pCal-n alone spot is not detectable. Although the 1:1 and 5:1 plates have some intense dots that can be aligned with colonies on the plates, the 3:1 reaction appears to have numerous detectable signal that can be aligned with colonies on the transformation plates.

We cultured the five colonies (circled) shown in Figure 4-12, and isolated plasmid DNAs from each. These plasmids were further screened by BamHI/SacI digestion, and the resulting agarose gel electrophoresis analysis is shown in Figure 4-13.

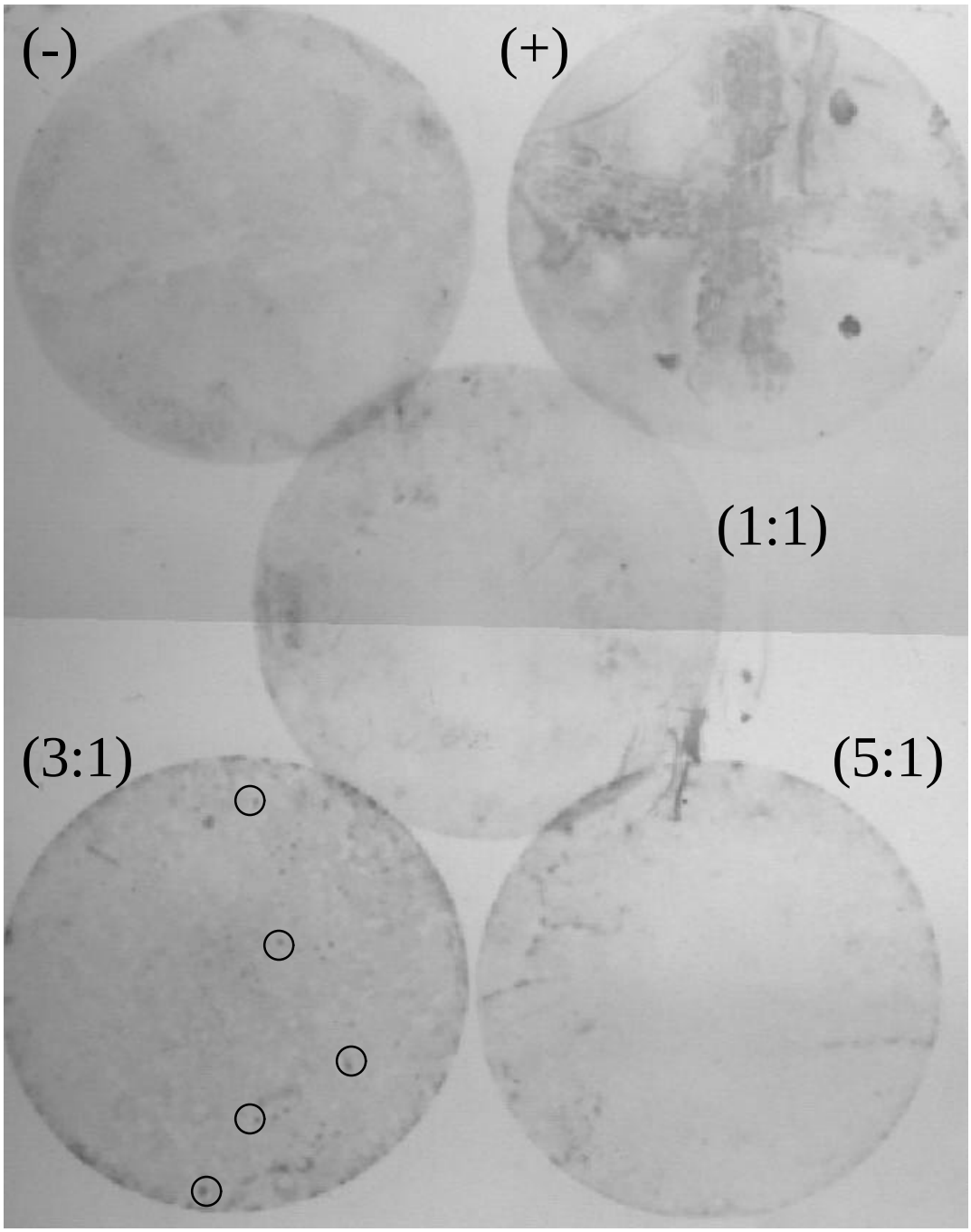

Figure 4-12: Dig® colony hybridization screening of the pCal-n + ptsH insert ligations, and controls. Upper left, negative control; upper right, positive control; middle, 1:1 insert:vector ligation; bottom left, 3:1 insert:vector; lower right, 5:1 insert:vector. Initially picked colonies from the 3:1 plate are circled.

We submitted plasmid-β (lane 2) to the Iowa State University DNA sequencing

facility for analysis and the resulting sequence is shown in Figure 4-14. The sequencing data confirmed that the insert was incorporated in the correct orientation, reading frame, and was devoid of any sequence errors. Thus, we achieved our initial goal of constructing a plasmid with the potential of producing large quantities of the native HPr protein.

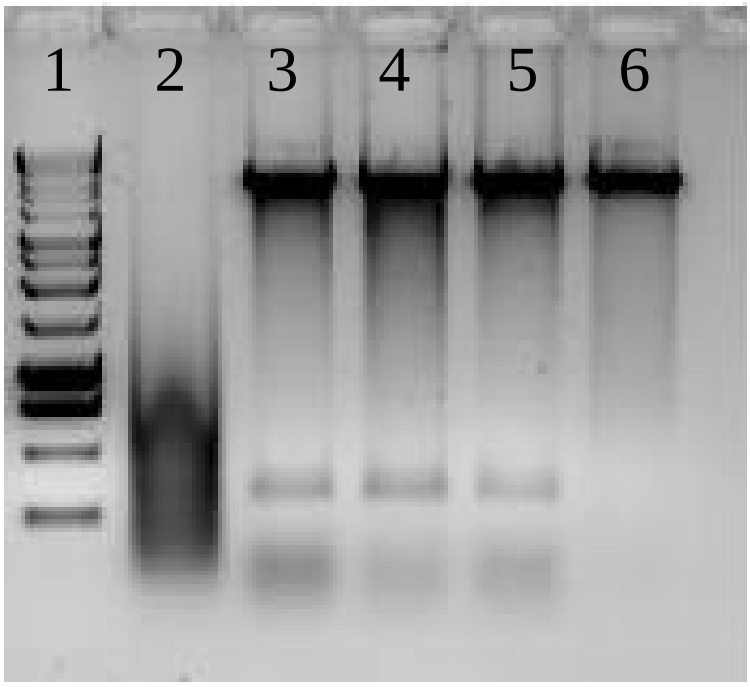

Figure 4-13: A 1.2% agarose gel electrophoresis of the pCal-n + ptsH insert transformants. Lane 1, 1 kb DNA ladder; Lane 2, colony α digest; Lane 3, colony β digest; Lane 4, colony χ digest; Lane 5 colony δ digest; Lane 6 colony ε digest.

4.3 HPr*g* MUTANT GENE PREPARATION, SUBCLONING AND CLONING

To express and purify the mutant HPrγ protein, we must generate the targeted mutations in the native ptsH gene sequence, and then subclone and clone this new gene into pCal-n in a manner analogous to the native HPr strategy. Successful incorporation of the native gene sequence into the pNoTA/T7 vector provided us with suitable template DNA to begin construction of the HPrγ mutant gene.

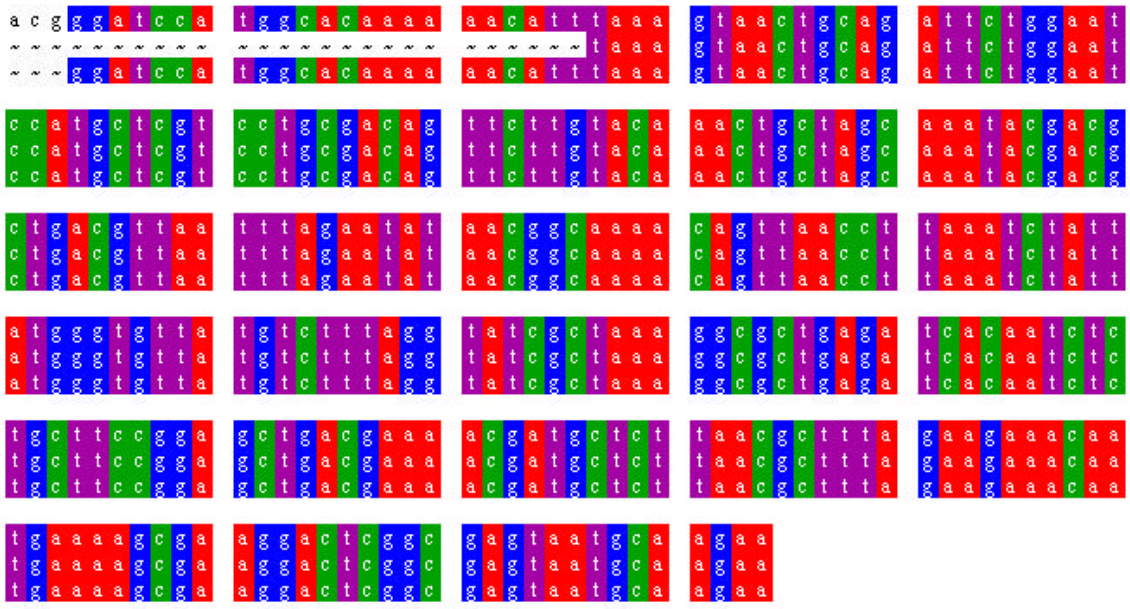

Figure 4-14: Sequence analysis of the native ptsH gene within the pCal-n vector. The top strand is the target sequence, the middle sequence is the upstream primer sequence, and the bottom is the reverse sequence.

As discussed in the chapter 3, this mutation procedure requires that three codon changes be made. The codon coding for serine-12 of native HPr must be changed to a tyrosine coding sequence (tct→tat), arginine 17 to a histidine codon (cgt→cat), and glutamate 84's codon replaced with a tyrosine directing sequence (gaa→tac). Experimentally these mutations were generated by a two-cycle PCR strategy called recombinant PCR. The process, in general terms is summarized in Figure 4-15. Four oligonucleotide primers are designed and synthesized such that they include the desired mutations. The α primers are combined in one reaction with template, and the β primers in a separate reaction with their own template. Both reactions are performed, and each product is purified to remove the dNTPs, old primers, enzymes, buffers etc.…

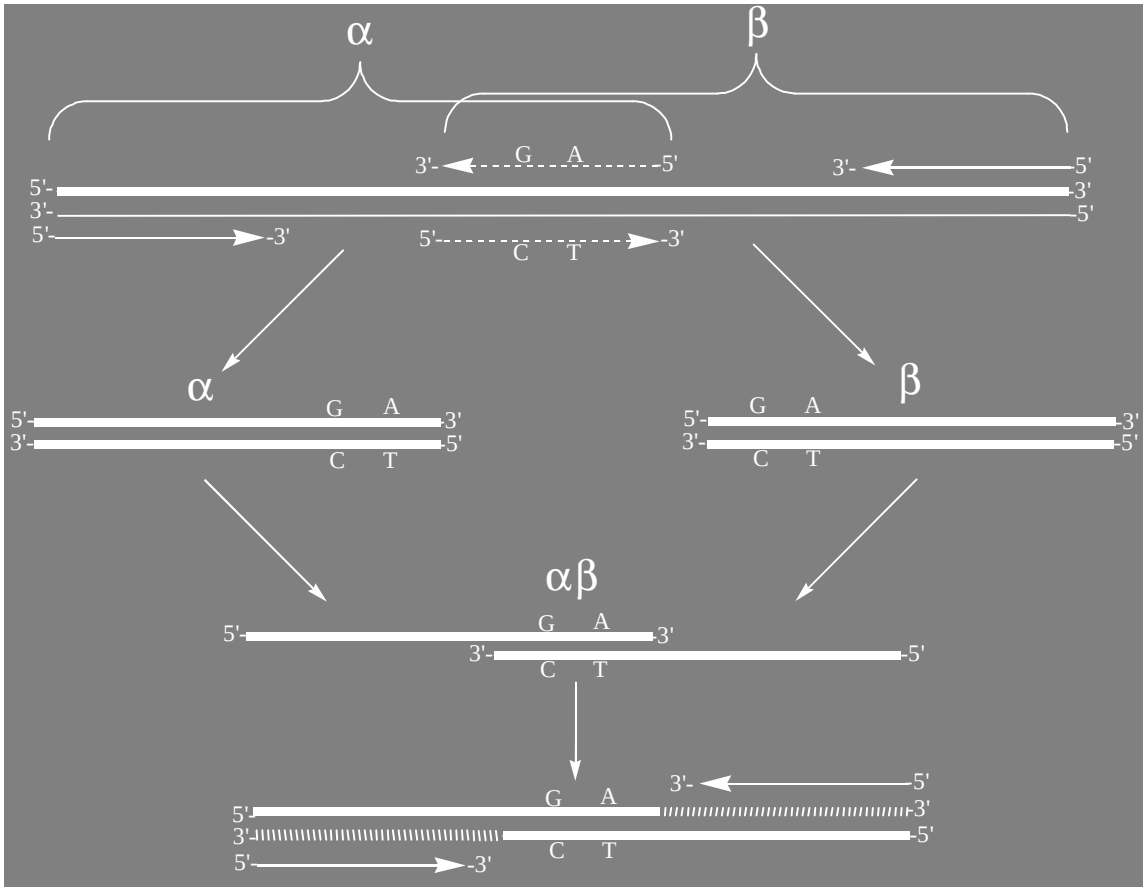

Figure 4-15: Generalized schematic representation of the recombinant PCR method

Subsequently, the α and β products are combined, and denatured such that as they renature, they can recombine to produce an αβ dimer. The two possible αβ dimer combinations afford only one product with a terminal 3' hydroxyl terminus capable of serving as a starting point for Taq DNA polymerase to extend the complete gene with desired mutations. Subsequent amplification of this product with the external primers produces sufficient quantities of the complete mutant gene sequence for subsequent manipulations.

For HPrγ, this process required an upstream α primer that was designed to bind significantly upstream of the gene sequence to produce a product large enough to visualize on an agarose gel. Figure 4-16 illustrates our experimental design. The internal primers contain two of the mutations tct→tat and cgt→cat, and the downstream β primer creates the E84Y conversion gaa→tac.

Figure 4-16: Primer design and binding for the α and β PCR reactions utilized to construct the HPrγ mutant gene sequence. Mutated codons in the primers are underlined.

The α reaction was performed with standard concentrations of all components (see experimental 2.3). The upstream α and downstream α primers were added to this reaction along with the template pNoTA/T7+ptsH plasmid generated previously. This reaction was run with an annealing temperature of 60^{o}C with a standard temperature profile. The resulting PCR product was analyzed by agarose gel electrophoresis, and is shown in Figure 4-17. Lane 2 shows the presence of an approximately 220 bp band that matches the expected mass for this reaction.

Figure 4-17: 2.0 % agarose gel electrophoresis of the α PCR reaction. Lane 1 contains the 100 bp DNA ladder, with the lower bands at 200 and 300 bp. Lane 2 contains the PCR α product, which is clearly in the 220 bp range (as expected). Lane 3 contains the 1 kb ladder with the lower band at 250 bp.

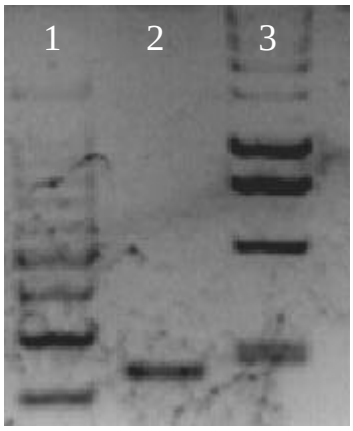

An analogous reaction was performed with the β primers and template DNA in a separate tube with an annealing temperature of 62 ^{o}C. An agarose gel analysis of this reaction is shown in Figure 4-18.

Figure 4-18: 2% agarose gel of the PCR β product. Lane 1 contains the 100 bp ladder. Lane 2 contains a PCR beta reaction control without template. Lane 3 contains the β PCR product at the anticipated 220 bp. Lane 4 is the 1 kb ladder with 250 bp at the bottom.

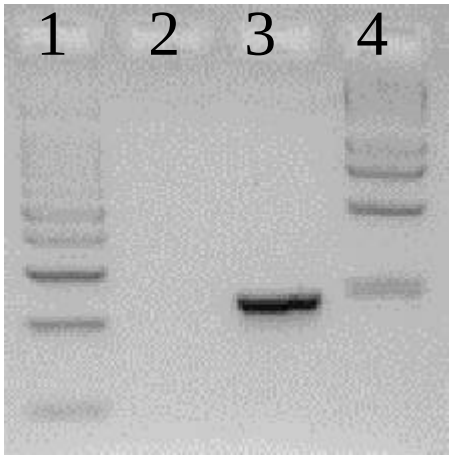

Following successful amplifications of the α and β segments of the HPrγ gene, each reaction was separately passed over a Qiagen PCR prep column to remove primers, oligonucleotides, buffers, and enzymes. Approximately 10 ng of each purified product

was added to a single tube, along with fresh aliquots of dNTPs, 10X Taq buffer, and **no primers**. Taq DNA polymerase was then added, and three cycles of 93^{o}C, 69^{o}C, and 72^{o}C @ 1 minute each were run. After completion of the third cycle, the external primers upstream α and downstream β were added at 1 μM each, and the reaction was run with continued for 20 cycles with a new annealing temperature of 62^{o}C. The resulting PCR products were analyzed by electrophoresis, which is shown in Figure 4-19.

The α + β PCR reaction from Figure 4-19 shows two distinct bands. One is a low molecular weight band at approximately 220 bp with a second, heavier fragment at approximately 450 bp. The recombinant product is expected at 420 bp, thus the

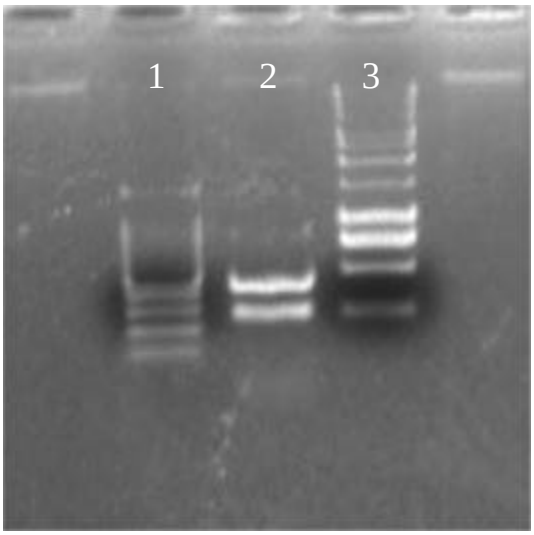

Figure 4-19: 2% agarose gel electrophoresis analysis of the recombinant PCR reaction which utilized the external primers → α and ← β. Lane 1 contains the 100 bp DNA ladder molecular weight marker. Lane 2 is the recombinant PCR reaction. Lane 3 contains the 1 kb DNA ladder molecular weight marker.

heavier PCR product was chosen as the band of our desired product. The source of the 220 bp fragment is not clear. However, its presence does not inhibit subsequent steps. We simply excised the 450 bp band and purified it out of the agarose slice in a procedure analogous to that described previously.

The gel purified recombinant PCR product was next subcloned into the pNoTA/T7 vector affords the advantages of facile DNA replication and sequencing. The BamHI/SacI digestion product of the purified plasmids (isolated from cultures taken from white colonies from the ligation transformations) is shown in Figure 4-20.

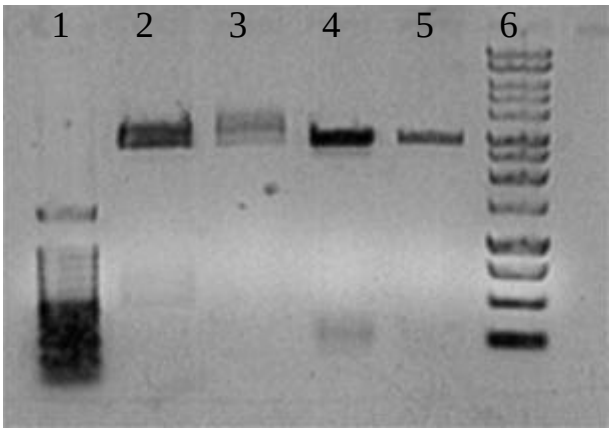

Figure 4-20: 1% agarose gel of isolated plasmids from the pNoTA/T7 subcloning of the recombinant PCR product. Lane 1 is 100 bp ladder. Lanes 2-5 are digested plasmids. Lane 6 is the 1 kb DNA ladder. The plasmid from lane 4 (HprγII#6) was chosen for sequence analysis.

The sequencing data for plasmid HprγII#6 showed that the recombinant PCR technique did produce a mutant ptsH gene, and every nucleotide in this sequence was exactly as desired except for one mutation. In both directions of sequence data, the nucleotide immediately following the α and β primer regions had been unintentionally converted from a C to an A. This result was puzzling initially, however the result makes perfect sense if you recognize that Taq DNA polymerase often will add an A nucleotide at the terminus of amplified PCR products. The new A mutation was the product of not cleaving this A prior to recombination of the two products. To solve this problem we simply treated the initial α and β PCR products with modifying enzyme from the pNoTA/T7 system (which removes the A overhangs), cleaned up the DNAs, and re-ran the recombinant reaction as before. This PCR product was subcloned into pNoTA/T7 as

before, and submitted for sequencing. The resulting sequence from this preparation is shown in Figure 4-21.

As is evident in the sequence data, we were able to successfully change three of the native HPr codons to the desired mutant codons in one PCR strategy. Additionally, the BamHI and SacI sites utilized previously are also incorporated. In this gene, however, the SacI site occurs immediately after the stop codon due to the constraint of incorporating the E84Y mutation in the downstream-β external primer sequence.

Following the construction of the HPrγ gene in the pNoTA/T7 vector, ligation within pCal-n vector as was accomplished for the native gene. As before, we double-digested the pCal-n vector and the plasmid containing the HPrγ gene with BamHI and

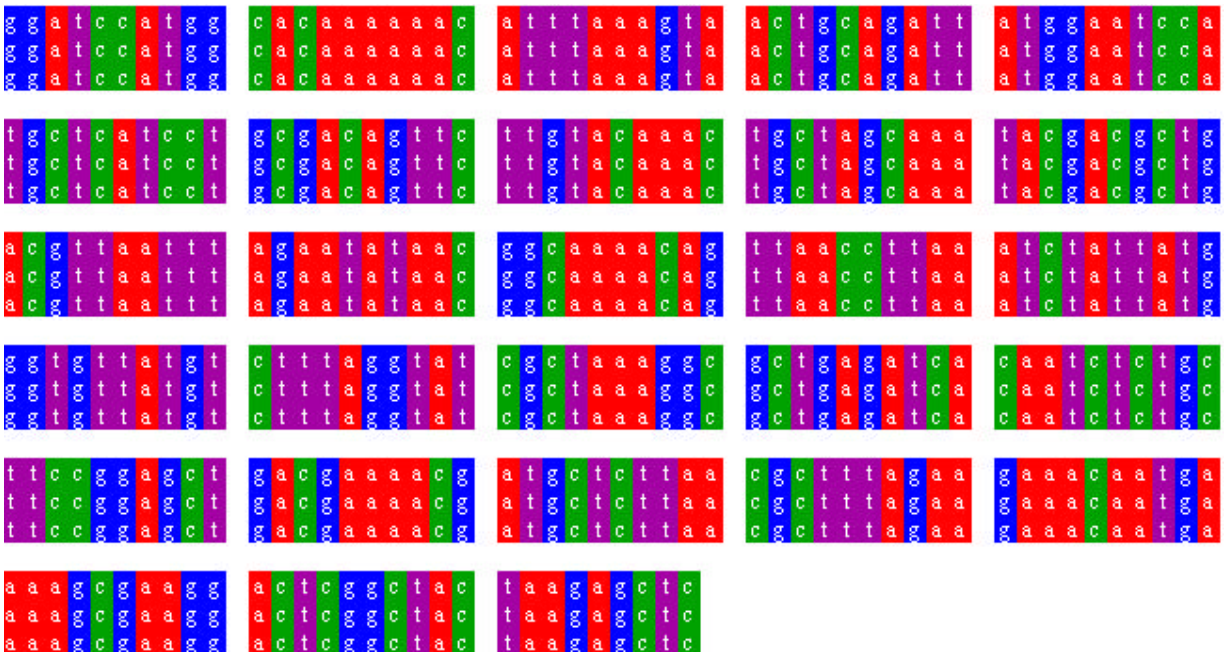

Figure 4-21: HPrγ sequence subcloned within the pNoTA/T7 vector.

SacI. The results of this are shown in Figure 4-22.

The pCal-n vector digest was purified differently than for the native HPr plasmid

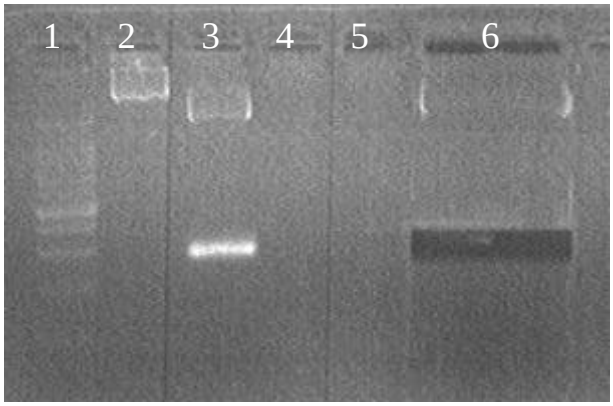

Figure 4-22: 1% agarose gel electrophoresis analysis of the preparative digestion of the HPrγ gene and the pCal-n vector. Lane 1 contains the 100 bp ladder. Lane 2 is 2-cut pCal-n. Lane 3 is a small aliquot of the 2-cut HPrγ + pNoTA/T7 construct. Lane 6 is the preparative gel slice removed to prepare the HPrγ insert DNA for ligation into pCal-n.

construction. Instead of gel purifying the cut vector, we applied it to a QiaQuick column (see experimental 2.4). This purification column can remove all contaminating DNAs of 50 bp length or smaller. Gel purification was required for the insert digest. Figure 4-22 presents the results of these operations. The band in lane 6 was excised, and purified with the QiaexII resin as described previously. Ligation reactions with purified vector and insert DNAs were performed for insert to vector ratios of 2:1 and 4:1, and were transformed into $CaCl_2$ competent *E. coli*. Media plates with 50 and 80 colonies respectively were produced from the transformation. Twenty-five colonies were selected from each of these plates to make duplicates for DIG analysis. The results are shown in Figure 4-23. We chose four of the colonies from this plate for further work and these are indicated with asterisks in Figure 4-23. These colonies were cultured, and plasmids from each were isolated and double digested with BamHI and SacI to screen for the presence

of the HPrγ insert. Figure 4-24 shows the results of this digest. Lane 5 of this gel has a

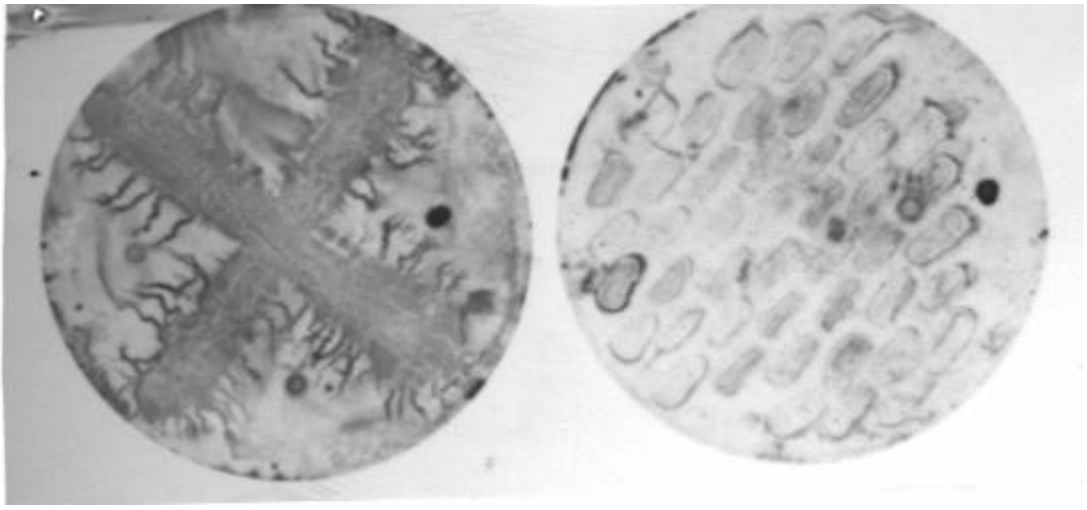

Figure 4-23: DIG analysis of the potential HPrγ containing colonies with pCal-n. On the left is the positive control plate and on the right is the replicate plate of transformants. Colonies with * symbols were chosen for screening by plasmid mapping.

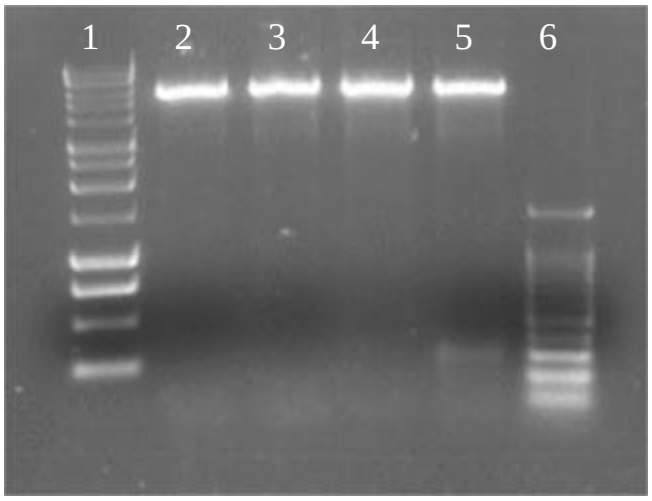

Figure 4-24: Digestion of pCal-n ligation products with the HPrγ gene. Lane 1 is the 1 kb ladder. Lanes 2-5 are plasmids 8, 23, 39, and 41 respectively. Lane 6 is the 100 bp ladder.

band of approximately 300 bp, which is consistent with the expected mass of 280 bp. Plasmid 41 from lane 5 was submitted to the Iowa State DNA Sequencing Facility, and the resulting sequence is shown in Figure 4-25. This DNA sequence data confirms that we have successfully incorporated our constructed HPrγ gene and inserted it within the

pCal-n vector in the proper orientation and reading frame. All three of the desired codon changes have been made, and induction of this pCal-n construct should result in the generation of a fusion protein containing our mutant HPrγ protein. This represents our

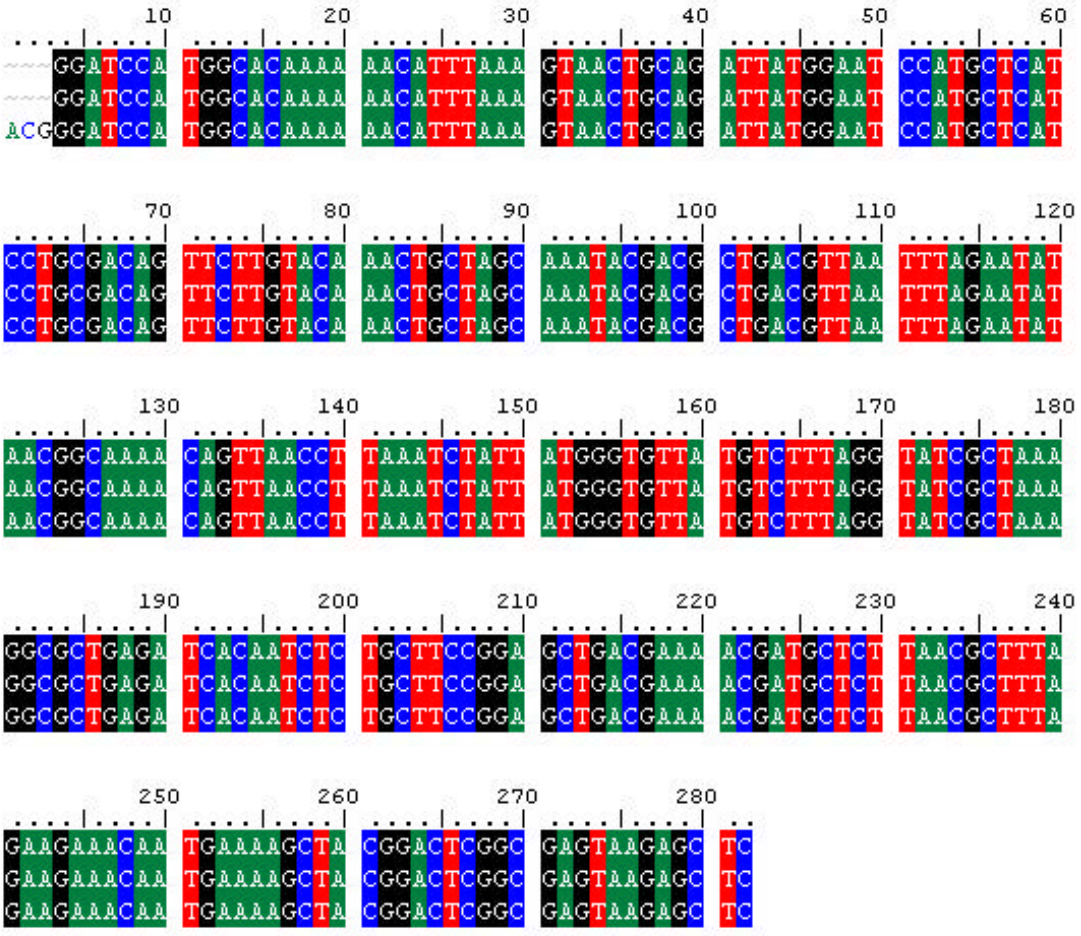

Figure 4-25: DNA sequence alignment of plasmid 41 from the pCal-n + HPrγ gene ligation. The top and middle strands are the forward and reverse PET primer sequences, while the bottom is the desired HPrγ sequence.

first successful mutant gene insertion within the pCal-n vector, and completion of this genetic construction and manipulation allows us to begin production of mutant protein.

4.4 HPrβ MUTANT GENE CONSTRUCTION AND CLONING

As discussed in Chapter 3, in our initial strategy to generate the HPrγ mutant, we planned to incrementally mutate HPr by first converting S12Y (Harπ), and then mutate Harπ to HPrβ through the R17H mutation. Finally, HPrβ was to be converted to HPrγ by the replacement of glutamate 84 with tyrosine. Due to time constraints, we were not able to carry out this strategy as planned, but instead directly converted HPr to HPrγ through the recombinant PCR technique discussed in Section 4.2 of this Chapter. However, we expected that the individual contribution of the E84Y mutation, located at the C-terminus of the protein sequence, was critical for our ability to make a PCD-type metalloprotein site with HPrγ. To test the importance of the E84Y mutation, the HPrβ was generated from HPrγ. To generate this gene, we designed a downstream primer containing the gaa codon at the 84 position, while using the HPrγ gene within the pNoTA/T7 vector as

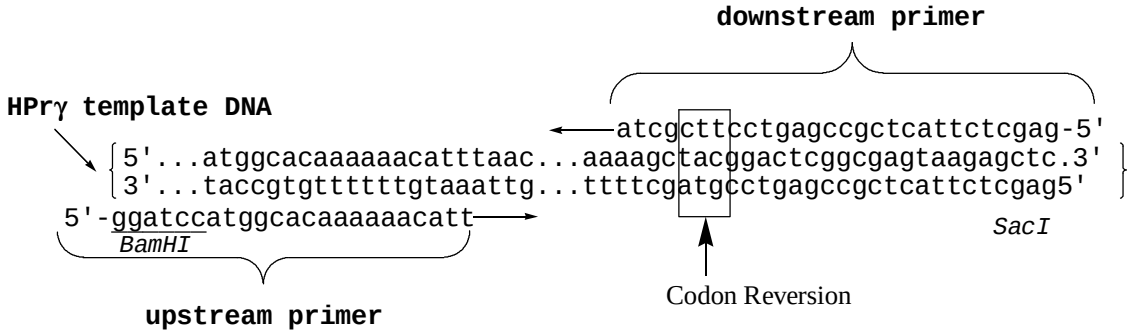

Figure 4-26: HPrβ gene construction strategy by reconversion of the E84Y mutation made for HPrγ back to the native glutamate.

template. Figure 4-26 shows the experimental design of this reaction.

This reaction was performed analogous to our previous PCR experiments except the annealing temperature used was 69 ^{o}C. The products of this reaction were run on agarose gel electrophoresis and the gel is shown in Figure 4-27. An approximately 300 bp band is present, which matches the expected product. The reaction was purified, and

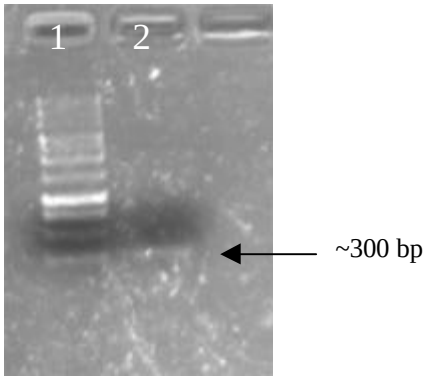

Figure 4-27: HPrβ gene PCR product. Lane 1 contains the 1 kb DNA ladder. Lane 2 is the PCR reaction containing the anticipated ~300 bp product.

the PCR product was subcloned into pNoTA/T7 analogous to our previous procedures. Figure 4-28 presents the agarose gel analysis of the plasmids screened by BamHI/SacI digestion. From this image, plasmids 1, 2, and 3 all contain insert DNA, and plasmid 3

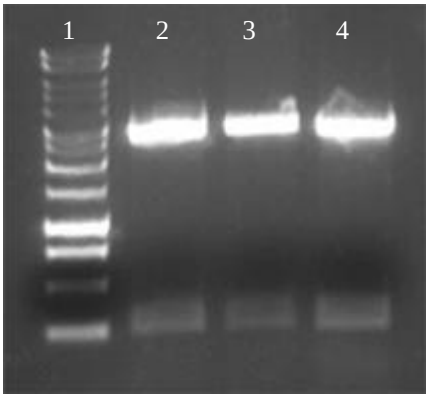

Figure 4-28: pNoTA/T7 subclones of the HPrβ gene. Lane 1 contains the 1 kb DNA ladder. Lanes 2-4 contain plasmids 1, 2, and 3 respectively. The plasmid from lane 4 was chosen for submission for sequence analysis.

was chosen for sequence analysis. The DNA sequence from this analysis is shown, Figure 4-29, confirms we were able to successfully revert the tac codon back to its native gaa sequence.

Ligation of pCal-n with the HPrβ gene was performed analogously to our previous procedures. The transformations of these ligations produced only 30 colonies,

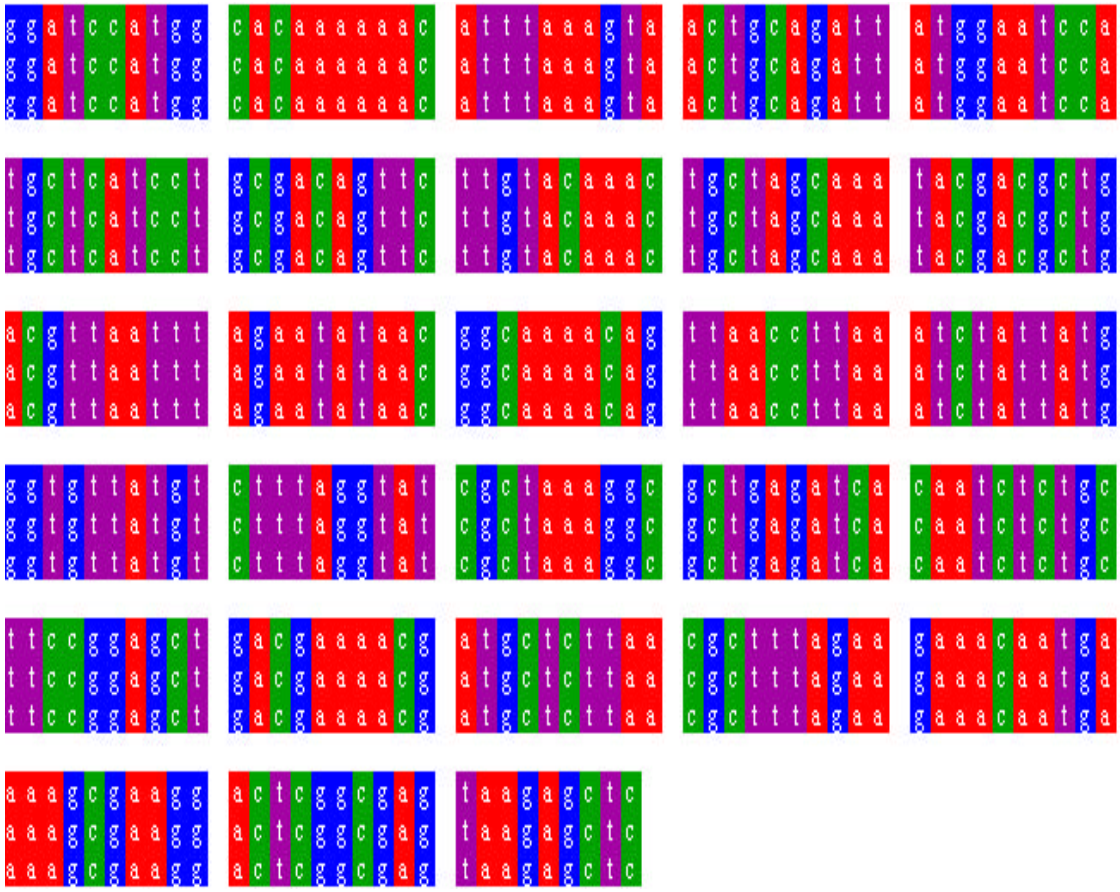

Figure 4-29: HPrβ DNA sequence alignment within the pNoTA/T7 subcloning vector.

that were screened by digestion methods. Plasmid Y was found to contain insert by the agarose gel analysis shown in Figure 4-30.

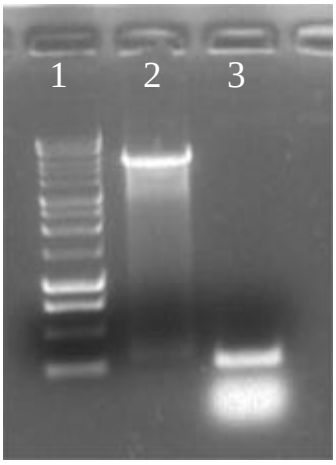

Figure 4-30: Agarose gel analysis of plasmid Y digestion with BamHI and SacI. Lane 1 contains the 1 kb DNA ladder. Lane 2 is the digested plasmid Y. Lane 3 contains an old PCR product of HPrβ as a mass reference.

This plasmid Y was submitted for sequencing and the alignment is shown in Figure 4-31. This successful cloning concludes our genetic manipulations for HPrβ.

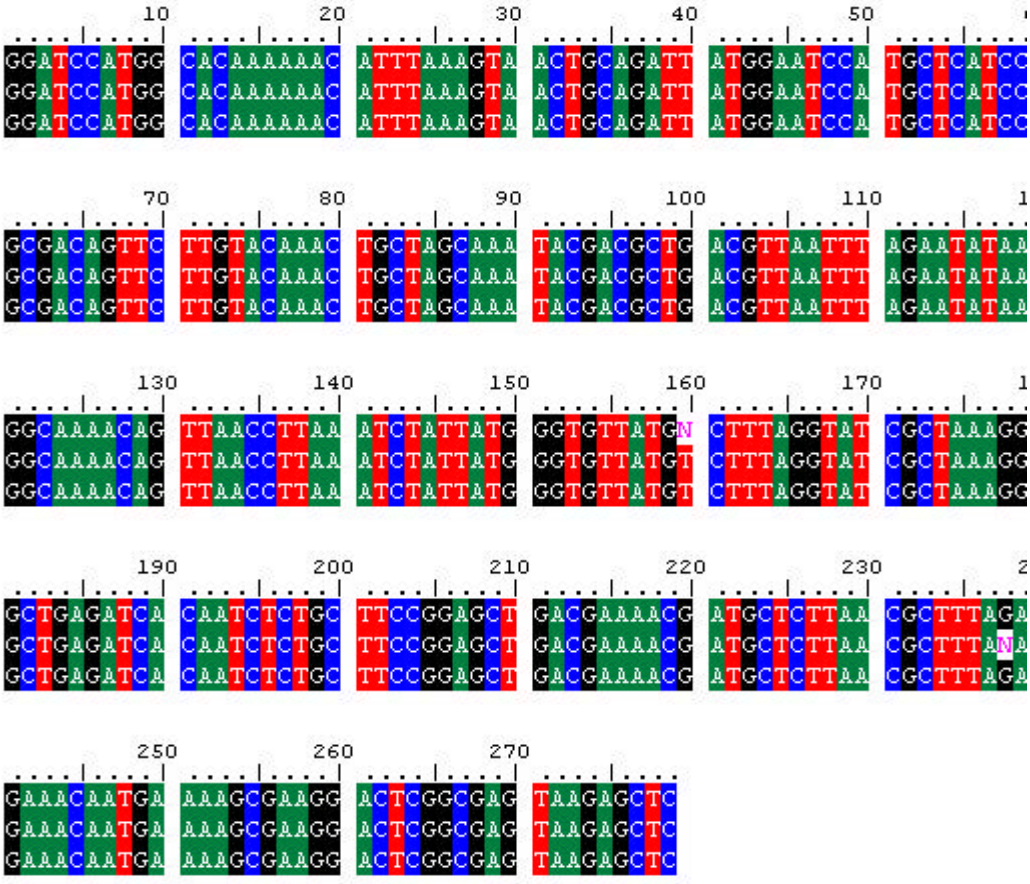

Figure 4-31: Hprβ + pCal-n sequence alignment confirming completion of the HPrβ DNA manipulations

4.5 SUMMARY

Through our subcloning and cloning strategy we have successfully incorporated the native ptsH gene into pCal-n. Recombinant PCR techniques allowed us to mutate three codons of this native ptsH gene sequence to create the HPrγ mutant gene that codes for S12Y, R17H, and E84Y mutations. We subsequently subcloned and cloned this mutant gene into pCal-n analogous to the native HPr gene sequence. Finally, using a single PCR reaction, we reverted the E84Y mutation back to its native glutamate to produce the HPrβ mutant construct designed to test the role of tyrosine 84 in metal-binding. These three genetic constructs will enable us, if successfully expressed and purified, to explore the metal-binding properties of the modified phosphate-binding sites.

4.6 REFERENCES

[1] Reizer, J. Sutrina; S. L.; Saier, M. H.; Stewart, G. C.; Peterkofsky, A.; Reddy, P. The Embo Journal, 1989, 8, 2111-2120. ref.
[2] Reizer, J.; Sutrina, S. L.; Wu, Long-Fei; Deutscher, J.; Reddy, P.; Saier, M. H. *J. Biol. Chem.* **1992**, *267*, 9158-9169.
[3] Simcox, T. G.; Zheng, C. F.; Simcox, M. E.; Vaillancourt, P. *Strategies***, 1995**, *8*, 40-43.
[4] PCR Cloner system manual, 1997, 5-prime 3-prime Inc.
[5] Sambrook, J. et al., eds 1989 Molecular cloning: a laboratory manual, 2nd ed., Cold Spring Harbor Laboratory Press, Cold Spring Harbor.

Chapter 5

PROTEIN EXPRESSION, PURIFICATION, & CHARACTERIZATION

5.1 INTRODUCTION

A critical step in this research project is the effective production of large quantities of recombinant protein. As described in Chapter IV, we utilized the pCal-n expression vector to construct our gene-containing plasmids. This vector DNA, illustrated in Figure 5-1, contains a T7 promoter sequence followed by a lac operator

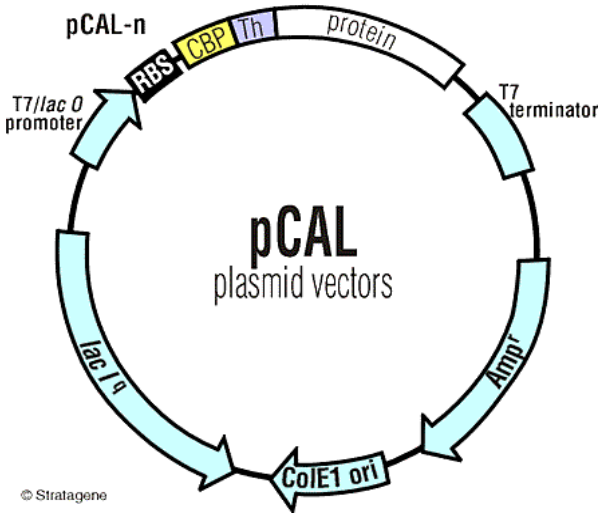

Figure 5-1: pCal-n expression vector map from Stratagene®.

sequence immediately downstream of the promoter. It also contains the natural promoter and coding sequence for the lac repressor protein (lac I), which is inducible with the lactose analog IPTG. For our three constructs, proper incorporation of the target genes into the BamHI site of the pCal-n vector should allow effective transcription and translation of a calmodulin binding peptide followed by our target sequences. Once expressed, the proteins can be purified from the crude cellular lysate, and characterized. Cleavage of the affinity tag can also be performed if necessary to evaluate the role it might play in the structure of our recombinant proteins. In this chapter we describe our

efforts to express and purify HPr and its mutants. Additionally, activity analyses, tag cleavage, and mass spectrometric analyses will be described to provide characterization of the proteins and their inherent activity.

5.2 NATIVE HPR EXPRESSION

The DNA sequence for HPr was confirmed from plasmid-β isolated from a single colony of the XL1Blue strain of *E. coli*. This strain of *E. coli* is not suitable for pCal-n induction because it lacks the lacUV5 promoter, lacI gene, and the gene for T7 RNA polymerase. Thus we transformed our plasmid into the BL21(DE3) strain of *E. coli* (Novagen) This host does not inherently afford antibiotic resistance, thus successful incorporation of the pCal-n vector results in resistant colonies that can grow in LB media containing ampicillin. For plasmid-β, this transformation resulted in 490 individual colonies. One colony was selected, and plasmid DNA was isolated with the Qiagen miniprep protocol described previously. Sequence analysis of this plasmid matched that of the plasmid from the subcloning host.

For our expressions of HPr protein, we followed the method described in Section 2.14. One goal of our early expression work was to establish the optimal conditions of native HPrs expression, while minimizing the background, uninduced protein levels. To accomplish this, we performed a titration of the inducing agent IPTG with the addition of increasing amounts to four identical cultures at OD600 = 0.6. Figure 5-2 illustrates an analysis of this titration experiment with sodium dodecylsulfate polyacrylamide gel electrophoresis (SDS-PAGE) (section 2.2) of the resultant crude lysates. For these

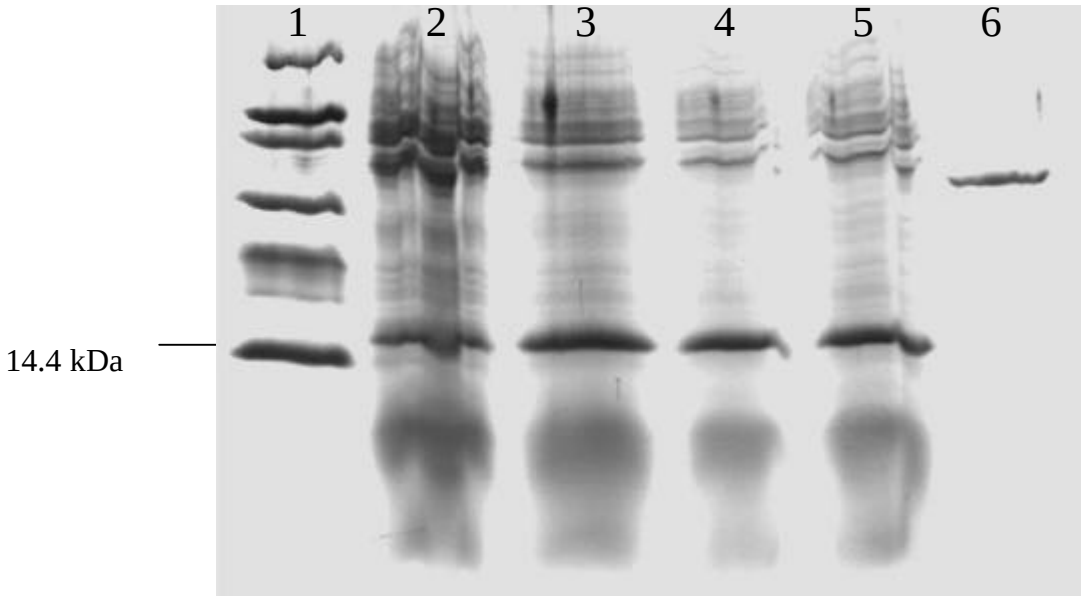

Figure 5-2: SDS-PAGE analysis of cell free extracts obtained from cultures induced with increasing concentrations of IPTG. Lane 1 is mass marker. Lanes 2-5 contain 0.5, 1.0, 1.5, and 2.0 mM concentrations of IPTG. Lane 6 is a reference protein (Yop51*Δ162).

bacterial lyses, 10 μL Lamelli buffer was added to 20 μL aliquots of resuspended cells, then each was boiled for 10 minutes to rupture the bacterial cells. From this gel, it is evident that an overexpressed protein with apparent molecular near 16,000 Da is present using all four IPTG concentrations. We believe that this band, although larger than the anticipated mass of our native HPr protein (12, 900 Da), is the desired protein, which is migrating with a heavier apparent molecular weight. From this analysis, we chose 1 mM IPTG as our standard induction concentration because it gives the highest levels of target (apparent) protein relative to background protein levels. Inductions with no IPTG and 1.0 mM IPTG at various culture densities were also performed. No IPTG in the BL21 (DE3) strain did produce some "leaking" expression, that at approximately one tenth the protein level of induced expression. In the BL21 (DE3) pLysS strain of *E. coli*, which is

designed for expression of extremely toxic proteins to minimize uninduced "leaking", no expression above background was observed without induction. Furthermore, induced levels of ~ 16 kDa protein were much lower than their BL21 (DE3) counterparts. Therefore, due to the non-toxic nature of HPr, and the reduced expression levels under tighter regulation, we chose to utilize the BL21 (DE3) strain throughout our studies. The influence of cell density prior to induction was also tested and did not produce significant differences in expression levels of target protein.

In summary, the plasmid-β construct of pCal-n containing the native HPr gene was apparently inducible in the BL21 (DE3) strain of *E. coli*, and the conditions for overexpression were optimized. The apparent molecular weight of this tagged protein is approximately 3,000 Da heavier by SDS-PAGE analysis than anticipated. We found that induction at a culture OD600 from 0.6 to 1.0 in the presence of 1.0 mM IPTG was most effective in generating large quantities of template HPr protein. Further examination of this expression product through purification, activity analysis, and spectroscopic characterization should provide further evidence to support our observation that the ~ 16 kDa band is our recombinant HPr protein.

5.3 HPR PURIFICATION

Although our expression experiments produced high levels of protein in the desired region, we did not have concrete evidence that this protein was actually our target HPr protein. Therefore, we turned to the purification procedures. Successful binding

and elution of tagged protein would identify, from the multiple proteins in the cell free extract, which protein(s) contain the calmodulin purification tag.

The pCal-n purification system, illustrated in Figure 5-3, was chosen for several key advantages to other expression systems available at the time of our experimental design.[1] - First, the purification process does not involve direct metal coordination to the purification tag such as the His-tag purification system. - Secondly, the binding and elution conditions are mild in terms of pH and ionic strength that will inhibit loss of protein, due to structural disruption, during the purification process. - Finally, the purification tag is cleavable with low concentrations of thrombin. This feature was very important to allow us to probe the metal-binding properties of the protein in the presence

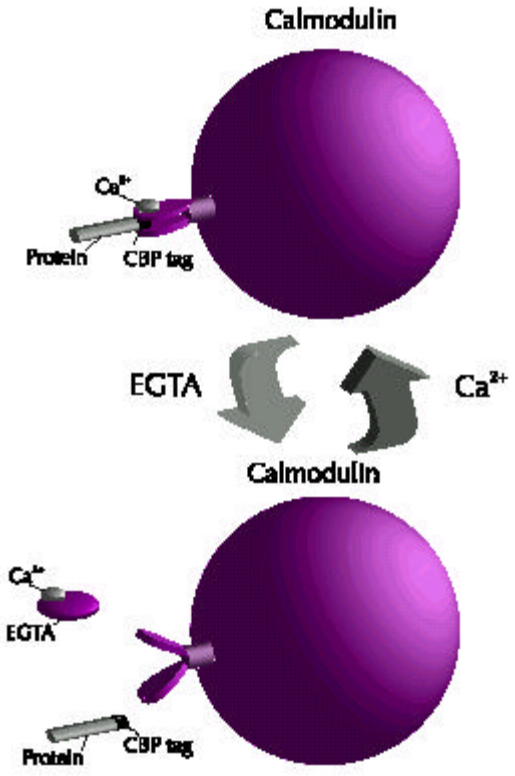

Figure 5-3: An illustration of the pCal-n purification process-Stratagene.[1]

and absence of the purification tag.

The purification procedure utilizes a calmodulin affinity resin that, in the presence of low concentrations of Ca^{2+} ions, forms a structural conformation with high affinity ($K_d = 10^{-9}$) for the 26-amino-acid calmodulin binding peptide expressed at the N-terminus of our HPr protein sequence. Thus cell free extract passed over the resin in the presence of Ca^{2+} ions will flow through, while the calmodulin binding peptide (CBP) and attached target protein will remain bound. Addition of EDTA, EGTA, or other strong Ca^{2+} chelators will remove the calcium from the calmodulin resin, and cause the calmodulin to undergo a conformational change which releases the CBP and attached target protein.

Our initial attempts to purify tagged HPr were based on the pCal-n system recommendations.[1] Small scale purifications were performed to optimize the conditions of purification with mixed results (Section 2.16-A) Repeatedly we were able to bind and elute the ~16kDa band which we felt was our desired protein, however several other proteins also appeared to bind and elute under the conditions of the purification. This non-specific binding caused us to alter the concentration of Ca^{2+}, the scale of the purification, and finally the ionic strength of the solution during binding and elution. Neither Ca^{2+} concentration nor purification scale appeared to significantly reduce the non-specific binding, however the ionic strength changes did appear to slightly reduce these binding of theses undesired proteins. We continued to increase the ionic strength from 50, to 100, 200, 300 and finally 400 mM NaCl. This highest ionic strength did eliminate the non-specific binding.

We also tested the feasibility of binding at 400 mM NaCl, then eluting with much lower ionic strength. Although this did result in the elution of some ~16 kDa protein, the yield was quite low. Subsequent elution with CABB-400 resulted in full elution of bound protein.

From these small-scale experiments, we were able to optimize the conditions to purify HPr from the cell free extract, and subsequently scale-up the purification procedure to produce large quantities of protein. Our procedure for the large-scale purification differed from the small-scale experiments in several areas. First the resin was equilibrated with cell free extract (10 mL of resin per liter of culture) on an orbital shaker for 1 hour on ice. This resulting slurry was packed into a 2.5 cm x 20 cm column, and washed with CABB-400 until the absorbance at 280 nm was less than 0.01. The resin was then eluted with 3x50 ml washings of EB-400, and each elution fraction was collected and run on SDS-PAGE. Figure 5-4 shows a SDS-PAGE analysis of a successful large-scale purification. From this gel, it can be seen that our French Pressure method of lysis is much more effective than sonication method used for this strain evidenced by the concentration of proteins in lane 2 vs. lane 3. From lanes 1-4 it can be seen that an intense band is present at ~16 kDa. The presence of this band in the flow through (lane 4) suggests that the purification procedure is allowing some of the target protein to pass through. This is probably the result of an insufficient resin to protein ratio. Lane 5 contains a single, intense band of ~16 kDa is present in this first elution fraction of 50 mL. Lanes 6 and 7 contain subsequent 50 mL elution fractions 2 and 3. These results show that our tagged HPr protein does migrate at ~ 16 kDa, and the reasons

for are unclear. Perhaps HPr's amino acid composition, or stability to denaturation in

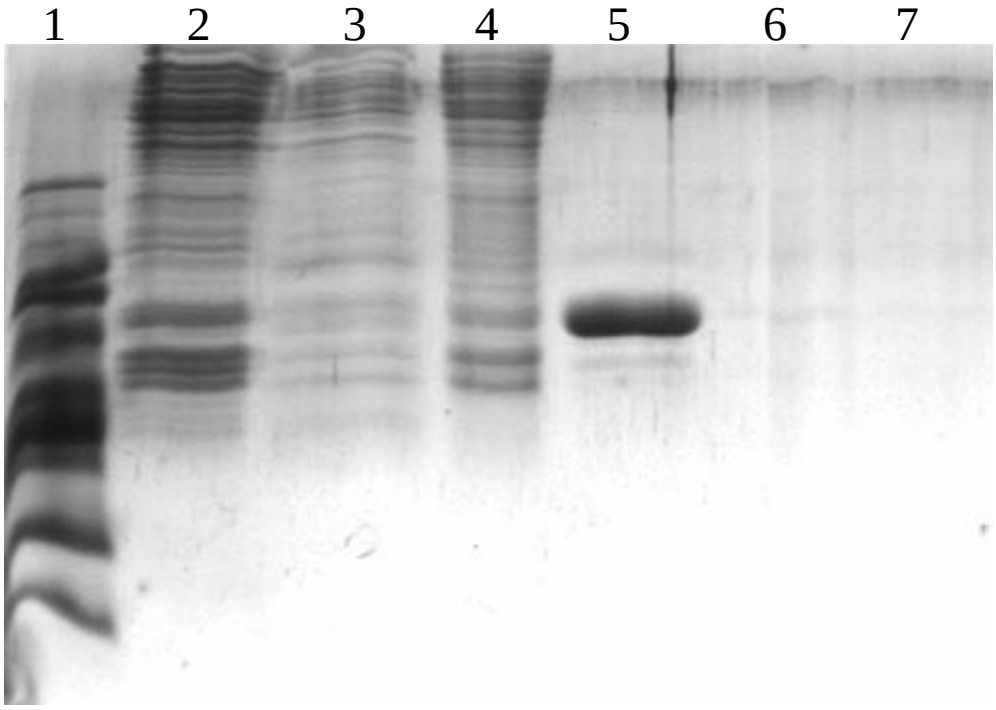

Figure 5-4: Large scale purification of HPr. Lane 1 contains molecular weight marker. Lane 2 shows the French Pressure lysate. Lane 3 contains sonicated lysate. Lane 4 is the column flow through. Lane 5 is elution 1. Lane 6 is elution 2. Lane 7 is elution 3.

SDS relative to the standard proteins differs enough to produced the observed. Alternatively the pCal-n construct is not functioning properly, and is producing the wrong protein. Further evidence is needed to prove this is our template HPr protein, and explain this migration discrepancy.

Spectroscopic analysis of fraction 1 by UV-Vis spectroscopy is a valuable tool to assist in the quantitation of protein levels through A280 measurements and protein assays. Additionally, UV-Vis spectroscopy serves to identify the levels of nucleotide, which absorb at 260 nm, in the "pure" protein samples. Thus comparison of the A280 versus the A260 values provides a reasonable estimate of the levels of nucleotide

contamination in purified protein. Figure 5-5 shows the UV-Vis spectrum of an undiluted sample of fraction 1 from the purification of Figure 5-4. The A280/A260 ratio of 0.26 indicates that little nucleotide contamination is present in the purified protein

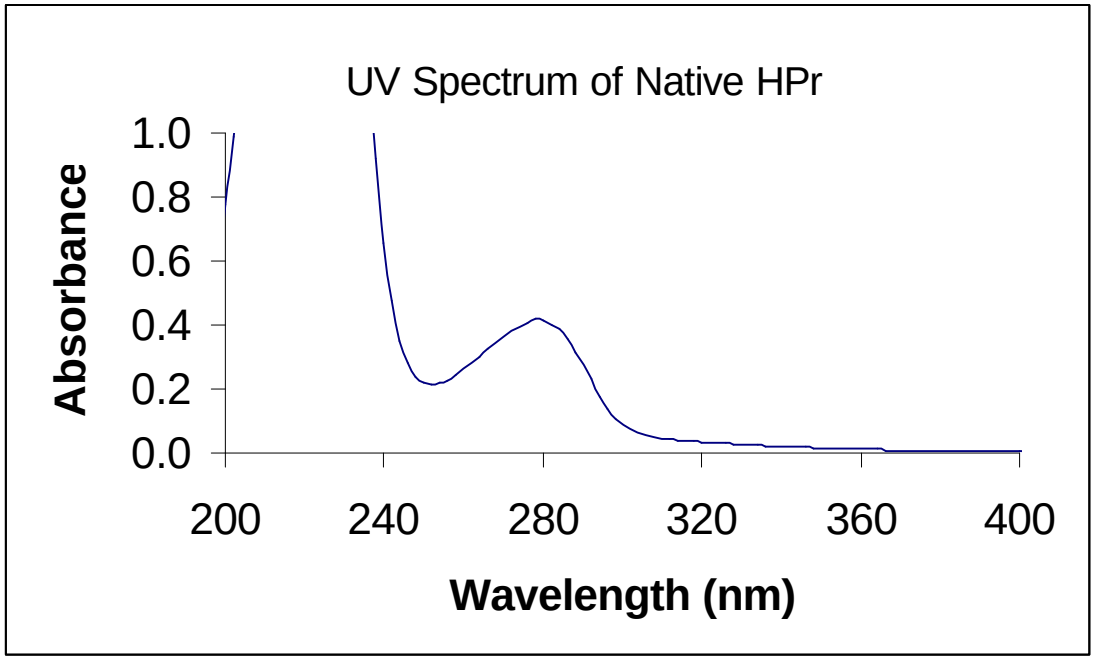

Figure 5-5: UV-Vis of fraction 1 from the HPr large scale purification from Figure 5-4.

preparation.

Based on the amino acid sequence, an extinction coefficient of 0.6 mg/mL can be calculated.[2] If this value were correct, it would result in an HPr concentration of 0.7 mg/mL.

The protein levels were also analyzed using Hartree-Lowry and Biuret assays as described in section 2.12. The results of these assays were consistent within 10 %. We chose to use the Hartree-Lowry method routinely, and the results of this assay indicated that the extinction coefficient of native HPr was 0.71. Thus, fraction 1 from our large

scale purification has a protein concentration of 0.58 mg/ml at a total volume of 50 ml. Thus from 1 L of culture, we have generated 30 mg of pure HPr.

Although we have successfully purified HPr, the higher NaCl concentrations necessary to eliminate non-specific binding during purification were somewhat of a concern. Would the high ionic strength affect activity or metal binding studies? In an effort to address this question, and to test HPr's solubility in various buffer conditions, we performed several dialysis procedures in which we lowered the salt concentration, exchanged the buffer, and altered the solution pH. We found that overnight dialysis in 10,000 MW dialysis tubing did not result in significant loss of protein through the dialysis membrane. Lowering the salt concentration from 400 to 100 mM did not effect protein stability; however, a further decrease to 20 mM caused precipitation of approximately 10 % of the protein sample. Neither exchange of the buffer from 50 mM to 20 mM Tris nor pH changes from 7.0 to 8.5 in Tris cause a decrease in soluble protein levels. Exchange of buffer solutions from 20 mM Tris (pH = 8.0) to 20 mM Sodium Acetate (pH = 4.8) also did not result in HPr precipitation. Exchange of HPr into HEPES buffer at 20 mM NaCl caused a loss of approximately 40 % of HPr, while DMG buffer caused nearly 90 % of HPr in solution to form insoluble material which was not redesolvable.

In summary, these results conclusively show that we are able to express and purify tagged HPr protein, which in conjunction with the DNA sequence data indicates we are producing high levels of pure HPr (with the affinity tag). The small-scale purifications were extrapolatable to the large-scale procedure, and resulted in production

of 50 mL of a pure protein at approximately 0.6 mg/mL. We also found that steep ionic strength changes and exchange of buffers to DMG and HEPES resulted in significant loss of the protein due to precipitation. Further analysis is still necessary to explain the SDS-PAGE migration discrepancy.

5.4 HPr PURIFICATION TAG CLEAVAGE

To further verify the integrity of the 16 kDa protein, we attempted to cleave the purification tag. At the interface between the calmodulin binding peptide tag (CBP) and HPr protein sequences is a six amino acid thrombin protease recognition site, which should allow thrombin to cleave the protein at a single point between peptides arginine and glycine. In our construct, this would produce a 3.5 kDa and a 9.4 kDa fragment. Utilizing 1/250 w/w addition of thrombin, we incubated the protein at 37^{o}C for 4 hours and ran an SDS-PAGE analysis of the digestion along with control samples from the immediately preceding expression (Figure 5-6). Lanes 2-5 indicate that we can reproducibly produce pure HPr (tagged), although expression levels in this batch appear to be lower (relative to background protein) than our earlier or subsequent preparations. Regardless, the resin appears to be able to isolate the target protein from even low-level expression. The most important feature of this gel is lane 7, in which the purified protein has been reduced in mass to near 10,000 Da. This result further supports the notion that the ~16 kDa protein is indeed HPr. In addition, this conclusively shows that the ~16 kDa protein does contain the purification tag, and it is fully cleavable. This cleavability suggests that the purification tag is in a conformation with HPr that does not bury, but

exposes the link between the HPr and the CBP tag to allow thrombin to bind and cleave its recognition site.

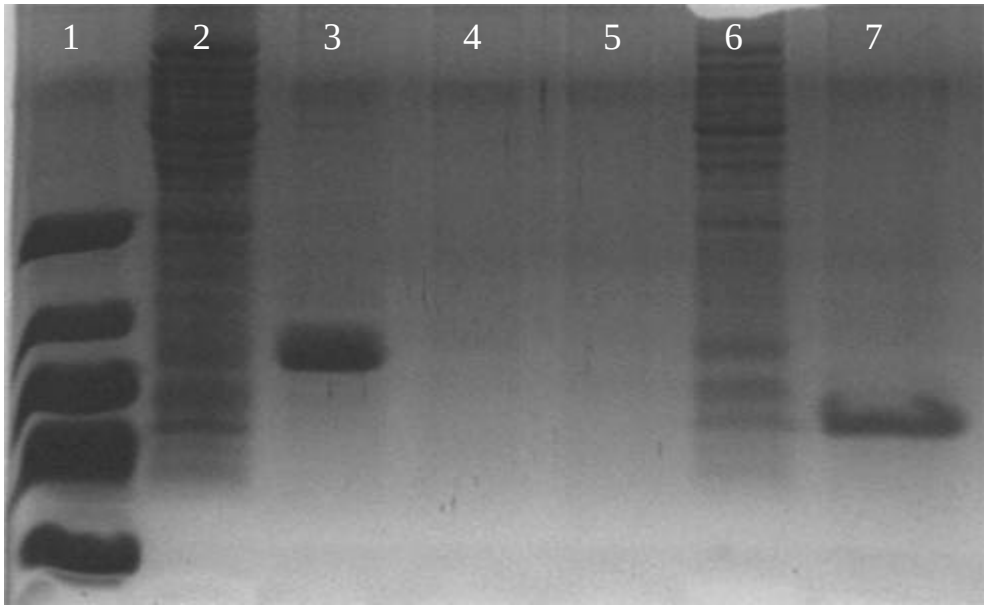

Figure5-6: HPr purification and Thrombin digestion. Lane 1 contains MW marker. Lane 2 is crude lysate. Lane 3 is elution fraction 1. Lanes 4 & 5 are elutions fractions 2 & 3. Lane 6 is dilute crude lysate. Lane 7 contains the HPr digestion.

We also probed the temporal profile of tag cleavage to optimize the conditions for maximum cleavage with minimum digestion time and thrombin. Figure 5-7 depicts an SDS-PAGE analysis our first time-course experiment.

From this gel, it is apparent that over time, a 1/500 w/w addition of thrombin increasingly cleaves tagged HPr. However, the cleavage is not complete under these conditions over an 8-hour period. We were to observe the presence of the 3.5 kDa calmodulin binding protein tag, which migrates in the expected mass range.

The SDS-PAGE analysis of Figure 5-8 also shows several new bands. This is especially apparent in lane 5 (~ 12 kDa band without thrombin present) and lane 9 in

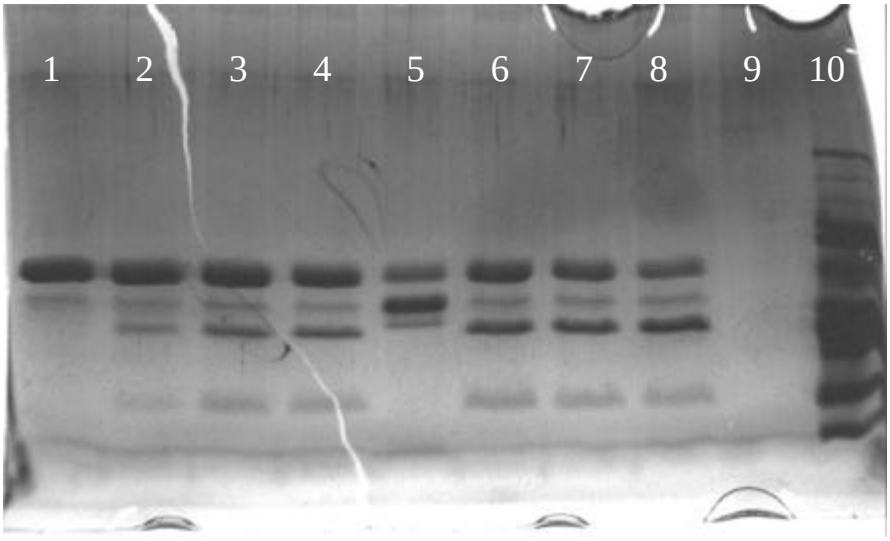

Figure 5-7: SDS-PAGE analysis of a thrombin cleavage reaction monitored over time. Lane 1 is time=0. Lanes 2-4 contains times of 1.0, 2.0, and 3.0 hours respectively. Lane 5 contains uncut protein 8 days old. Lanes 6-8 are times 4.0, 5.0, and 7.6 hours. Lane 9 contains a 22 hour digested sample. Lane 10 is MW marker.

which all the protein has been consumed. This can be explained by bacterial contamination, which was observed in the protein solutions after prolonged storage (bacterial smell) To eliminate this problem, we filtered our protein solutions with a 0.2 micron sterilization filter, which alleviated the problem and all subsequent protein preparations. Although this time course experiment was contaminated, it provided the necessary information to perform subsequent digestions with 1/250 w/w thrombin and achieve complete cleavage over a 4-hour incubation period.

The masses of the digested protein appeared to be more consistent with expectations relative to the molecular weight marker. This suggests that the fusion protein combination of HPr and tag migrates more slowly, possibly due to the existence of two spatially separated structural domains (HPr and tag). To fully clarify this issue, we used Matrix Assisted Laser Desorption Ionization-Time of Flight mass spectrometry

(MALDI-TOF MS) analysis to obtain more accurate masses of the tagged and cleaved protein. This is a standard method for analyzing protein samples due to its soft ionization ability and its large mass window. MALDI-TOF MS is less accurate than other method; however, for our purposes, 0.1 % error suitable accuracy to confirm the identity of our recombinant protein. The results for tagged HPr are shown in Figure 5-8. From this analysis, the tagged protein has a m/z of 12,862, which assuming a Z = 1) is the same as the calculated mass of tagged HPr, 12859 utilizing external calibration. This confirms that the ~16 kDa band on SDS-PAGE actually has a mass of 12,862 +/- 13 Da as expected based on the DNA sequence.

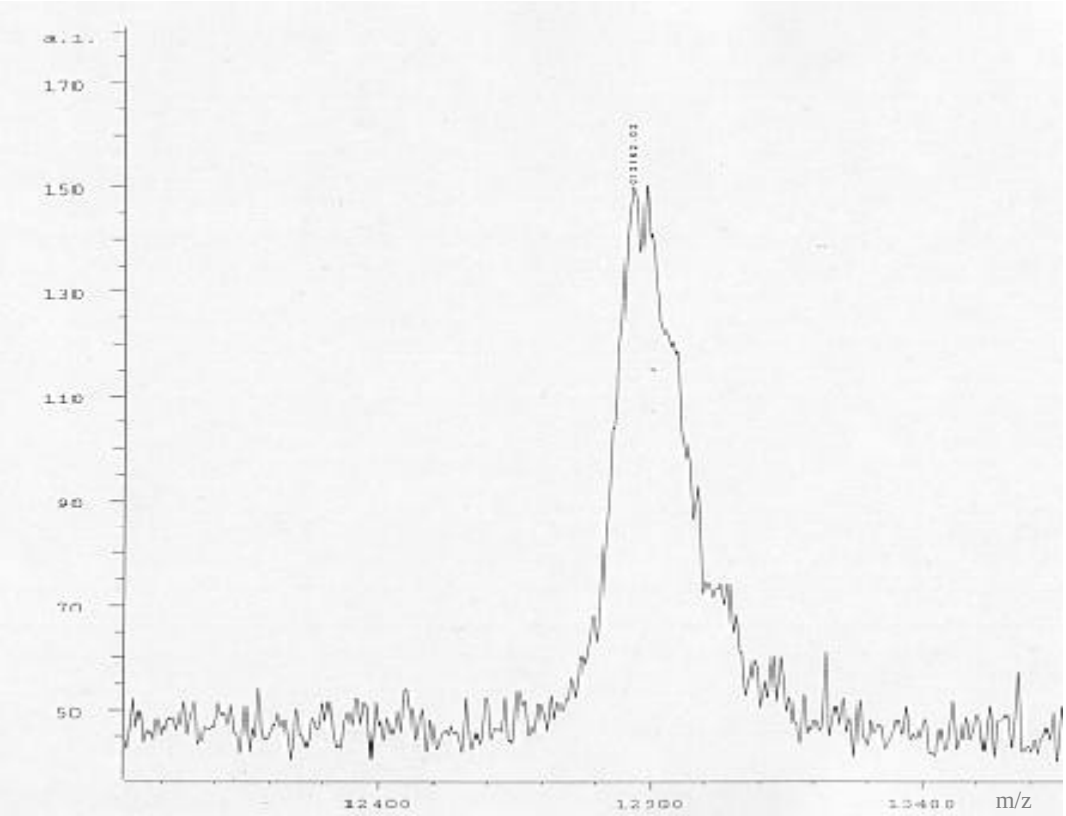

Figure 5-8: MALDI-TOF MS spectrum of native HPr calibrated against horse heart myoglobin.

We also ran MS on the thrombin digestion reaction products. These partial digests allowed us to observe signals from both the uncut HPr and the digestion products. Figure 5-9 shows this analysis, and reveals the presence of several key features. First, the uncut protein is observed at 12,862, and its doubly charged signal is also present at 6,431 is also present. These are consistent with the calculated values of 12,859 and 6,430 respectively. At 9,317 an intense band is observed, consistent with the cleaved HPr

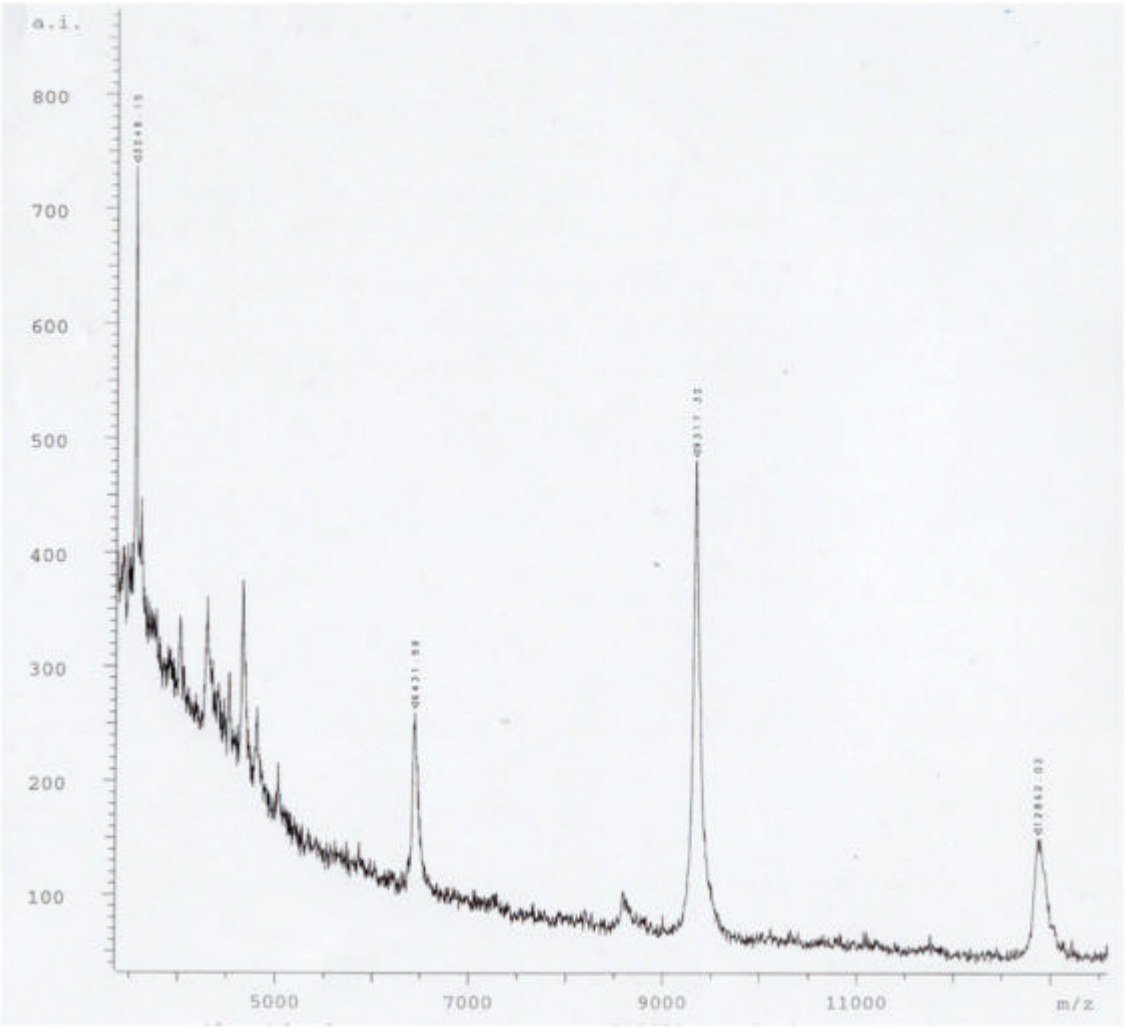

Figure 5-9: MALDI-TOF MS spectrum of a thrombin digestion reactions of native HPr.

fragment which has a theoretical mass of 9,315 Da. Finally, the CBP tag protein fragment should be observed at m/z = 3,543 for the singly charge species. In the spectrum we see an intense band at 3,548 which matches the calculated value within the limits of the measurement. Taken together, these MS results confirm that the recombinant protein we have expressed and purified is our native HPr protein, and both the masses of tagged and thrombin cleaved fragments match those anticipated for their respective amino acid sequences. In addition, these results show that the apparent migration properties of our tagged HPr at ~ 16kDa are not the result of the production of an incorrect protein. Therefore, the large mass displayed on SDS-PAGE analysis must be caused by the fusion proteins structure presence, or the HPr amino acid composition.

In summary, we successfully overexpressed native HPr from B. subtilis with the calmodulin binding peptide at its N-terminus. We optimized the conditions for expression, and developed a protocol to purify the tagged protein on both small and large scales. We solved the problem of non-specific binding during HPr purification by increasing the NaCl concentration to 400 mM during the binding and eluting steps. We elucidated the buffer conditions in which HPr could be stably handled by successfully dialyzing it in various buffer and ionic strength environments. We successfully cleaved the purification tag, which suggested that the ~ 16 kDa protein is indeed our desired CBP-HPr fusion protein, and we optimized the conditions for tag cleavage. MALDI-TOF MS data confirmed expected molecular masses of the CBP-HPr fusion protein as well as HPr itself. The disparity between the calculated and observed protein masses as determined by SDS-PAGE probably derived from the presence of the CBP tag, or HPr's

amino acid composition. These results provide definitive evidence that we are expressing and purifying an HPr fusion protein with a function and cleavable CBP.

5.5 HPRγ EXPRESSION AND PURIFICATION

Expression of HPrγ was performed in an analogous manner to the native protein. Again BL21 (DE3) cells were transformed with, in this case the gamma-Y plasmid. French Pressure lysis and a large scale purification of the resultant cell free extract with 3 elutions of 50 ml each yield the samples depicted in the SDS-PAGE gel from Figure 5-10.

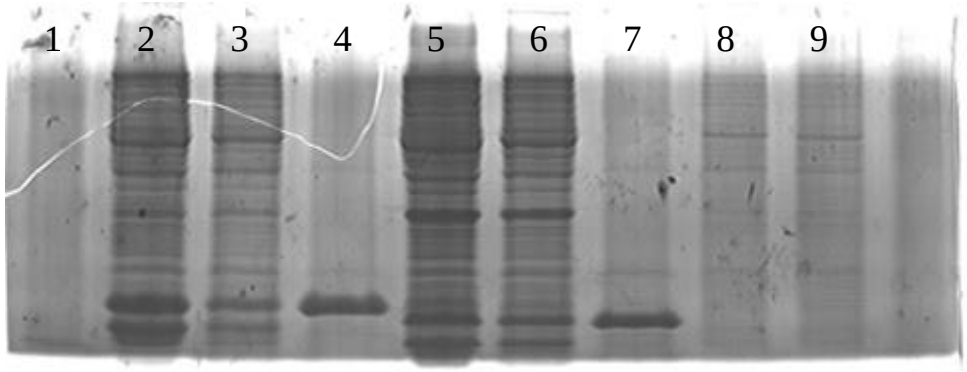

Figure 5-10: HPr purification vs. HPrγ purification. Lanes 2-4 contain crude, flow through, and eluate 1 respectively for native HPr. Lanes 5-9 contain crude, flow through, and eluates 1-3 respectively.

Figure 5-10 indicates we are indeed expressing a protein in the region near our native HPr band. In this particular purification, it appears as though the native HPr and mutant HPrγ proteins were not efficiently purified from the cell free extract due to the relatively high concentration of apparent target protein in the column flow-through. Nevertheless, the purification appears to be a success, and as with the native HPr

purification, the CABB-400 and EB-400 solutions were effective in reducing non-specific binding and producing approximately 50 ml of pure protein solution. Also notice that all of the eluted protein is contained in the first fraction, with fractions 2 and 3 containing low levels of a heavier, non-specific binding proteins. One notable observation from this gel is that HPrγ appears to migrate much faster through the acrylamide gel than HPr. This is a curious result since HPrγ should, in mass, be approximately 12,950 Da that is ~ 90 Da larger than native HPr. Perhaps some conformational change in the formation of SDS-protein aggregates results in this differential migration pattern. Alternatively, HPr may be more easily denatured in SDS solution, while HPrγ is more stable to denaturation with SDS, thereby decreasing the fusion proteins overall volume, and allowing it to migrate more rapidly. Another possibility is that HPrγ's mutations have changed the protein charge, however the S12Y, R17H and E84Y at physiologic pH should have the same overall charge since we have removed both a positive and negative charge.

MALDI-TOF MS analysis, presented in Figure 11 shows singly and doubly charged fragments at 12,963 +/- 13 and 6,473 +/- 6 respectively. Again, the SDS-PAGE analysis differs from the MS observed data, suggesting denaturation or charges differences between the HPr proteins and the molecular weight standard.

We also performed thrombin cleavage digestions of the HPrγ mutant which, as with the native protein, resulted in the formation of the tag and HPrγ protein fragments. Figure 5-12 shows the MS spectrum that contains signals from both the digest products and the uncut HPrγ protein. Here bands of 9,420 and 3,556 are observed and demonstrate

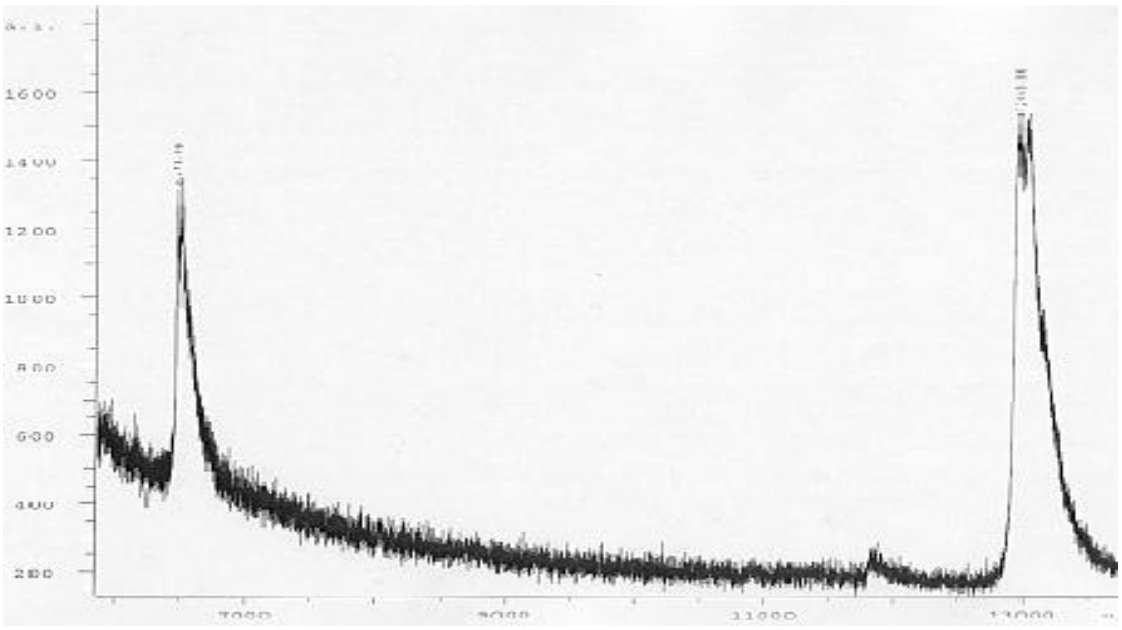

Figure 5-11: MALDI-TOF MS spectrum of uncut HPrγ showing both singly and doubly charged species.

our ability to successfully digest the CBP-HPrγ fusion protein to obtain the cleaved HPr mutant and the CBP purification tag. No observable uncut protein signal was observed in this analysis. These MS results confirm that HPrγ has the correct mass in both cleaved

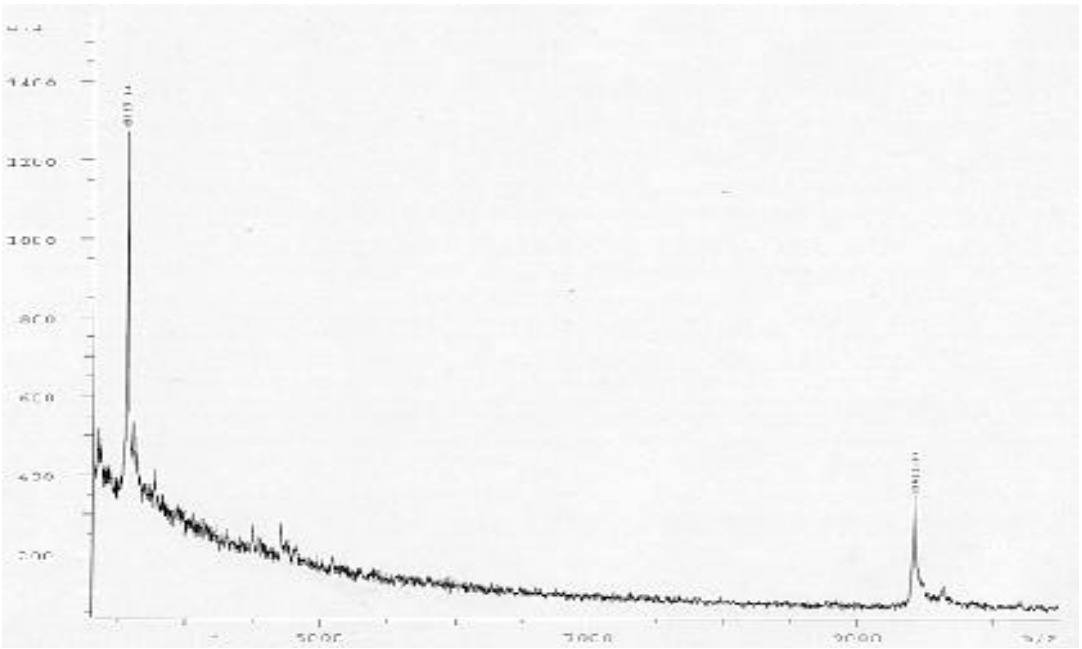

Figure 5-12:MALDI-TOF MS MS spectrum of cut HPrγ.

and uncut forms, and provides conclusive evidence that we are generating the directed HPrγ amino acid sequence.

The purified HPr protein was handled analogous to the native protein, however, HPrγ did distinguish itself from HPr in its solubility. Reducing the NaCl concentration by dialysis following purification did not result in the loss of protein due to precipitation. This result could potentially be linked to its differential migration rates in SDS-PAGE as compared to native HPr. Perhaps HPrγ excludes salt more efficiently from its structure, therefore lowering the salt concentration does not significantly perturb its structure as is apparent for native HPr in similar solutions. Hartree-Lowry assays were also performed on HPrγ, and the extinction coefficient at 280 nm was determined to be 0.806, consistent with the presence of an additional tyrosine relative to the native HPr protein.[3] From this analysis, we determined that the yield of our first HPrγ purification was 50 mL at 0.55 mg/mL, which is similar to the yields obtained for native HPr.

In summary, HPr expression and purification procedures were directly applicable to HPrγ, and we have successfully prepared pure solutions of HPrγ at a yield of 25 mg per liter of culture. SDS-PAGE comparisons of HPr and HPrγ reveal that HPrγ migrates much faster than HPr despite its larger mass.

5.6 HPRβ EXPRESSION AND PURIFICATION

HPrβ expression and purification was performed in a manner analogous to the native and HPrγ proteins. However, during the purification of HPrβ we modified the purification protocol to expedite the purification of large-scale preparations. We utilized

30 mL of resin with a 2 L culture cell free extract (essentially increasing the resin/L of expressed culture by a factor of 1.5) and increased the yield of pure protein. In addition, instead of applying approximately 80 ml of CABB-400 on the column and allowing the solution to flow through while maintaining the 80 ml overhead volume (as was performed previously), we added 500 ml in a reservoir above the column. This modification not only increased the rate of the flow, but also increased the relative speed at which the flow through A280 fell below 0.01 absorbance units. Elution of HPrβ was accomplished as before with 300 mL of EB-400 per 2 L of culture. Closely monitoring the elution, we began collecting elution fractions when A280 increased to 0.1 absorbance units, and stopped the collection process when the absorbance fell below 0.2. We believe the rapid washing resulted in less loss of bound protein due to the abbreviated length of the washing phase. The combination of these modifications along with the close monitoring of the elution profile allowed us to increase our overall protein yield from an average of 20 mg/L to 40 mg/L. All subsequent purifications of native and mutant proteins were performed in this manner.

Figure 5-13 shows a SDS-PAGE analysis of a purification of HPr, HPrγ, and HPrβ using this modified protocol. The most notable observation from this gel is that all three proteins are purifiable as is evidenced in lanes 4, 7, and 10. The lower intensity of the HPrβ crude and flow through is a result of loading more dilute samples, however the intensity of the purified HPrβ band is clearly as strong

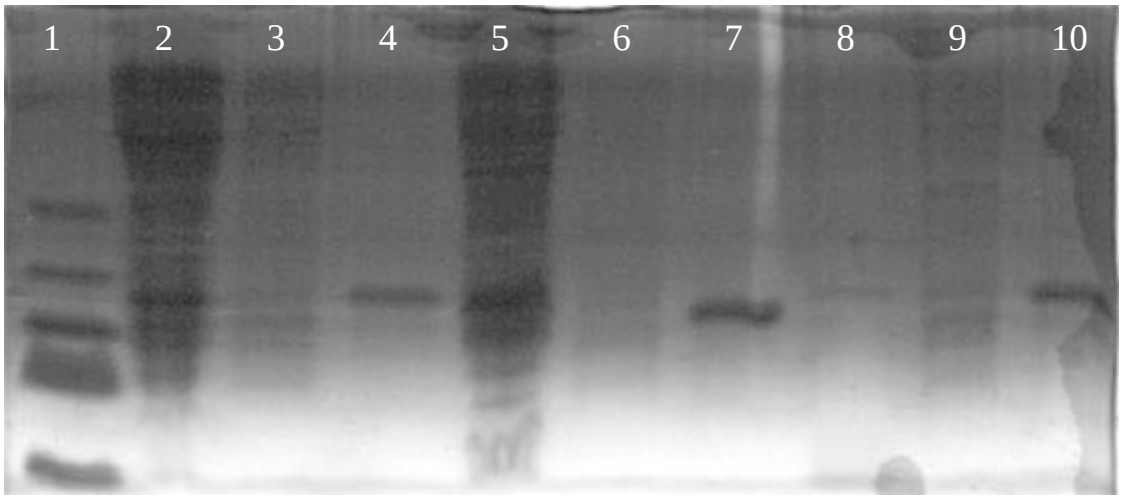

Figure 5-13: SDS-PAGE of HPr, HPrγ, and HPrβ purifications. Lane 1 contains MW marker. Lanes 2-4, 5-7, and 8-10 contain crude lysate, flow through, and elutions for HPr, HPrγ, and HPrβ respectively.

as the native and HPrγ batches. A key point to note here is the migration differences. HPr and HPrβ appear to migrate at similar apparent molecular weights, while HPrγ runs significantly faster. This is consistent with what we have seen previously, however the HPrβ migration is puzzling. A single amino acid change from tyrosine 84 back to the native glutamate 84 makes the two residue mutant HPrβ migrate similar to native HPr and not the three residue mutant HPrγ. Perhaps protein stability to denaturation in SDS solution differs significantly with HPrγ from the native and HPrβ mutants. We will address this question with protein denaturation studies monitored by Circular Dichroism spectroscopy to examine this possibility. Another feasible explanation is that the charge difference retards HPrβ relative to HPrγ. This possibility is limited by the fact that the electrophoresis is performed in a highly ionic system, thus minimizing the charge contribution to migration.

MALDI-TOF MS analysis of HPrβ is shown in Figure 5-14, and the two observed signals at 12,930 and 6,457 are consistent with the calculated values of 12,916 Da and

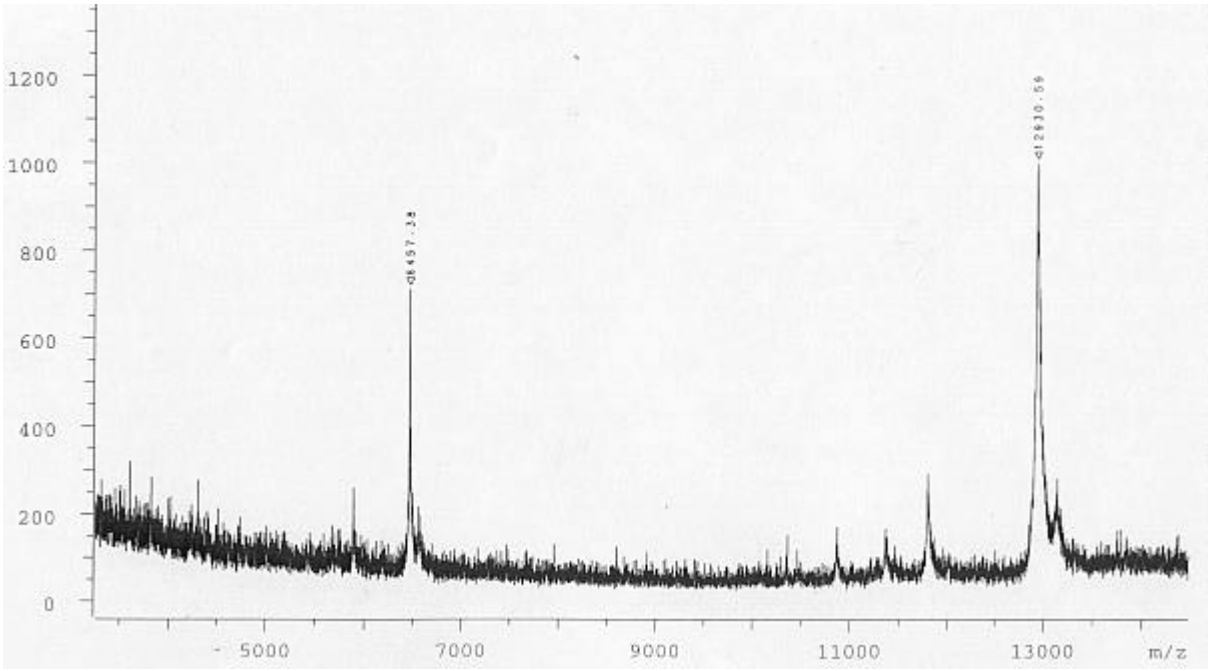

Figure 5-14: MALDI-TOF MS of a 2 month old sample of HPrβ.

6,458 Da for the singly and doubly charged species respectively. Subsequent analysis of samples containing combinations of HPrβ with HPr and HPrγ showed that the calculated mass differences of 70 Da and 31 Da respectively were consistent with observed, resolvable shoulders on the MS signals. Figure 5-15 shows the MS spectrum of the HPr shoulder on the HPrβ signal.

From this MS data, we have definitive evidence that we are producing the correct recombinant proteins. The anomalous SDS-PAGE migration patterns observed for these recombinant proteins provide mass estimates that are 25 % larger for HPr and HPrβ, while only ~15% larger for the faster migrating, heavier HPrγ.

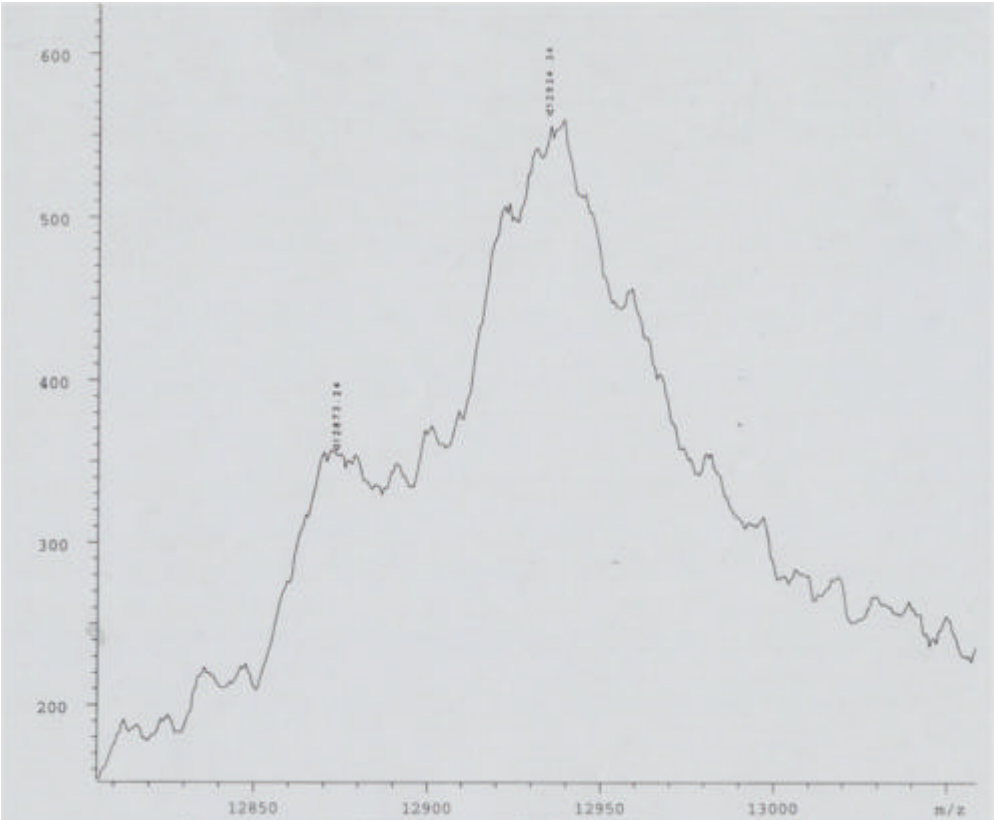

Figure 5-15: MALDI-TOF MS of HPr and HPrβ proteins mixed together.

Thrombin cleavage was not performed on HPrβ because studies (to be described below) on HPr and HPrγ showed that cleavage of the purification tag does not result in significant changes in protein properties. However, HPrβ, with its identical positioning of purification tag at the N-terminus, should also be cleavable.

In summary, HPrβ expression and purification was achieved in a manner analogous to the native and HPrγ mutants. Perturbation of the purification conditions led to a two-fold increase in the yield of protein, which was also effective in HPr and HPrγ. The migration differences between the three proteins provide an interesting result that will be discussed further in section 6.9.

5.7 CD MEASUREMENTS AT 280 nm

To further explore the identity of our HPr proteins, we performed circular dichroism spectroscopy on the three proteins near 280 nm to assess differential chirality of the incorporated residues. This procedure at 280 nm can often provide valuable information to assess structural changes resulting from tyrosine, tryptophan, or phenolalanine modifications. Native, tagged HPr contains 3 tyrosine residues, while HPrβ has 1 more, and the HPrγ gene encodes for 2 additional tyrosine residues. Therefore if the orientation of these new tyrosine residues is chiral, we may be able to observe differential absorption spectra to circularly polarized light. Figure 5-16 shows the results of the average of 10 scans made for HPr, HPrγ and HPrβ. Near 280 nm peaks at 277 nm and 285 nm, and a valley at 281 are observable. Comparison of the native signal with HPrβ shows a similar profile with slightly reduced signal, while HPrγ shows a dramatic increase in both peak and dip intensities. A new signal in both HPrβ and HPrγ is present as a shoulder at 279 nm. This could possibly arise from our S12Y mutation although the intensity is relatively weak in HPrβ. A new dip at 280 nm is also present for HPrγ that could potentially arise from the E84Y mutation. Additionally, a clear red shift in the 285 nm peak of the native and HPrβ samples to near 286 for HPrγ is evident.

These observations, although not definitive, do show that our protein mutations

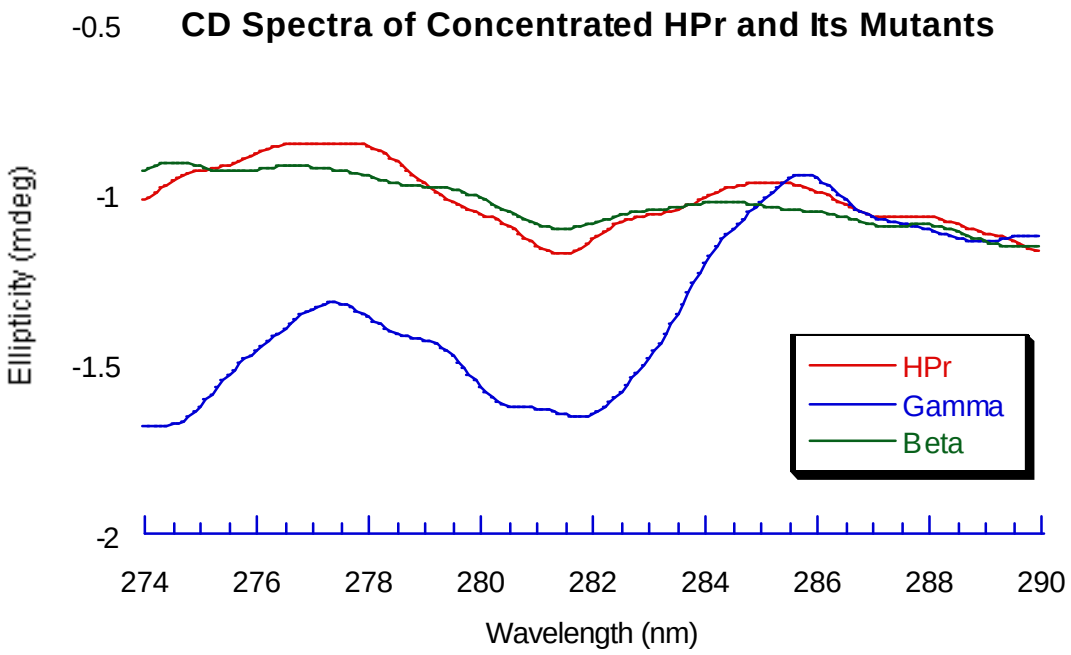

Figure 5-16: CD spectra near 280 nm of HPr, HPrγ, and HPrβ in 20 mM phosphate buffer at pH = 8.0

do cause changes in the chirality of the 280 nm absorbing residues of our HPr proteins, and are not inconsistent with the engineered mutations encoded from the prepared gene sequences.

5.8 ACTIVITY STUDIES

In the study of proteins using recombinant techniques, it is important to establish that the recombinant form of the produced protein be similar in structure and function to the native protein. For instance, expression of a native protein from the gram positive *B. subtilis* organism within the gram negative organism *E. coli*, could result in the formation of a protein having the correct amino acid sequence, but lacking suitable secondary and

tertiary structure. In our case, the *E. coli* and *B. subtilis* proteins are very similar in structure and function, and others have expressed recombinant HPr in *E. coli*.[4] Still, verification of the activity of our native protein is a critical step in evaluating the validity of our recombinant constructs, the role of the purification tag near the active center, and the effects on our targeted mutations.

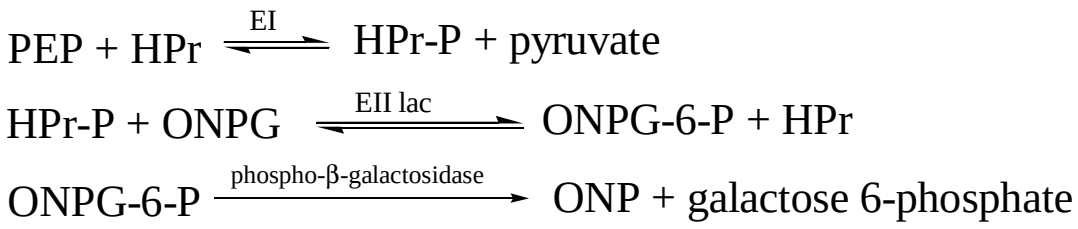

Figure 5-17: Reactions involved in the mutant complementation assay for the determination of phosphotransfer activity of HPr in S. auerus.

To assay HPr activity, we used a colorimetric mutant complementation assay developed by Dr. Wolfgang Hengstenberg for HPr in the gram positive organism S. aureus.[5] This assay has been used on recombinant HPr from *B. subtilis* by several groups.[6] The method is summarized by the reactions shown in Figure 5-17. In the PEP-PTS, HPr transfers a phosphate ion from Enzyme I to Enzyme II. In this assay, HPr in the presence of phosphoenolpyruvate and enzyme I is phosphorylated to form HPr-P and a free pyruvate. In the presence of o-nitrophenyl-β-D-galactoside and Enzyme II, HPr can phosphorylate the galactoside at the sixth carbon-OH, and release free HPr. Phosphorylated ONPG can then, in the presence of a phospho-β-galactoside liberate orthonitrophenol that has an intense absorption at 410 nm that can be seen as a bright yellow color. In the assay developed by Dr. Hengstenberg, all of the necessary components for this cycle are present in an HPr deficient strain S797A of *S. aureus*.

Simple addition of the S797A cell free extract, PEP, and ONPG with the recombinant HPr yields colorimetric activity data.

For our experiments, Dr. Hengstenberg graciously donated a stab culture of this S797A strain. Thus we grew the organism, and proceeded to follow the assay outlined in his publication with some modification. First, 100 mL of the S797A strain was grown overnight at 37 ^{o}C and centrifuged at 10,000xG for 10 minutes. The paste was weighed, resuspended in 2 mL of buffer matching the published protocol, then frozen at –80 ^{o}C for 1 hour. Next the cells aliquoted into a two 1.5 mL microcentrifuge tubes and lysed via the bead beating method (section 2.14-D). 50 µL of this clarified extract were added to 2 µmol of ONPG and 3.1 µmol of PEP to a total volume of 100 µL with buffer and varying amounts of HPr. This mixture was incubated at 37 ^{o}C for 20 minutes, quenched with 800 µL of 0.25 M Na_2CO_3. This reaction mixture was centrifuged at 20,000xG for 20 minutes, and the absorbance at 410 nm was measured. The results of our complementation assays on native, pure, HPr are shown in Figure 5-18. Increasing amounts of HPr, above an apparent low-level threshold, produces increasing absorbance at 410 nm. This data was corrected for background absorbance of HPr, buffer, and cell free extract contributions. These results prove that HPr is active, and with the purification tag still attached, demonstrates several key points. First, our recombinant approach to expressing and purifying HPr was effective in the generation of an active protein capable of carrying out native HPr function. This strongly suggests that HPr has been produced in the proper conformation to allow directed phosphorylation and dephosphorylation. Secondly, our choice of positioning the purification tag at the N-

terminus, which is located on the opposite face of the protein (away from the phosphate-binding site in the crystal structures), appears to have allowed for complete access to the phosphate binding site. Also, this active HPr is the first HPr construct to be generated with a calmodulin binding peptide purification tag. Thus the mild binding and elution conditions of this pCal-n purification system does not destroy the integrity of HPr during the purification. This observed reactivity is retained for over one month with HPr solutions stored at 4 ^{o}C in 20 mM Tris, 20 mM NaCl, and sub-nM levels of EGTA and $CaCl_2$, thus demonstrating stability upon storage of the purified protein. Finally, these positive results show that our system can support formation of active, tagged HPr. Thus

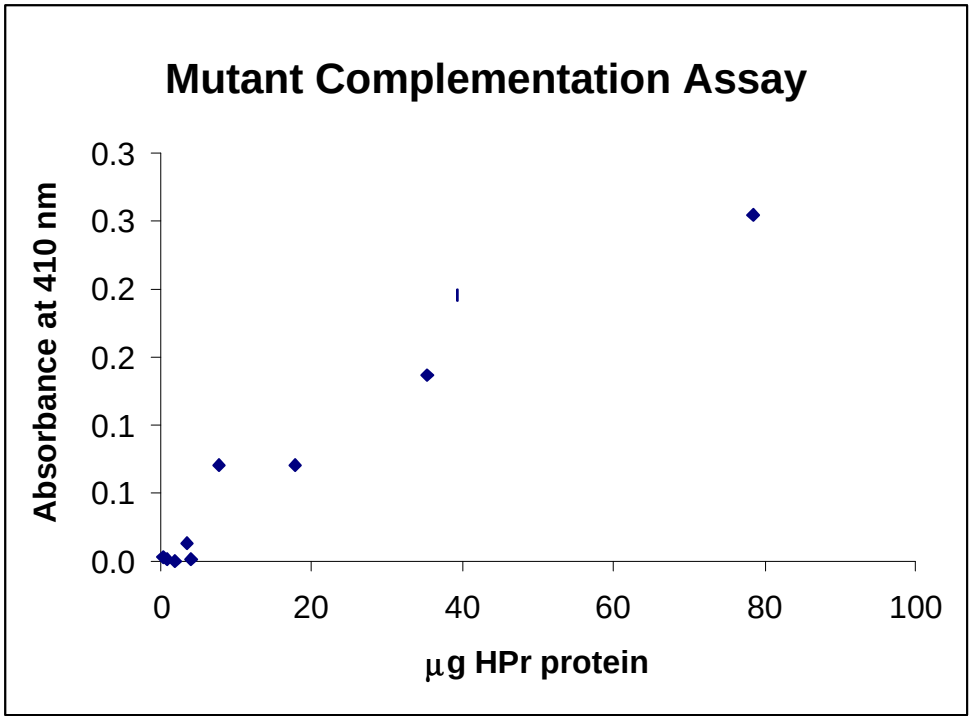

Figure 5-18: Mutant complementation assay of native HPr with its attached purification tag.

preparation of our mutants, which differ by only 2 or 3 residues, should also form structures inherent to their amino acid sequences in the presence of the purification tag.

With these positive results for the native protein, we next turned to our mutants. We anticipated that mutations to such critical residues as R17 and E84 in would likely result in inactive mutant proteins. To verify this we examined the reactivity of HPrβ and HPrγ relative to native HPr and the results are presented in Figure 5-19. Both HPrγ and HPrβ are essentially inactive. This result does not mean that HPrγ and HPrβ are grossly different in secondary and tertiary structure from native HPr, simply that they do not have the necessary residues to provide recognition and binding of one of the components of the phosphotransfer reaction. One possibility is that Enzyme I can not bind properly to the new active sites. Perhaps the phosphate is transferred to the mutants, but is very unstable

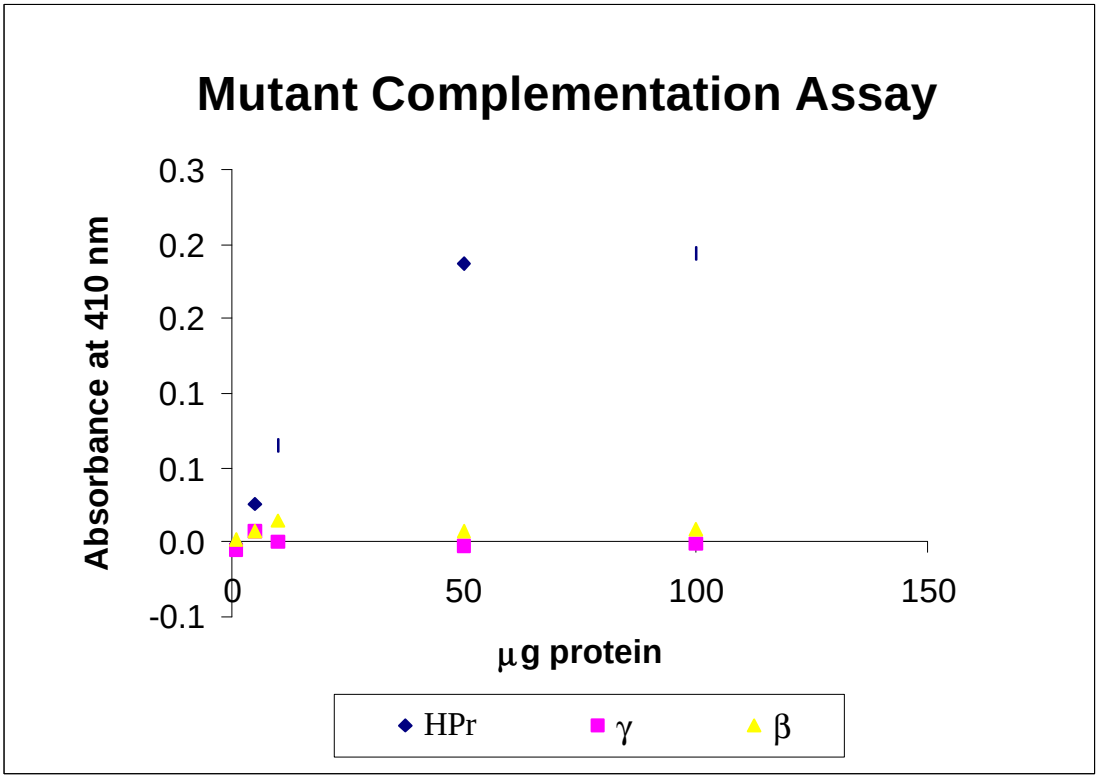

Figure 5-19: HPr activity assay on HPr and the purified mutants.

without its native residues in the active site and is immediately released. Alternatively, perhaps Enzyme II can not bind to HPr, thus leaving the mutants phosphorylated until they naturally hydrolyze in solution (usually 1 to 2 hours for native HPr in the literature).[7]

In summary, our recombinant HPr has phosphotransfer activity, while HPrβ and HPrγ lack any observable activity under comparable conditions. These results validate our approach to expression and purification, and provide a foundation to begin probing the metal-binding properties of the native and mutant proteins.

5.9 SUMMARY

In this chapter we have described the expression and purification of native HPr and two of its mutants HPrγ and HPrβ. Through our efforts, we have successfully generated these recombinant proteins at a yields of 40 mg with concentrations of 0.6 mg/mL. Characterization of the proteins by mass spectrometry, thrombin digestion, and SDS-PAGE, has provided us with information that collectively confirms that our approach to producing pure samples of these recombinant proteins was successful. Several interesting observations were made that may have implications on the proteins' metal-binding properties. Mutant complementation assays on the native and mutant HPr proteins confirmed that we were able to generate an active native protein, and that the directed mutations resulted in expected loss of phosphotransfer ability. This observed activity for native HPr suggests that the covalently attached CBP does not interact with the phosphate-binding site such that it precludes activity. This is consistent with its positioning at the N-terminus of the HPr peptide chain. These studies serve as building

blocks to examine the ability of our native and mutants to coordinate iron in a manner analogous to PCD.

5.10 REFERENCES

[1] Simcox, T. G.; Zheng, C. F.; Simcox, M. E.; Vaillancourt, P. *Strategies***, 1995**, *8*, 40-43.
[2] Bollag, D. M.; Rozycki, M. D.; Edelstein, S. J. *Protein Methods*, 2nd ed, 1996, Wiley-Liss, Inc. New York.pp 76-79.
[3] Pain, R. Current protocols in Protein Science, 1996, Wiley & Sons, Inc. pp. 3.2-3.5.
[4] Reizer, J. Sutrina; S. L.; Saier, M. H.; Stewart, G. C.; Peterkofsky, A.; Reddy, P. *The Embo Journal*, **1989**, *8*, 2111-2120.
[5] Hengstenberg, W.; Penberthy, W. K.; Hill, K. L.; Morse, M. L. *J. Bacteriol*. **1969**, *99*, 383-388.
[6] (a) Reizer, J.; Bergstedt, U.; Galinier, A.; Kuster, E.; Saier, M. H.; Hillen, W.; Steinmetz, M.; Deutscher, J. *J. Bacteriol*. **1996**, *178*, 5480-5486. (b) Witt, E.; Frank, R.; Hengstenberg, W. *Protein Engineering*, **1993**, *6*, 913-920. (c) Kowolik, C. M.; Hengstenberg, W. *European J. Biochem*, **1998**, *257*, 389-394.
[7] Anderson, J. W. *Biochem. Cell Biol.* **1995**, *73*, 219-222.

Chapter 6

METAL-BINDING STUDIES

6.1 INTRODUCTION

Strategic incorporation of a single iron ion within the engineered binding site of HPrγ, in a manner similar to the metalloenzyme PCD, is the ultimate goal of these studies. Successful large-scale expression and purification of HPrγ enables us to examine its iron-binding properties. Subsequently, utilizing PCD-type substrates and inhibitors, we can probe and evaluate our constructed metalloprotein's reactivity, through physical methods, by comparison of iron-HPrγ adducts with established characteristics for PCD. First we must demonstrate iron complexation within the engineered site of HPrγ. In this chapter, we outline the steps taken to produce and characterize iron coordination to our mutant HPrγ protein, and additional experiments conducted to probe the protein structure by addition of alternate transition metals. Comparison of these metal interactions with HPrγ analyses, under identical conditions, will be made to native HPr and our Y84E reversion mutant HPrβ.

6.2 QUALITITATIVE IRON ADDITIONS

Our initial iron additions were qualitative. Since PCD-type coordination of iron to tyrosine produces a burgundy-red color with characteristic absorption at 450 nm, we began our metal-binding analyses by performing small-scale (30 μl) spot tests on parafilm with purified, concentrated HPrγ. In these experiments we added various concentrations of iron in both the ferrous and ferric forms vs. buffer control samples. These attempts did not produce a visible red color in either short (within 10 minutes) or longer (overnight-days in reaction tubes) incubations. With the limited solubility of

ferric ion in basic/neutral conditions, we turned to addition of ferrous ion, with hopes of oxidizing the metal to its ferric form either aerobically, or with oxidizing agents. Using our spot tests we utilized various oxidants such as ferricyanide, permanganate, and hydrogen peroxide. None, in the presence of 500 μM iron (II) produced a red color significantly different from buffer control. We also lowered the pH of the metal reactions to more effectively examine iron (III) binding. Near physiological pH, iron oxides/hydroxides are dominant, which inhibit soluble iron (III) from coordinating to our HPrγ protein. We exchanged the standard Tris-HCl buffer with a sodium acetate buffer at pH = 4.8 by dialysis of HPrγ. Addition of ferric chloride and ferric sulfate equivalents to HPrγ spots also failed to produce a red colored protein solution.

Additional spot tests were run with iron and the PCD substrate protocatechuate (PCA). This was attempted with the idea that introducing a known PCD substrate, which also has affinity for iron, might facilitate complexation within the HPrγ active site to coordinate tyrosine in an analogous manner to PCD. Using variable reaction conditions this also failed to produce the desired red solution.

From these preliminary tests of HPrγ's reactivity with iron ions, it was apparent that the desired coordination would not be easily discovered by simple addition of iron ions. This could be due to several factors such as: the absence of iron-tyrosine coordination, the binding constant of iron coordination to the HPrγ ligand set is too low to observe at the applied conditions, ferrous complexation is preferred over the ferric form, the protein structure is not capable of supporting the iron coordination requirements and rapidly denatures, the HPrγ active site is not oriented in a manner consistent with the

X-ray crystal structure of the protein. Thus, our spot test studies revealed that the desired complexation is not qualitatively observable, and more quantitative measurements are needed.

6.3 IRON BINDING STUDIES MONITORED BY UV-Vis AND EPR SPECTROSCOPIES

Examination of the PCD literature revealed reconstitution experiments had been conducted to remove, and re-coordinate iron within the metalloenzyme's active center.[1] They reduced the resting-state iron (III) ion with sodium dithiothionite, then removed it by complexation with o-phenanthroline and dialysis. To reconstitute the apoprotein, they found that aerobic addition of iron (II) ions in the presence of ascorbic acid resulted in recovery of the red color and catalytic activity. This activity was also restored by anaerobic iron (II) addition followed by treatment with the oxidant ferricyanide.

We performed these additions to HPrγ under similar conditions to these reconstitution experiments, and the UV-Vis spectra recorded for these titrations are shown in Figure 6-1. In the visible region of these spectra, no absorption bands are observed for HPrγ that are consistent with the desired 450 nm transition characteristic of iron (III)-phenolate coordination. Comparison of the HPrγ titration with buffer control reveals little differential absorption. Therefore, HPrγ does not, under these conditions, produce a target site consistent with that found in PCD.

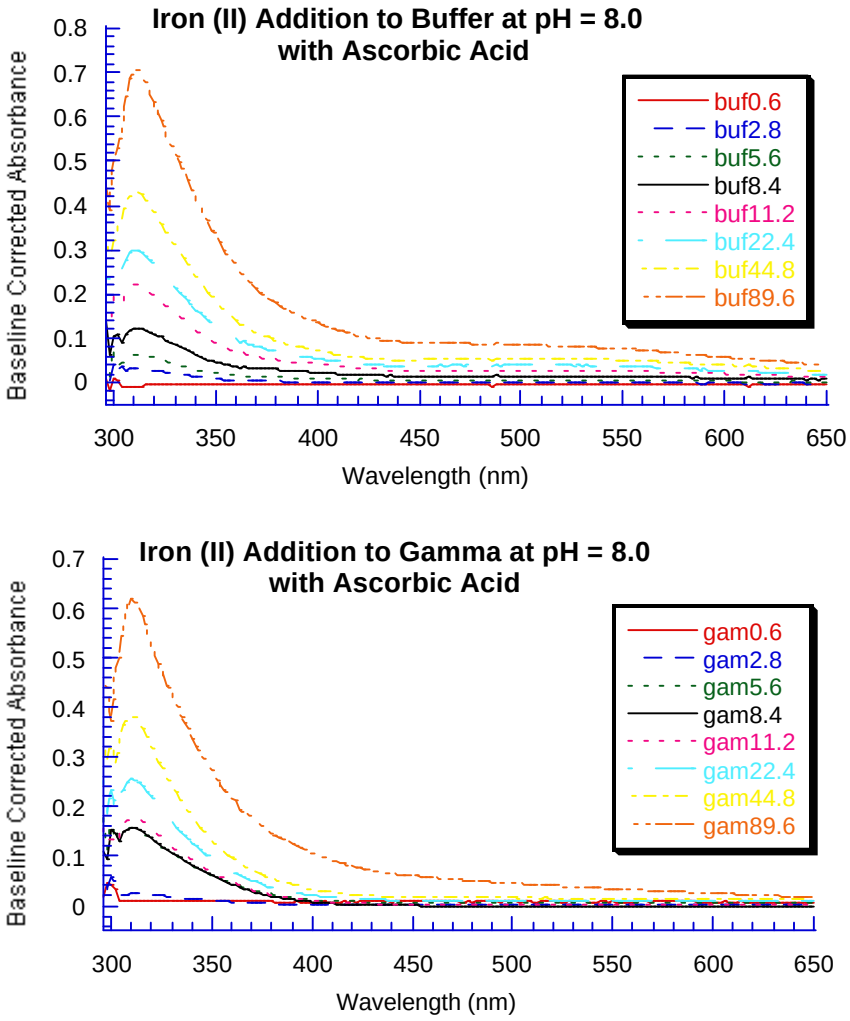

Figure 6-1: Iron (II) additions at pH = 8.0 in the presence of 500 μM ascorbic acid. The spectra have been baseline corrected by the subtraction of the 0.0 iron equivalent spectra, and μl of 10 mM iron (II) are indicated in the legends.

To further probe the iron-HPrγ interactions, we titrated iron (III) with HPr, HPrγ, and HPrβ. These additional controls enable us to compare differential protein interactions with iron, and test the effect of the E84Y mutation on iron binding. In order to keep ferric ion in solution during these analyses, we dialyzed each protein in acetate

buffer at pH = 4.8, and used the resulting exterior dialysis solution as our buffer control. The UV-Vis spectra recorded from these titrations is shown in Figure 6-2. Comparison of these spectra does appear to result in changes between the buffer control and the HPr

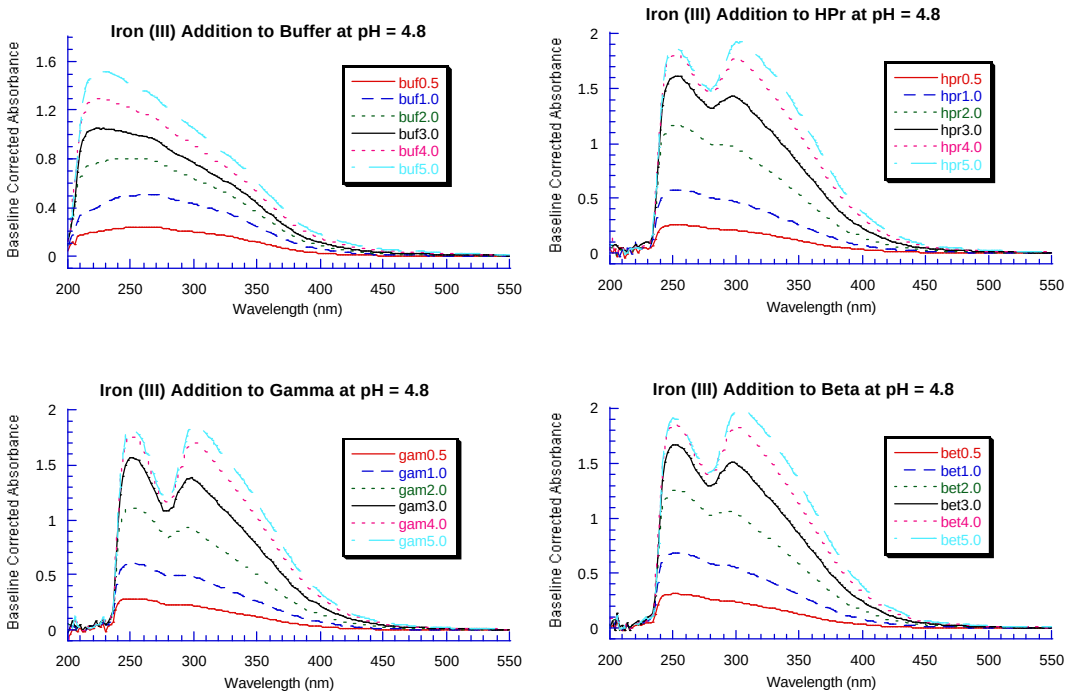

Figure 6-2: Iron (III) additions to buffer, HPr, HPrγ, and HPrβ samples at pH = 4.8 that have been baseline corrected by subtraction of the 0.0 iron equivalents spectra from each iron addition respectively. Equivalents of iron (II) added are indicated in the legends.

protein samples. This observation, however, is misleading because the three proteins were at high concentrations (~ 150 μM), and the baseline correction procedure of subtracting the 0.0 iron equivalents sample results in a dip at 280 nm for samples whose uncorrected spectra rises above the scale of the spectrometer. Thus, iron (III) addition at pH = 4.8 produces no differential absorbance for HPrγ relative to buffer, HPr, or HPrβ. This result correlates with the reconstitution experiments by Hayaishi and coworkers who also failed to re-activate PCD with ferric ion. In their attempts, however, they used pH =

8.0 which would likely preclude effective iron (III) complexation due to ferric ions insolubility in basic solutions.

To further analyze the products of these titrations we used EPR spectroscopy to probe the paramagnetic properties of the iron ions in each solution. Figure 6-3 contains

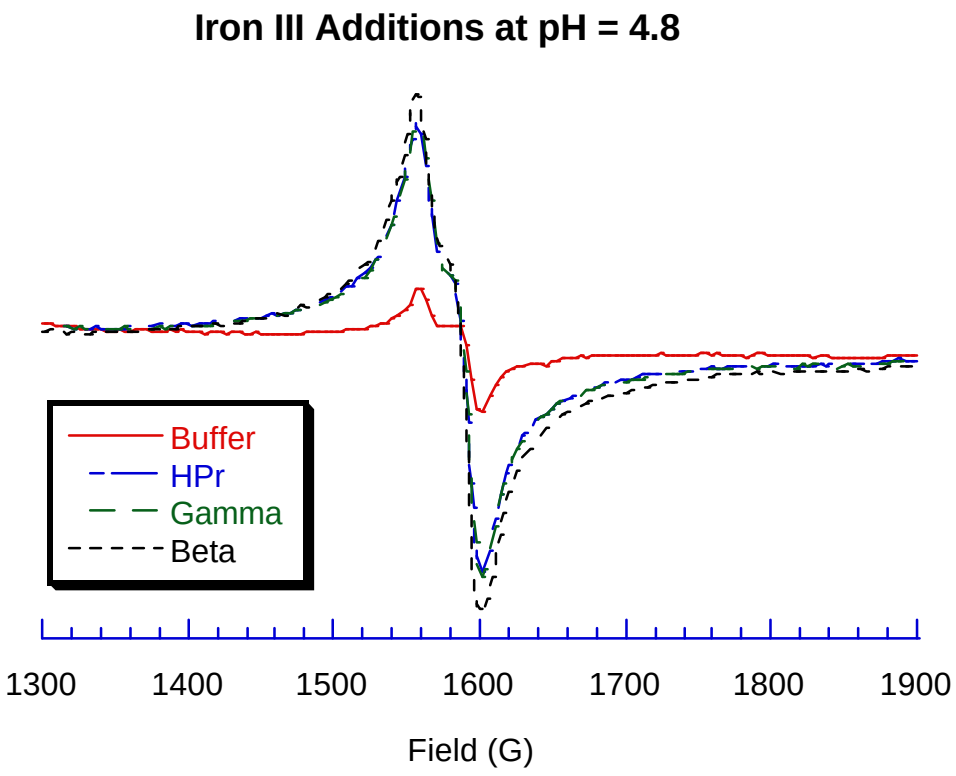

Figure 6-3: EPR spectra of iron (III) additions to dialysis buffer, HPr, HPrγ, and HPrβ at pH = 4.8 derived from the UV-Vis monitored titrations from Figure 6-2.

the resulting spectra. These observed signals are found at g = 4.28. These rhombic EPR signals are also found for PCD, and arise from the iron (III) ion. Notice that the buffer signal has a much lower intensity than those of the HPr proteins. One explanation for the intensity difference is that, in the presence of protein, the iron ions are stabilized and do not form insoluble (EPR silent) iron oxides. In buffer alone, the soluble iron is decreased

through the formation and precipitation of iron oxides. This observation is strong indirect evidence for the formation of iron (III)-protein adducts. However, since all three proteins give the same spectrum -- that of rhombic, high spin iron(III) – it is unlikely that the iron-protein interaction is associated with our designed active site.

In summary, our iron (III) binding experiments show that we do not produce the desired PCD-type iron coordination with HPrγ or HPrβ by the addition of ferric ions at pH = 4.8.

Comparative ferrous additions at pH = 4.8 were made, and the UV-Vis spectra recorded for buffer, HPr, HPrγ, and HPrβ samples are shown in Figure 6-4.

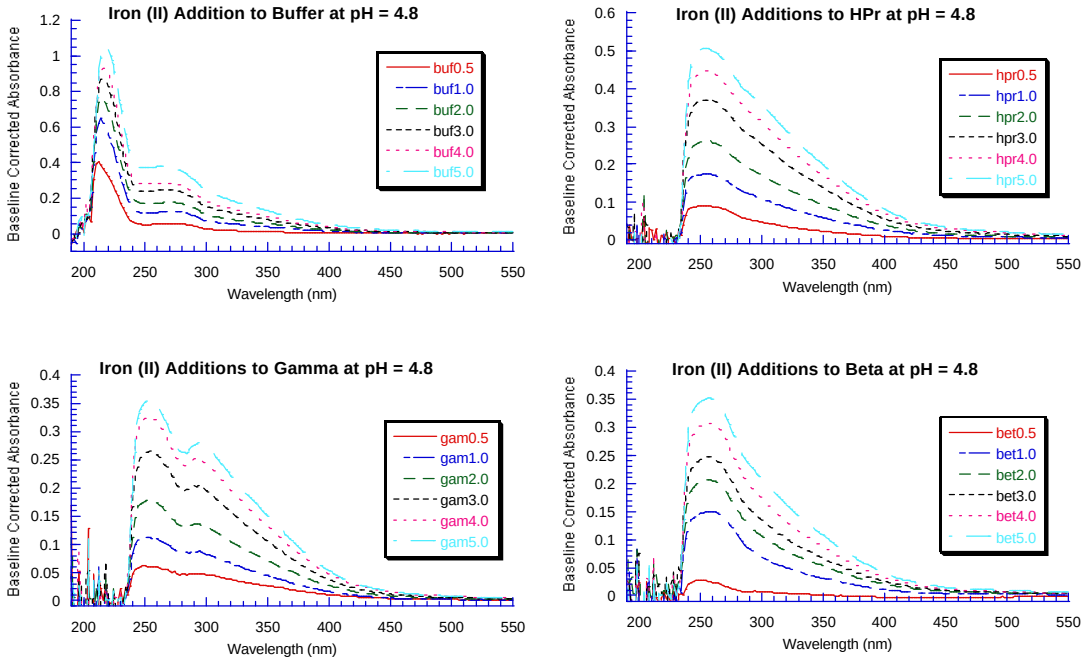

Figure 6-4: UV-Vis spectra of iron (II) additions to dialysis buffer, HPr, HPrg, and HPrb at pH = 4.8. Spectra were baseline corrected by subtraction of the 0.0 equivalents samples, and iron equivalents are indicated in the figure legends.

These spectra support our observations made in the spot test experiments, and show that the visible region is devoid of transitions near 450 nm. The HPrγ spectra shows the 280 nm dip discussed above, but does not differ greatly from HPr or HPrβ.

EPR spectra were taken for these iron (II) additions at pH = 4.8, and Figure 6-5

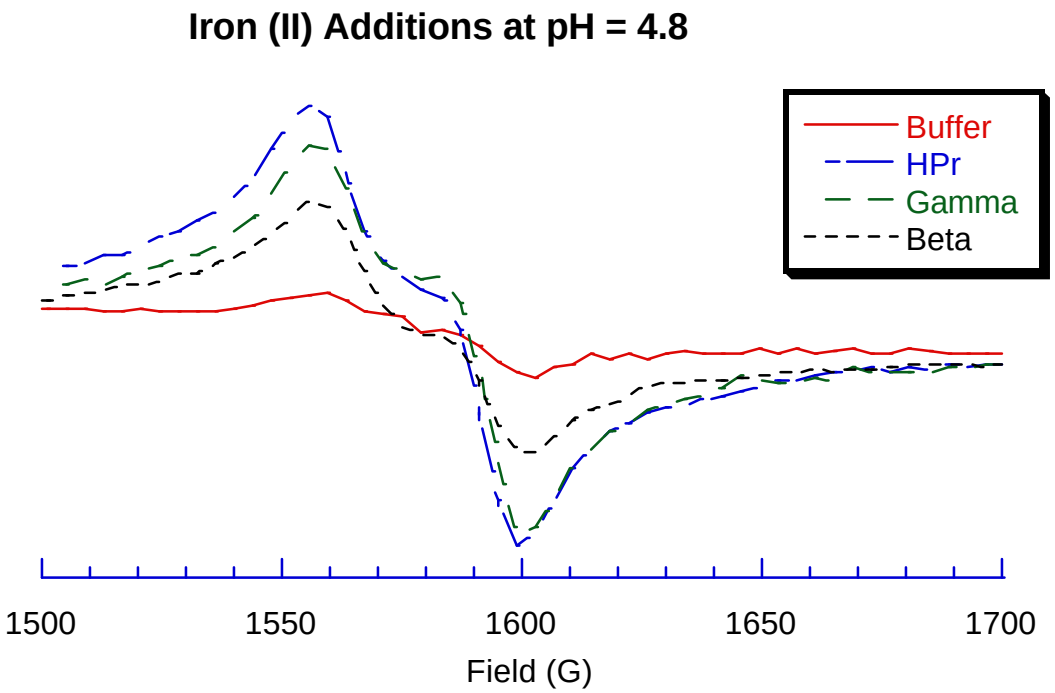

Figure 6-5: EPR spectra of iron (II) additions at pH = 4.8 for buffer, HPr, HPrγ, and HPrβ.

shows the results. Here we see a transition at g = 4.28. This is similar to our iron (III) examination at pH = 4.8. The intensity of these signals is ¼ that of the iron (III) titrations, however, the relative ratio of buffer signal to the protein containing samples remains the same. This EPR transition is likely due to the air oxidation of iron (II). Subtle differences are detectable among the three protein-containing samples in certain features and signal intensities, however, their overall profiles are very similar.

In summary, ferrous additions to HPr, HPrγ, and HPrβ compare well with the ferric studies at pH = 4.8, and show that our HPrγ and HPrβ proteins do not produce detectable interactions that are different from native HPr as monitored by UV-Vis and EPR spectroscopies.

Ferrous additions at pH = 8.0 were also performed to test our proteins iron-binding ability at a more physiological pH. Figure 6-6 depicts the UV-Vis spectra used to monitor these titrations. These analyses compare well with our ferrous data at pH = 4.8 and spot tests, however, they further demonstrate our apparent inability to bind iron in a manner analogous to PCD.

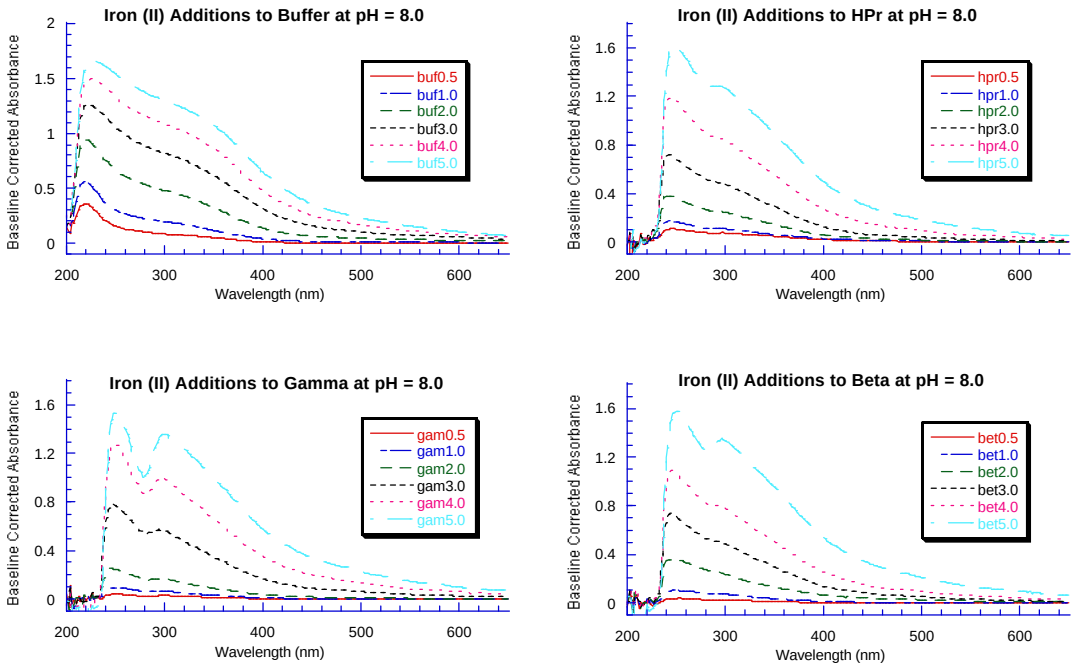

Figure 6-6: UV-Vis spectra of iron (ii) additions at pH = 8.0 to buffer, HPr, HPrγ, and HPrβ. Spectra are baseline corrected by subtraction of 0.0 iron equivalent spectra. The Fe (II) equivalents added are indicated in the figure legends.

EPR analysis of these iron (II) additions at pH = 8.0 is displayed in Figure 6-7, Here, an extremely weak g = 4.28 signal is observed for dialysis buffer and HPr, while no

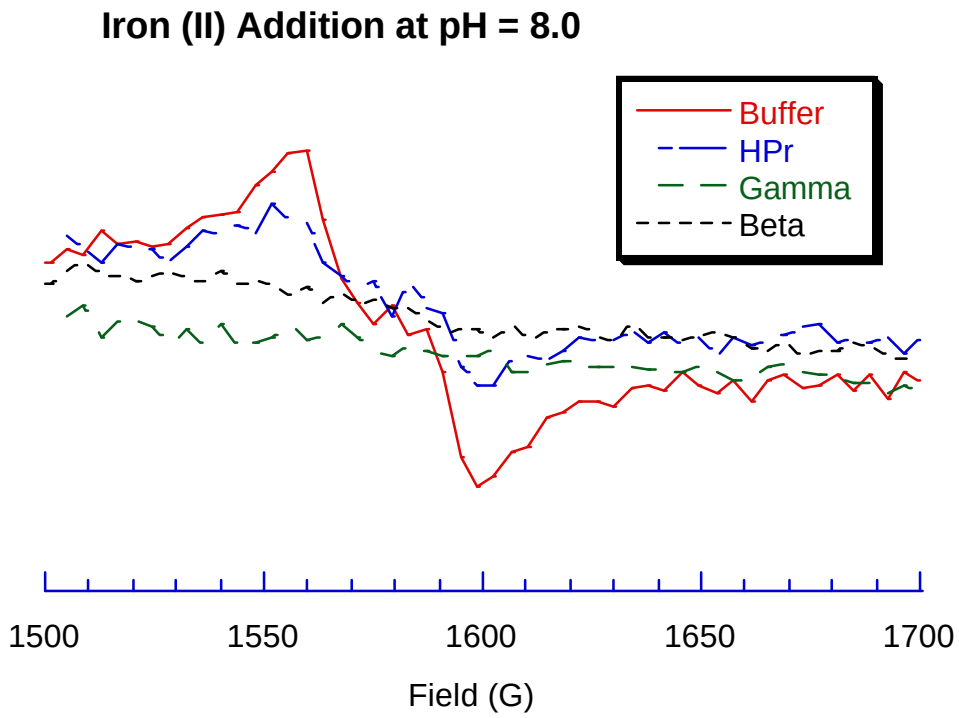

Figure 6-7: EPR spectra of iron (II) additions at pH = 8.0 for dialysis buffer, HPr, HPrγ, and HPrβ.

observable signal is evident for HPrγ and HPrβ. This observation is puzzling, but does not alter the conclusion that at pH = 8.0 soluble ferric ion is virtually non-existent, and these extremely weak-to-absent signals confirm that no iron (III) coordination to our HPr proteins is established.

The bottom line of these iron binding studies is that we are not forming the anticipated iron (III)-tyrosine complex with our HPrγ and HPrβ proteins. In the

following section, we will describe our efforts to explore the causes of this unexpected outcome through transition metal binding studies with copper, manganese, and vanadium.

6.4 ALTERNATIVE TRANSITION METAL PROBES TO HPr, HPrγ, AND HPrβ

To probe our mutant proteins' inability to bind iron as anticipated, we explored our proteins' interactions with the transition metal-copper. Copper (II) ions are known to coordinate histidine residues in several metalloenzymes.[2] Our HPrγ and HPrβ mutants contain two histidine residues separated by a single alanine residue. Therefore, they both have the potential to form copper complexes within their re-designed active sites. Native HPr conversely is less likely to strongly coordinate copper with only one histidine (residue 15) in its phosphate-binding pocket. Using these unique properties of copper-histidine affinity, we can probe the accessibility of the engineered active sites in HPrγ and HPrβ relative to native HPr. This procedure could clarify the causes of our apparent inability to form iron (III)-tyrosine coordination, and by comparison of the HPrγ and HPrβ profiles, we can specify the specific role of our E84Y mutation on the proteins' metal-binding properties.

Our copper experiments were performed on the same protein batches as those utilized in our iron additions, and a similar procedure for HPr, HPRγ, and HPrβ proteins was performed as described in the preceding section. Figure 6-8 shows the UV-Vis spectra for the copper additions at pH = 8.0. In these spectra, peaks observed for buffer alone are present (misleadingly shifted by the correction procedure) and grow with increasing copper (II) concentration for native HPr and our HPrγ and HPrβ mutants.

These spectra provide little new information except that copper interactions with our proteins do not produce a UV-Vis profile that is suitable for monitoring copper binding at pH = 8.0.

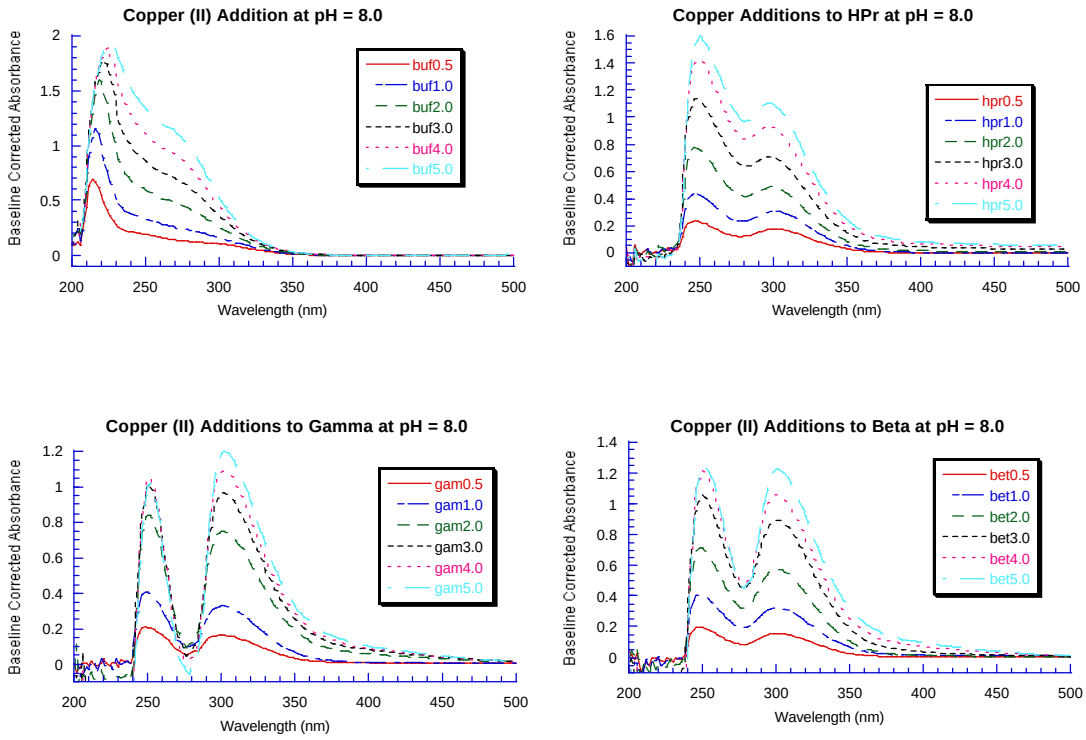

Figure 6-8: Copper (II) additions to buffer, HPr, HPrγ, and HPrβ at pH = 8.0. Spectra were corrected by subtraction of 0.0 equivalent metal additions. Copper equivalents are indicated in the figure legends.

Analysis of this addition by EPR spectroscopy (Figure 6-9), in stark contrast to the UV-Vis spectra, shows some very interesting results. The signals appear to be normal copper axial signals with $g_{\parallel} \sim 2.24$ and $g_{\perp} \sim 2.04$. In comparison of the signals, notice that buffer and HPrγ look essentially identical. This result is surprising since HPrγ has two proximate histidine residues at positions 15 and 17 in the amino acid sequence. From this it appears as though the copper ions in the HPrγ solutions do not interact with

the protein any differently than copper reacts to buffer alone. This is an important

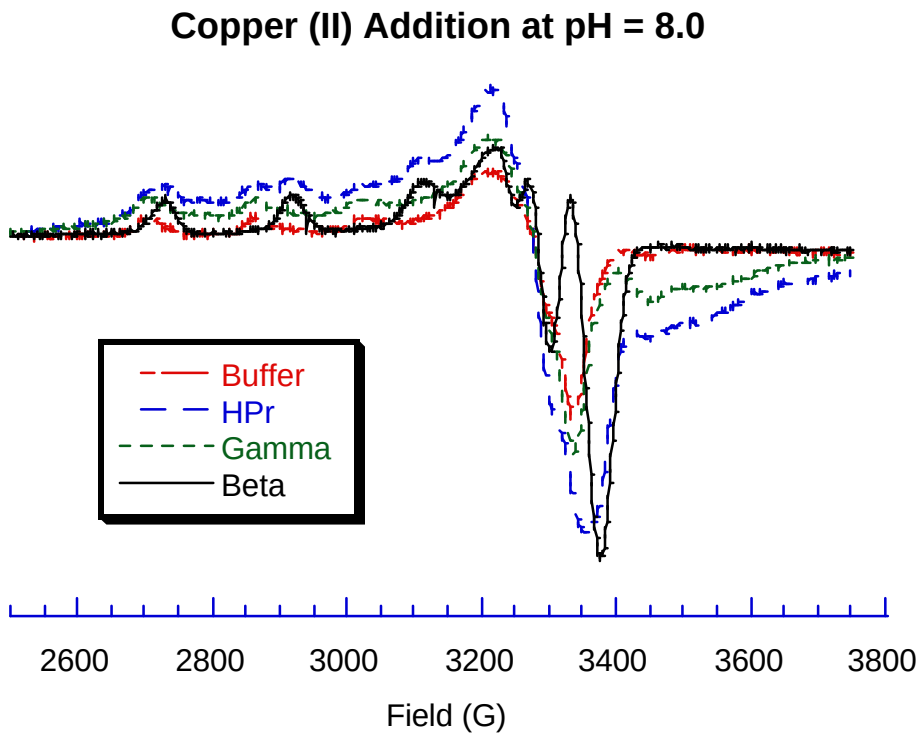

Figure 6-9: EPR spectra of copper (II) additions at pH = 8.0 for buffer, HPr, HPrγ, and HPrβ.

observation. Also, notice that native HPr has some of the same transitions as the buffer and HPrγ, but also has a set of different signals as well. Perhaps this is the result of His-15 coordination to the copper ion. Finally, look at the HPrβ signal. It is distinct from the other samples in several ways. First, parallel signals are seen that appear to match the new signal seen for native HPr, and there is no evidence of the transition observed for the buffer and HPrγ reactions. This signal could arise from the coordination of copper to His-15 as was suggested from the copper addition to native HPr. In addition, the

perpendicular region for HPrβ shows a distinct signal that has an observable hyperfine coupling to the copper nucleus with a relatively large coupling constant. This observation is not seen for buffer and HPrγ reactions. Some low intensity hyperfine coupling is observed for native HPr, however its intensity is much lower, and the coupling constants do not correspond to those of the HPrβ signal. In light of these EPR data, it is plausible that copper ions can enter the active sites of HPr and HPrβ at pH = 8.0, while HPrγ seems to exclude the metal ion from its engineered pocket. This point will be elaborated further below.

Copper binding experiments were also performed in acetate buffer at pH = 4.8. The UV-Vis spectra of these titrations are shown in Figure 6-10. From these spectra, HPr

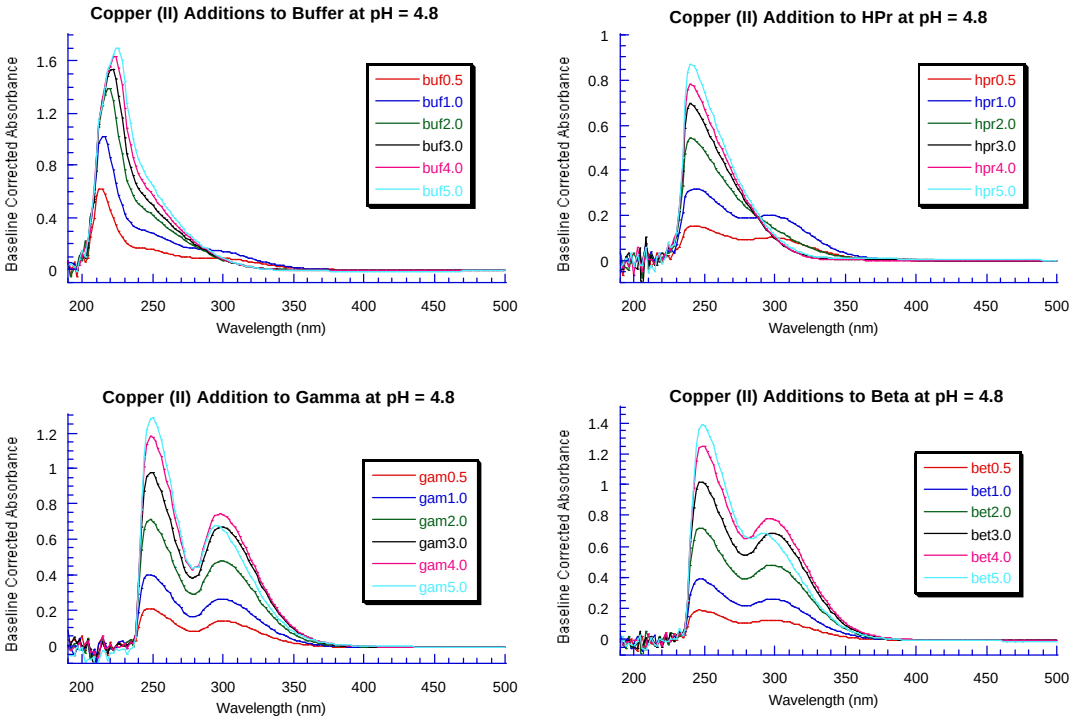

Figure 6-10: UV-Vis spectra of copper (II) additions to buffer, HPr, HPrγ, and HPrβ at pH = 4.8. Spectra were baseline corrected by subtraction of 0.0 copper equivalent spectra. Equivalents of copper added are indicated in figure legends.

and buffer appear to have similar profiles upon copper (II) addition, while HPrγ and HPrβ appear similar. At closer examination, differences in the 600 nm absorbance regions are also observable. Figure 6-11 contains magnified views of this region and shows that all

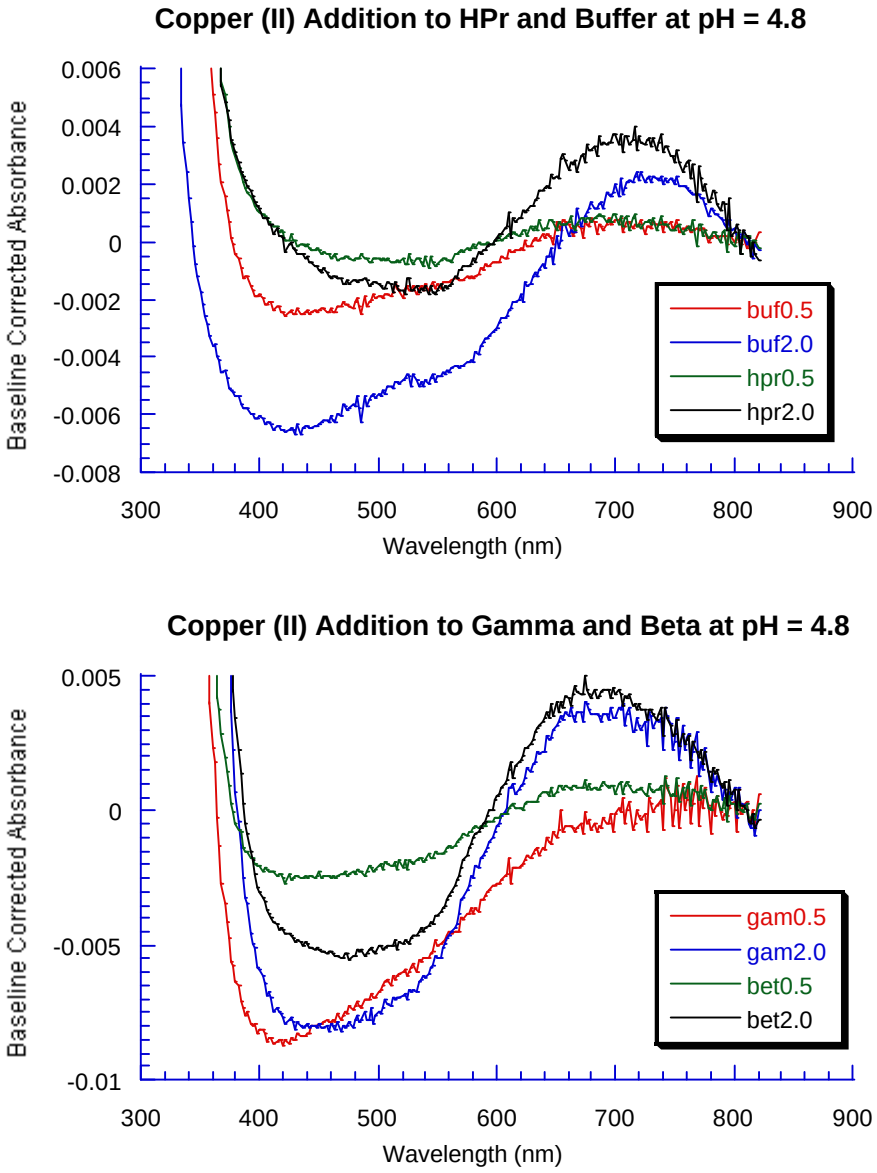

Figure 6-11: Magnified view of the 600 nm region of copper (II) additions a pH = 4.8 showing shifts in transition energies with increasing concentrations of copper ions. Spectra baseline corrected by subtraction of 0.0 copper equivalent spectra. Equivalents added shown in figure legends.

four samples have observable isosbestic points near 687 nm. Notice from comparison of the transition energies, buffer and HPr bands (both the increasing and decreasing peak) are shifting toward lower energy with increasing copper concentrations. By comparison, HPrγ and HPrβ display converging shifts with the lower wavelength, diminishing peaks red-shifting while the longer wavelength, growing peaks, blue-shift. Thus, both the UV and visible regions of these copper spectra at pH = 4.8 show that HPr and buffer are similar. However, these controls differ from the HPrγ and HPrβ mutant proteins. Another interesting observation is that lowering the pH from 8.0 to 4.8 appears to cause native HPr, which at pH = 8.0 showed spectra similar to HPrγ and HPrβ, to display copper-binding characteristics similar to the control buffer.

EPR spectra of the pH = 4.8 copper (II) titrations also proved informative. Figure 6-12 (A) contains the parallel region, while 6-13 (B) shows a magnified view of the perpendicular region. From Figure 6-12 (A), we see a normal copper EPR signal with a large coupling constant. In comparison of the four spectra, we see that HPrγ and buffer seem to share matching signals as was the case at pH = 8.0. HPrβ and HPr also show matching perpendicular signals that are clearly different from the buffer and HPrγ signals. The coupling constant in the parallel region at pH = 4.8 is ~45 G, while at pH = 8.0 it is ~60 G. The perpendicular coupling constant for HPrβ is different at the two pH values with ~25 G for pH = 4.8 and ~65 G for pH = 8.0. This indicates that near physiological pH values, the hyperfine coupling to the copper nuclear spin with HPrβ becomes stronger, consistent with decreased copper covalency with its ligands.

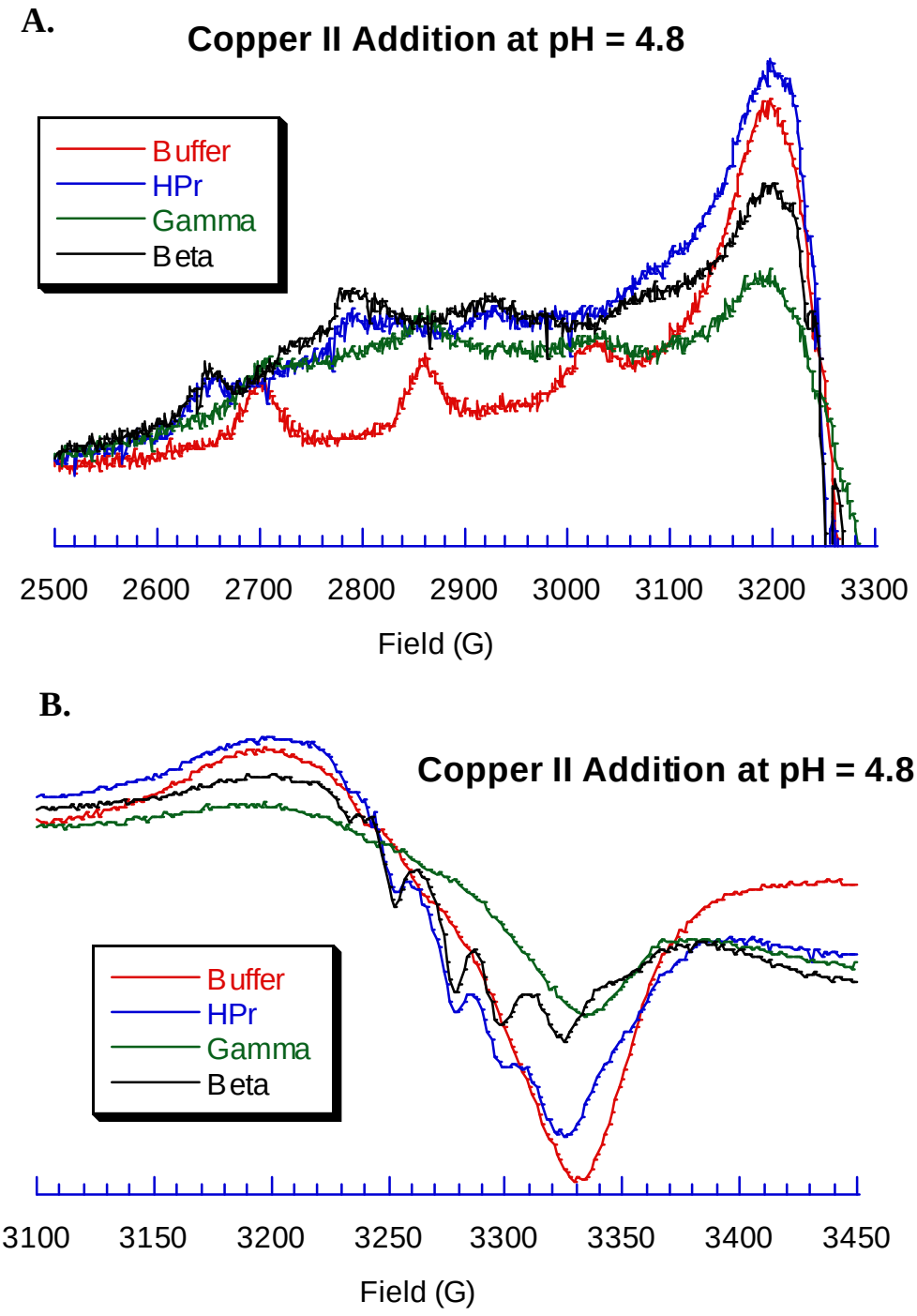

Figure 6-12: EPR spectra of the copper (II) addition at pH = 4.8

Overall, these copper studies on HPr and its mutants suggests that HPrγ is not

effective at binding copper at pH = 8.0, while HPrβ does show copper complexation characteristics. HPr and HPrβ have similar binding properties, however, the observed EPR signals for HPrβ are more intense and complex. These observations lead us to the conclusion that something about HPrγ's structure, with the E84Y mutation causes the engineered binding pocket to exclude copper ions. One explanation can be made by the observation that at pH = 8.0, our engineered two tyrosine and two histidine residues are uncharged and essentially hydrophobic. Perhaps the proximity of these four residues facilitates formation of a hydrophobic pocket that excludes both iron and copper from coordinating to the HPrγ ligands. Using HPrβ, we reverted the E84Y mutation back to the negatively charged (at pH = 8.0) carboxylate glutamate that has also been observed to coordinate copper ions. This might alleviate the hydrophobicity of the engineered metal binding site, and allow copper ions to enter pocket, and bind His-15 (native and HPrβ) and His-17 (only) for HPrβ. This explanation would be consistent with the SDS-PAGE analyses where HPrγ appears to migrate much faster than HPr or HPrβ, potentially due to increased stability of HPrγ to denaturation by SDS. To further probe this possibility we perform protein denaturation studies of the three proteins, and monitor their structural stability by circular dichroism spectroscopy (discussed in section 6.8).

From these copper titrations, valuable information about our proteins metal-binding properties was learned, and subsequent analyses with manganese and vanadium was also conducted. Manganese ions have been used in metalloprotein experiments to replace iron as their metal ion, therefore we titrated manganese (II) in a manner analogous to our iron and copper studies. These additions did not, however, produce

experimental data that differentiated HPrγ from HPrβ or HPr. Vanadium was also added to our protein samples to test its ability to interact with our engineered sites. Vanadate has been shown to mimic the coordination properties of phosphate. Thus probing our native HPr, which transfers phosphate ions in vivo, with vanadate could provide useful information. Our additions of vanadium (IV) and vanadium (V) did not, however, produce any distinguishable features by UV-Vis, EPR, or ^{51}V NMR spectroscopies.

As a result of these metal-binding studies, we do have a clearer picture of our proteins' metal binding properties, however, an explanation of why our HPrγ mutant has not produced the anticipated results has not been fully established. To further address this question, we turned to the CD spectroscopic investigation of our proteins.

6.5 CD DENATURATION STUDIES

As discussed above, our metal-binding analyses have shown that HPrγ does not coordinate iron ions by generating an iron (III)-phenolate bond. The reasons for this apparent inability could be complex, however one line of reasoning begins by noticing that at pH = 8.0, the two tyrosine, and two histidine residues engineered into HPrγ's phosphate binding pocket are essentially hydrophobic residues. Thus the congregation of all four of the close in proximity, greasy, residues in the presence of 55 M water induces a collapse of the potential metal-binding residues which excludes hydrophilic ions from entering. One approach to solving this dilemma is to lower the pH of the protein solutions below the pKa of histidine. This should result, under normal conditions, the protonation of His-15 and His-17 of HPrγ and alleviation of some of the hydrophobic

character of the binding pocket. Unfortunately lowering the pH to non-physiological values can cause other changes in the protein structure that may also preclude metal incorporation into the engineered pocket. Histidine residues buried in a relatively hydrophobic environment may also possess very different pKa values, thus potentially lowering their pKa well below the standard value of 6.4. In addition, if the histidine residues are buried in a hydrophobic pocket during expression and purification, no pH level may be attainable which will both protonate the histidine residues and maintain the structural stability of the protein. Our experimental attempts at iron binding at pH = 4.8 were unsuccessful in producing the desired complex. Therefore it is feasible that protonating the histidine residues in HPrγ, assuming a relatively standard pKa, does not alleviate the structural collapse developed *in vivo*.

To address the possibility that HPrγ does possess a hydrophobic interactions at its engineered binding loop relative to the functionally active native HPr, and metal-binding HPrβ, we can probe the overall stability of the HPrγ mutant relative to the native and HPrβ structures. Protein stability can be viewed as resistance to denaturation. If we are forming a hydrophobic pocket in HPrγ, its relative resistance to denaturation, compared to native HPr and HPrβ, should be increased. Evidence from SDS-PAGE analyses hints at this potentially increased stability to denaturation of HPrγ, however definitive evidence is necessary to support this argument.

Circular Dichroism (CD) spectroscopy has been developed over the last 30 years to probe chiral molecules, such as proteins, for their differential absorption of right and left circularly polarized light. CD spectroscopy is a powerful tool for examining

asymmetric molecules. The chirality associated with the secondary and tertiary structure of the protein can be probed with this technique.[3] UV absorbance measurements from 178 nm to 240 nm have been deconvoluted by fitting these spectra with linear combinations of standard spectra of known protein motifs such as α-helix, parallel and antiparallel beta sheets, beta turns etc…-to predict the structural features of unknown proteins. Figure 6-13 contains CD spectra of our native HPr, HPrγ, and HPrβ proteins at

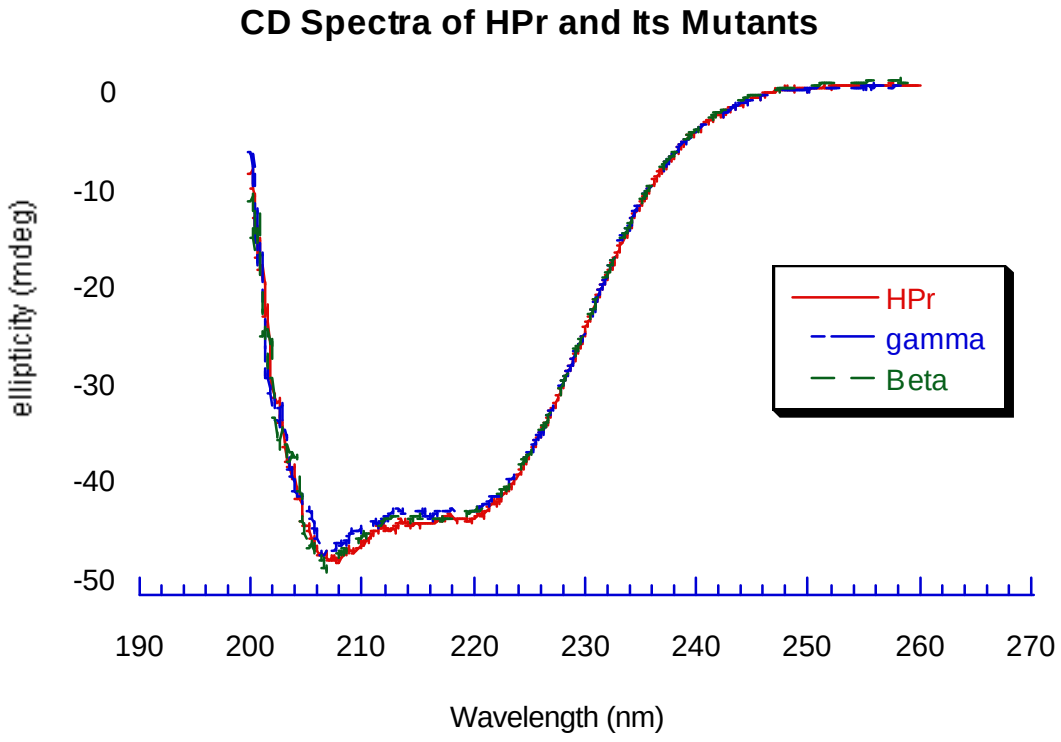

Figure 6-13: CD spectra of native HPr and our engineered mutants

room temperature. In the range from 260 nm down to 200

nm, these spectra match the known secondary structure of HPr containing contributions of α-helix, antiparallel β-sheet, and β-turn.

Expansion of this link between CD signals and protein secondary structures has led to analysis of protein stability toward denaturation by monitoring the loss of specific CD signals (which derive from specific secondary structure features) as proteins transform from their native structure, to a denatured, randomly oriented linear strand(s). Such studies have been reported for native HPr from E. coli.[4] Due to the strong structural homology, our B. subtilis protein should reasonably compare to these findings, and serve as a benchmark to measure the thermal stability of our HPrγ and HPrβ proteins.

In our CD experiments, we varied the temperature from 30 ^{o}C to 90 ^{o}C (according to the published procedure for *E. coli* HPr) and took CD spectra from 250 nm down to 200 nm at 5 ^{o}C increments for the native and two mutant HPr proteins. The striking results of these experiments are shown in Figure 6-14 where we plot the A_{222} ellipticity vs. temperature for duplicate analyses. From these revealing experiments, it can be seen that both HPr and HPrβ share similar profiles at 222 nm during heat denaturation from 30 ^{o}C to 80 ^{o}C with temperatures of most rapid denaturation (Tm) at approximately 60 ^{o}C. This value is consistent with the reported value for E. coli HPr of 60 ^{o}C. Contrast these similar profiles with the much more stable HPrγ protein that has a Tm value of approximately 65 ^{o}C. This is a full five degrees Celsius higher than HPr or HPrβ. This result provides definitive evidence that the HPrγ protein structure, through its E84Y mutation, is afforded a stabilizing force that protects it from denaturation.

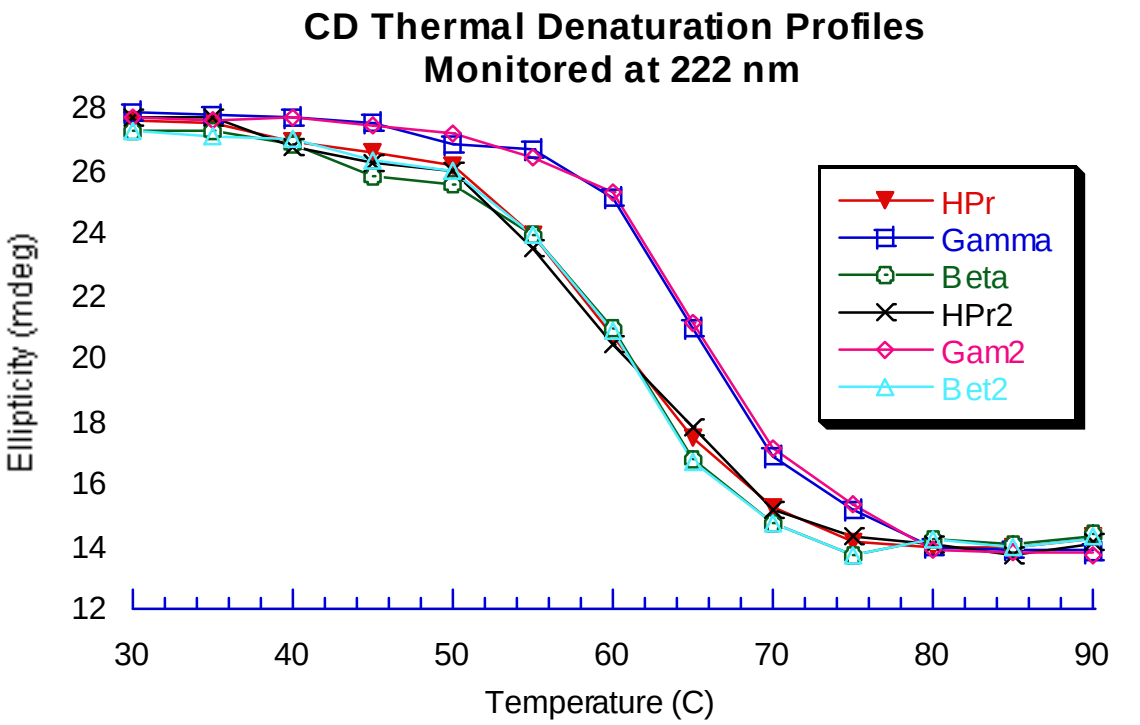

Figure 6-14: CD denaturation studies to probe the thermal stability of HPr, HPrγ and HPrβ

This result is consistent with our SDS-PAGE analyses, our ionic strength susceptibility to precipitation observations of HPr relative to HPr and HPrβ, and our metal-binding analyses. A likely cause of this effect at pH = 8.0 is the creation of a hydrophobic pocket which collapses the engineered segment of HPrγ and forces out the solvent molecules. One byproduct of this collapse, based on the HPr crystal structure, would likely be that the terminal α-helix (the helix E84Y mutation rests atop) would be pulled into closer contact and pack tightly against the protein structure. The results of such an effect would certainly reduce the degrees of freedom of this terminal loop and possibly assist in the exclusion of hydrophilic metal ions from the HPrγ engineered

pocket. If this is the case, it makes our endeavors to create such a site on the exposed surface of HPrγ essentially impossible.

In light of these findings, we made one last effort to incorporate iron by first denaturing HPrγ at 70 ^{o}C for 10 minutes, then adding 5.0 equivalents of iron (II) aerobically. Upon cooling, this reaction did not display absorbance in the visible region when monitored over time. This result was not unexpected, however, because in all three proteins only ~50 % of the CD signal was recovered when cooling the 90 ^{o}C denatured proteins back to 30 ^{o}C.

6.6 SUMMARY

In this chapter we have probed the metal binding properties of HPr, HPrγ, and HPrβ with iron (III), iron (II), copper (II), manganese (II), vanadium (IV) and vanadium (V) at pH's of 4.8 and 8.0. We found that iron does not coordinate to any of the proteins in a manner that is consistent with iron (III)-phenolate coordination similar to that found in PCD. Careful additions of iron showed no repeatable visible transition, and EPR spectra confirmed that all three proteins react to iron at both pH = 4.8 and 8.0 in a similar fashion.

Copper additions proved very informative as they showed that HPrβ did appear to coordinate the divalent transition metal in a new mode that was partially evidenced in the native HPr reactions as well. These copper studies showed that HPrγ's reactivity to copper was analogous to buffer alone, thus raising the question of why its very similar (in amino acid sequence)engineered pocket did not respond as the HPrβ protein.

Manganese titrations also hinted that HPrγ was incapable of coordinating metal ions, while HPrβ showed a dramatic loss of paramagnetic signal in its EPR signal. Vanadium results did not provide any information about HPrγ's structure because neither vanadium (IV) nor vanadium (V) showed reactivity to any of the proteins by UV-Vis or EPR spectroscopies.

Finally the CD denaturation studies gave conclusive evidence that HPrγ's structure is somehow stabilized by the E84Y mutation to thermal denaturation by 5 ^{o}C relative to HPr and HPrβ's Tm of 60 ^{o}C.

6.7 REFERENCES

[1] Nakazawa, T.; Nozaki, M.; Hayaishi, O. *J. Biol. Chem.* **1969**, *244*, 119-125.
[2] Bertini, I.; Gray, H. B.; Lippard, S.; Valentine, J. *Bioinorganic Chemistry*, 1994, University Science Books, Mill Valley, California.
[3] Pain, R. *Current protocols in Protein Science*, 1996, Wiley & Sons, Inc. pp. 7.61-7.6.23
[4] Nicholson, E. M.; Scholtz, J. M. *Biochemistry* **1996**, *35*, 11369-11379.

Chapter 7

SUMMARY & CONCLUSIONS

7.1 PURPOSE OF THESE STUDIES

Protein engineering has emerged as an important area of research. Our ability to synthesize, modify, and redesign protein structures has evolved in recent years, yet the field as a whole remains in its infancy. Currently, even the prediction of structural folding of a peptide based solely on its amino acid sequence, is difficult. Thus fundamental research in this area is essential to develop the tools to produce and modulate protein structure and function in a directed and predictable fashion.

A long-term goal of research in this area is to develop methods for the generation of "designer enzymes" which can catalyze *any* desired transformation. Included in this seemingly limitless number of transformations are those that require difficult reduction or oxidation reactions. Many of these reactions can not be carried out by purely organic proteins or cofactors. Transition metals, which are often found to coordinate proteins in nature, can perform many of these redox reactions. Therefore, the development of strategies to create "designer metalloenzymes" that specifically transform target substrates into the desired product(s) would be a significant accomplishment in protein engineering and chemical synthetic strategies.

The research presented herein focuses on the strategic incorporation of a transition metal into a phosphate-binding site. It is our hypothesis that the protein secondary and tertiary structure that supports phosphate coordination can also serve as a stable scaffold for metal coordination. To test this hypothesis, this research has accomplished:

- The design of mutant HPr proteins directed to support iron (III) coordination analogous to PCD
- The subcloning and cloning of the native ptsH gene from *B. subtilis*
- The synthesis, subcloning, and cloning of two mutant genes of the ptsH gene coding for HPrγ and HPrβ
- The overexpression and purification of recombinant HPr, HPrγ, and HPrβ
- Fe^{3+}, Fe^{2+}, Cu^{2+}, Mn^{2+}, V^{5+} and V^{4+} binding studies with HPr, HPrγ, and HPrβ monitored by UV-VIS and EPR and various metal addition experiments
- Protein stability studies monitored by circular dichroism on HPr, HPrγ, and HPrβ

7.2 TARGET DEVELOPMENT AND REDESIGN

The phosphate-binding protein HPr from *B. subtilis* was selected as a template protein for our studies. It is our expectation that the pre-existing protein structure of HPr (or phosphate-binding sites in general), which supports phosphate coordination, can stably support covalent metal coordination through directed mutagenesis of the amino acid residues within the phosphate-binding pocket. We also selected a naturally occurring iron-containing enzyme, PCD, to serve as an idealized goal for the conversion of our former phosphate-binding site. Strategic incorporation of iron within HPr in an analogous manner to the iron site found in PCD was modeled, examined, and simulated *in vacuo* to test possible routes of mutagenesis of HPr. Through a comparative analysis of the possible combinations of PCD-type metal ligand sets within HPr's phosphate-

binding pocket we found HPrγ (S12Y, R17H, E84Y) to require the least perturbation of the phosphate-binding pocket to support iron coordination analogous to PCD. Thus we restrained the HPrγ mutant ligands to the geometric constraints of iron ion in PCD and found that constrained minimization of HPrγ did not result in a gross perturbation of the HPr secondary or tertiary structure.

From this analysis, we set out to produce HPr and two of its mutants, with HPrγ (S12Y, R17H, E84Y) as our ultimate goal. However, the E84Y mutation is far removed, in a linear peptide sequence, from the other potential iron ligands, thus we wanted to test its individual contribution to metal coordination. Thus, we designed HPrβ (S12Y, R17H) to examine the role of residue 84.

7.3 GENE CONSTRUCTION AND CLONING

In our efforts to produce large quantities of proteins, we set out to construct and clone the HPr, HPrγ and HPrβ genes into a suitable expression system. We obtained the native ptsH gene (a generous donation from Dr. Jonathon Reizer) in the shuttle vector construct pCPP. Utilizing PCR techniques, we added a terminal BamHI restriction endonuclease site to the 5' terminus of the gene, and subcloned the PCR product into the pNoTA/T7 vector. DNA sequencing of the PCR product and the subcloned DNA in both directions confirmed that the native gene had been correctly synthesized and incorporated within the pNoTA/T7 vector. Finally we cloned the BamHI modified gene into the pCal-n expression vector via a BamHI and SacI forced cloning strategy. Colony hybridization analyses assisted in selection of putative clones, and DNA sequencing analysis confirmed

the correct construction of the ptsH gene within pCal-n had been achieved. This pCal-n construct can produce a fusion protein of HPr with an N-terminal, thrombin cleavable calmodulin binding peptide to allow facile purification of the target protein.

Mutagenesis of the ptsH gene was accomplished via a recombinant PCR technique. Three codons were changed to produce S12Y, R17H, and E84Y substitutions in HPr's amino acid sequence. The PCR product containing the three codon modifications was subcloned into pNotA/T7, and verified by sequencing prior to cloning within pCal-n. All three mutations were generated in a single mutagenesis strategy. The HPrγ mutant gene was constructed first, then codon 84 was reverted back to its native sequence to generate HPrβ gene. Both mutant genes were successfully cloned from pNoTA/T7 into pCal-n in a process analogous to the native ptsH gene.

This genetic construction is the first time an HPr protein has been cloned within the pCal-n vector, and neither HPrγ nor HPrβ mutant genes have been constructed previously.

7.4 PROTEIN EXPRESSION, PURIFICATION, AND CHARACTERIZATION

Successful cloning of the HPr and mutant genes into pCal-n allowed us to move forward to the next phase of our research, that of protein production, purification, and characterization. Production of high levels of HPr protein was accomplished through induction of the pCal-n/ptsH construct within the BL21 (DE3) strain of *E. coli*. Examination of the protein migration from SDS-PAGE analysis revealed an intense band migrating near the region expected for our tagged protein. Uninduced controls revealed

some leaky expression, however it was found that optimal intensity of the band relative to the background protein was produced at an IPTG concentration near 1.0 mM. To confirm that the overexpressed band was our desired protein, we applied cell free extract to the purification resin, and found it indeed preferentially binds to the resin in the presence of calcium ions, and is eluted by addition of EGTA. Thus the band contains the purification tag, and is very likely the desired protein.

Large-scale purification of the native protein was initially accompanied by a great deal of non-specific binding of background proteins. Optimization of the ionic strength conditions alleviated non-specific binding and subsequent protocol changes provided yields of 20 mg of protein / L of culture. A similar expression and purification process was applied to the HPrγ and HPrβ mutant proteins with similar results.

Characterization of HPr and its mutants was performed with SDS-PAGE, mass spectrometry, UV-VIS spectroscopy, and circular dichroism spectroscopy. Hartree-Lowery assays quantified the extinction coefficient for the three proteins at 280 nm. Activity assays revealed that our HPr construct is active with the purification tag at the N-terminus of the protein sequence, (far removed) from the phosphate-binding site. The purification tag was easily cleaved and separated from the uncleaved protein via Sephadex G-50 chromatography.

The combination of these characterization techniques confirms we overexpressed and purified an active HPr, that has characteristics consistent with the expected protein. In addition, our approach allowed us to readily express and purify the mutant proteins in an analogous manner without a probe for activity (since they had none). The purification

tag approach also provided a means to separate native HPr proteins from the BL21 (DE3) strain of *E. coli* from the recombinant proteins produced from the plasmid DNA with the organisms own machinery.

7.5 METAL-BINDING STUDIES OF HPR AND ITS MUTANTS

Upon successful completion of the protein expression and purification we investigated the iron-binding ability of our mutant HPr proteins by the addition of iron (III). At pH = 8.0, ferric ion readily precipitates, so we exchanged buffers to pH = 4.8 and added 1 to 200 equivalents of ferric chloride. No red color -with absorption near 450 nm was observed.

Attempts to coordinate iron ion within HPrγ's active site were modeled after reconstitution experiments of the native PCD by Nayaishi and coworkers. Analogous to those studies, we added iron (II) under aerobic conditions, and allowed the protein to equilibrate. Alternatively the experiment was performed anaerobically, and ferricyanide was added as oxidant to produce ferric ion. Our attempts on both HPrγ and HPrβ did not produce the red color characteristic of iron (III)-tyrosine coordination. These results were not anticipated. We repeated the metal additions several times, altering the conditions, however, PCD-type electronic transitions were not reproducibly observed. These results precluded our ability to probe the visible electronic transitions with PCD-type substrates and inhibitors, or assay our metallo-adducts for monooxygenase activity.

As a result of our apparent inability to create an iron coordination site analogous to PCD, we shifted our focus to the exploration of the metal binding with a panel of

transitions metals including: iron (III), iron(II), copper (II), vanadium (V), vanadium (IV), and manganese (II).

Iron (III) additions at pH =4.8 were performed. UV-Vis data showed no absorbance near 450 nm in additions from 0.5 to 5.0 equivalents of ferric chloride. These titrations also produced matching electronic spectra for the native and mutant proteins, indicating the iron (III) is not likely interacting with our mutant proteins. Examination of EPR spectra of these additions supported this conclusion, and revealed that all three proteins produced very similar signals consistent with soluble iron (III) appearing as the dominant species. Therefore iron (III) does not coordinate our mutant proteins as anticipated, and subsequent analyses to address probable causes were necessary.

Iron (II) was titrated from 0.5 - 5.0 equivalents, at both pH = 4.8 and 8.0, and monitored by UV-Vis and EPR spectroscopies. Our results show that no differential transitions were observed between HPr and our designed mutants. EPR analysis of the titrations shows that the post-dialysis buffer has a much weaker g = 4.3 (indicative of iron (III)) signal than our HPr proteins. These results demonstrate that we do have soluble iron (III) in solution, yet it does not interact with HPrγ at either pH = 4.8 or 8.0. The fact that HPrβ and HPrγ mutants have identical iron-binding signatures with UV-Vis and EPR spectroscopies suggests that the E84Y substitution is not important for iron (II) binding at either pH = 4.8 or 8.0. From these iron studies with our native and mutant proteins, we conclude that we are not forming the anticipated iron complex with either of our mutant HPrs. Additional studies to further explore the metal-binding properties of these mutants,

and address possible causes of our ineptitude to bind iron were performed, and are discussed below.

Copper additions, analogous to the iron (II) experiments were performed at pH = 4.8. UV-Vis analysis revealed that HPr and buffer produce similar spectral features with increasing concentrations of copper. An extremely weak isosbestic point at 687 nm was observed for each titration, and differences in energy shifts were noted. EPR spectra of these additions show that HPr and HPrβ have very similar signals which clearly differs from the dialysis buffer and HPrγ reactions. From the results of this comparison at pH = 4.8, HPrγ can not support the coordination requirements of copper, while both HPr and HPrβ show substantial evidence of copper (II) coordination.

Comparison of these results with similar experiments at pH = 8.0 indicates that copper additions produce identical electronic spectra for all three proteins, while the dialysis buffer control spectrum is similar to the pH = 4.8 buffer profile. EPR analysis of this addition shows that buffer and HPrγ have identical spectra, while HPr and HPrβ have distinct profiles. The most prominent feature of the four samples is that HPrβ contains a perpendicular signal with a large hyperfine coupling constant. HPr also has hyperfine coupling in the perpendicular region, however it is much lower in intensity and coupling constant. These results are good evidence that HPrγ does not allow copper to coordinate its histidine residues at pH = 8.0, while HPrβ and HPr appear to show no difficulties in the complexation with copper under identical conditions.

Addition of vanadium at pH = 8.0 was also performed in the 4^{+} and 5^{+} oxidation states to further probe our engineered proteins metal binding ability. UV-VIS and EPR

analyses, however, showed no distinguishing characteristics to establish vanadium binding to our HPr proteins.

Finally, manganese titrations were performed at pH = 4.8 and 8.0. The results show no absorption changes in the UV-VIS region for any of the samples. EPR data were obtained for these titrations, and produced standard manganese (II) signals that were identical for dialysis buffer and our three HPr proteins. Thus, manganese also fails to bind to our mutant proteins, which is consistent with our inability to bind ferrous ion under similar conditions.

To further probe our proteins, we examined their relative stability to thermal denaturation. Using CD spectroscopy, we monitored the loss of protein secondary structure for HPr, HPrγ, and HPrβ. The results of this analysis were eye opening. We found that HPrγ has a 5 ^{o}C higher melting temperature than do either HPr or HPr. This is clear evidence that our E84Y mutation imposes a stabilizing force to HPrγ since HPrβ shows no increased stability over native HPr. The native HPr annealing temperature was found to match the published value for HPr from *E. coli*.

In summary, from our metal binding studies with iron, copper, vanadium, and manganese at pH values of 4.8 and 8.0, we feel that HPrγ contains structural features that inhibit it from coordinating metal ions within its engineered binding site. One possible interpretation is that HPrγ, with four relatively hydrophobic residues, forms a hydrophobic pocket at pH = 8.0 that is not easily penetrated or protonated when lowering the solution pH to 4.8. This possibility is supported by SDS-PAGE, experimental observations, and CD denaturation studies. These stability studies that show HPrγ is

much more stable to denaturation than either HPr or HPrβ. It is likely that the overall structure of the native PCD enzyme inhibits this type of active site collapse, thus affording it the ability to reversibly coordinate ferric ions within its active site.

7.6 CONCLUSIONS

Efforts strategically create a ferric site within mutants of HPr proved unsuccessful. Through the results of additional metal binding analyses, we proposed possible explanations for these results. HPr could not be mutated into a PCD-type metalloprotein by our rational design process. Potentially alternate mutation pathways could be attempted, however it is likely that HPr's surface positioned phosphate-binding site could never possess the rigid backbone structure needed to prevent hydrophobic collapse of the PCD-type tyrosine and histidine ligands at physiological pH. In PCD, the active site is also slightly buried within the enzymes structure, thus reducing the solvent accessibility, potentially reducing the hydrophobic tendencies. Thus HPr, could be a poor match to PCD due to its small size and highly exposed binding pocket. Perhaps choosing a different metalloenzyme site with more hydrophilic character at pH = 7.2 would have resulted in the production of the desired protein.

Our inability to generate a PCD-type site does prove that HPr, from this experimental design, can not support the coordination requirements of iron in a manner analogous to PCD. Therefore our research does not support our hypothesis that phosphate-binding sites can serve as stable scaffolds for the creation of metal binding sites in proteins. Apparently other factors are involved. We did, however, propose a

plausible explanation for our difficulties, and through subsequent experimental probes, provided conclusive evidence that our suspicions about HPrγ were correct.

Protein engineering is an emerging field, and the insight gained through these studies contributes to the growing body of knowledge about protein structures, and what makes them so attractive and elusive.